COLORIMETRIC DETERMINATION OF METAL IONS USING SPIROPYRAN CONTAINING COPOLYMER THIN FILM SENSORS

by

KRISTEN HOLLIE FRIES

(Under the Direction of Jason Locklin)

ABSTRACT

Fabrication of sensors with a switchable surface that can alter between active (sensing) and passive forms provides a unique method for the development of optical sensors. In this context, spiropyran is an excellent candidate to use in designing a switchable surface using light. This dissertation details the design, synthesis, and characterization of a series of spiropyran-containing copolymers used as colorimetric thin film sensors. The copolymer with which spiropyran methacrylate is copolymerized was varied to study the effect of comonomer on the photoinduced conversion of spiropyran (SP) to merocyanine (MC). The composition of SP contained in the polymer backbone was also varied from 10 to 100 mol% to investigate the influence of free volume and sterics on the photochromic response, as well as the merocyanine-metal ion (MC-M^{2+}) interaction. Through UV-vis spectroscopy, we demonstrated that each metal ion gives rise to a unique colorimetric response that is dependent upon the amount of SP comonomer contained in the polymer backbone. Using chemometric methods, UV-vis spectra can be analyzed to selectively and quantitatively identify metal ions in a concentration range from 1 μM to 100 mM and simultaneously identify two metal ions in a binary mixture. We also used UV-vis spectroscopy to investigate the relative binding affinity of merocyanine to each metal ion by displacement studies of a bound metal ion with a second metal ion of higher binding affinity. In addition, we synthesized SP-containing copolymers that were used to investigate the influence of two different spiropyran derivatives, spiropyran methacrylate (SPMA) and the 8'-methoxy substituted derivative (MEO), on the metal ion complexation. FT-IR spectroscopy was used to characterize the photoinduced conversion of SP to MC, as well as the MC-M^{2+} complex in all of the copolymers. Principal component analysis was used to analyze the FT-IR spectra in order to elucidate the chemical binding environment between MC and the different metal ions.

INDEX WORDS: spiropyran, colorimetric, ultrathin film, optical sensor, polymers, chemometrics

COLORIMETRIC DETERMINATION OF METAL IONS USING SPIROPYRAN CONTAINING COPOLYMER THIN FILM SENSORS

by

KRISTEN HOLLIE FRIES

B.S., James Madison University, 2006

A Dissertation Submitted to the Graduate Faculty of The University of Georgia in Partial Fulfillment of the Requirements for the Degree

DOCTOR OF PHILOSOPHY

ATHENS, GEORGIA

2011

COLORIMETRIC DETERMINATION OF METAL IONS USING SPIROPYRAN CONTAINING COPOLYMER THIN FILM SENSORS

by

KRISTEN HOLLIE FRIES

Major Professor: Jason Locklin

Committee: I. Jonathan Amster
Bingqian Xu

Electronic Version Approved:

Maureen Grasso
Dean of the Graduate School
The University of Georgia
August 2011

DEDICATION

I dedicate this dissertation to my dad, David Fries. He lived his life with complete passion and exceptional energy, and I can only hope I will do the same. He held himself to the highest of standards not only at work, but with his family, friends, and even his love for running as well. My dad did not just go for a jog; he went for the Boston Marathon. He was an inspiration to everyone he met, a great friend to many, and a loving husband and father to his family. While his marathon ended too soon, his memory will live on forever. We miss you.

ACKNOWLEDGEMENTS

This dissertation would not have been possible without the guidance and encouragement of several individuals. First and foremost, I would like to thank my advisor, Dr. Jason Locklin, who has guided me with patience and support throughout the entire research process. I have come a long way since my first days in the lab, and I attribute all of my progress to him. He is a great teacher, and I cannot imagine having a different advisor.

I would also like to thank my committee members, Dr. Jon Amster and Dr. Bingqian Xu. They have always been kind and helpful, and I really appreciate their willingness to help me.

During my daily work, I have been blessed with a friendly and cheerful group of fellow lab mates. Sara Orski, Nick Marshall, Kyle Sontag, Gareth Sheppard, Joe Grubbs, Rachelle Arnold, Evan White, Vikram Dhende, Jenna Bilbrey, Shameem Giasuddin, and our former post doc, Satya Samanta, have all in some way or another made the lab a better place to work. This group made it possible for me to want to come to work day in and day out, and I consider them friends, not just coworkers. I would like to offer a special thanks to Sara Orski, as she became one of my closest friends over the years. We shared in each other's struggles and celebrated in each other's happiness, and her friendship throughout these last five years has been incredibly important to me. I have no doubt we will carry this friendship through life.

I would also like to thank my parents, who have been pivotal in all of my success. My mom has always been my biggest cheerleader, encouraging me in every aspect of my life. Whatever the goal, my mom is the first to say that I can achieve it. My dad was an inspiration to me. His hard work and dedication has always been something to which I aspire. I would also like to thank my brothers, Scott and Austin. They have always been willing to lend an ear when I need to vent.

Finally, I would like to thank Eric Gale. As my boyfriend, he has often had to bare the brunt of my frustrations and rages against the world, and he has done it amazingly well. He has stayed by my side throughout everything, and I truly cannot imagine going through these last several years without him. He has been my rock, and I love him dearly.

TABLE OF CONTENTS

CHAPTER

APPENDICES

LIST OF TABLES

LIST OF FIGURES

CHAPTER 1

INTRODUCTION AND LITERATURE REVIEW

Spiropyran

Photochromism is typically defined as the reversible, photoinduced transformation between two molecular states whose absorption spectra are significantly different.[1] The phenomenon of photochromism was first discovered by Fischer and Hirshberg in 1952 and was observed in both organic and inorganic molecules.[2] Besides the significant difference in absorption spectra of the two isomers, several other molecular and bulk properties are also different in the two forms, such as refractive index, redox potential, and dielectric constant. Several reviews describing these properties have been written.[1, 3-5] Photochromic materials have gained considerable attention in research due to their enormous potential in various devices, such as erasable optical memory media,[6-11] fast linear and nonlinear optical switches,[12-15] and chemical sensors.[16-18] Spiropyrans, azobenzenes, spirooxazines, fulgides, diarylethenes, and cinnamates are just a few of the more common organic compounds that exhibit photochromic properties, and their chemical structures are shown in Figure 1.1.

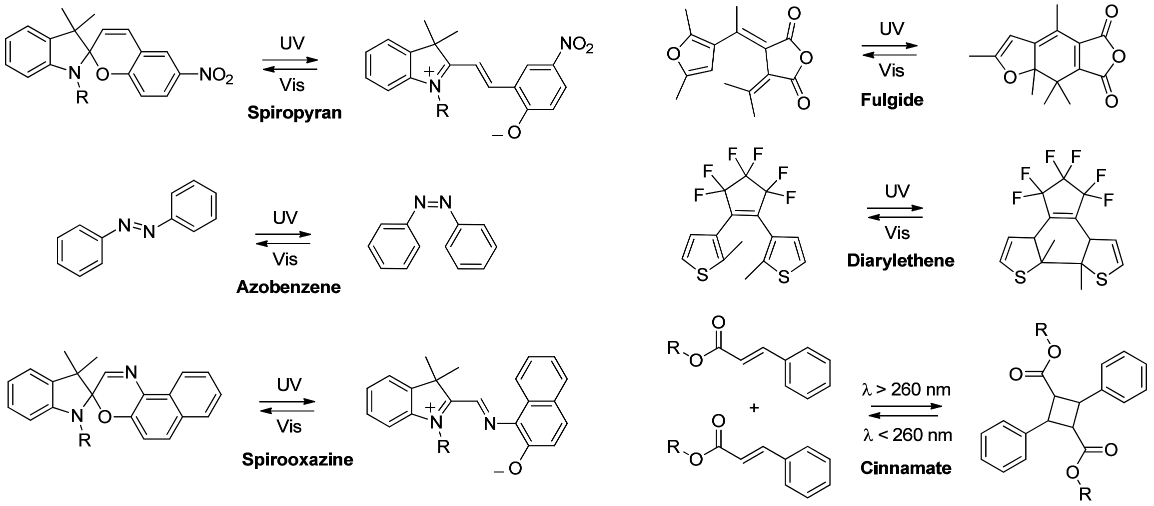

Figure 1.1. Isomeric structures of various photochromic compounds.

Of these many classes of photochromic compounds used for various applications, spiropyrans are the most extensively studied both experimentally and theoretically.[6, 19-21] The photoswitchability of spiropyrans has been exploited for a variety of chemical assemblies and has been used for photocontrol of enzyme activity,[22, 23] surface patterning,[24] optical transduction,[25] and surface wetting.[26-30] The majority of spiropyrans exist in the dark as a nonpolar, ring-closed form that absorbs light only in the ultraviolet region, with an absorption maximum in the range of 300 – 400 nm (Figure 1.2). When exposed to UV light, the spiropyran (SP) chromophore undergoes a molecular rearrangement in which the spiro C-O bond is cleaved and a polar, ring-opened merocyanine (MC) is formed.[19, 31] The MC isomer has an intense color with an absorption maximum in the range of 500 – 700 nm. It has been shown that there are eight possible conformers that correspond to different values of the three dihedral angles, α, β, and γ, describing the rotation about the bonds in the central segment.[32-34] Those four conformations with the central transoid segment, where $\beta = 180^{\circ}$ (Figure 1.3), are the lowest energy conformations and provide the optimal conjugation of the 2 π-electron systems, the indoline and benzopyran. This gives rise to the long wavelength absorption, *trans*-MC, between 500 and 700 nm. Merocyanine can revert back to the ring-closed form by the use of visible light or heat. Figure 1.4 shows the typical color change between SP and MC in a solution of dichloromethane (Figure 1.4a) and the typical UV-vis spectra of each isomer in the solid state (Figure 1.4b).

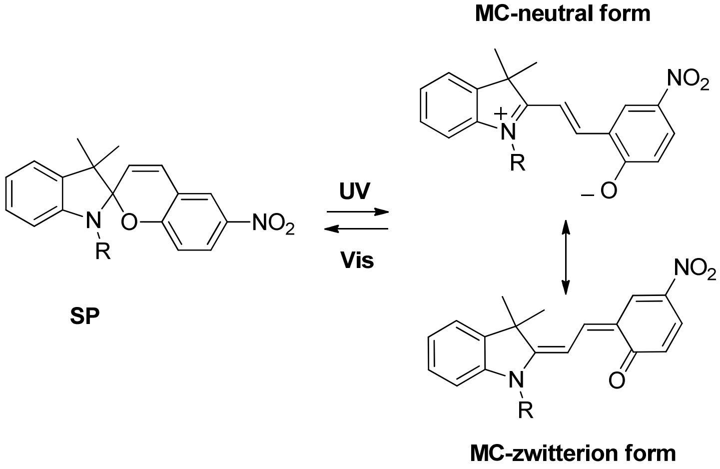

Figure 1.2. Reversible photoinduced conversion between spiropyran (SP) and merocyanine (MC). The resonance between the MC-neutral form and the MC-zwitterionic form is also depicted.

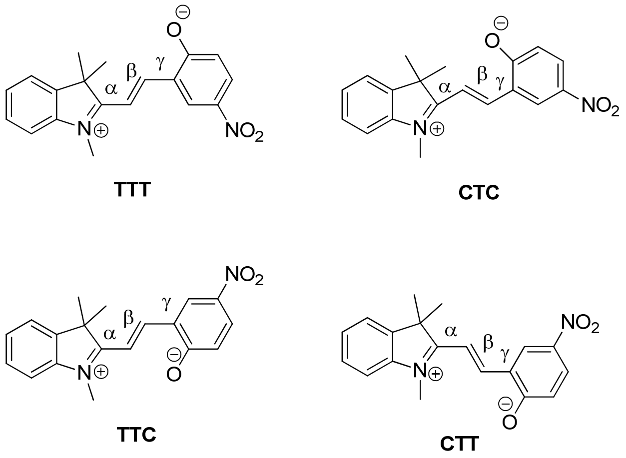

Figure 1.3. The four conformations of merocyanine with a central transoid segment (β = 180°).

The photoinduced change in geometry from SP to MC is accompanied by a large change in dipole moment (4.3 – 17.7 D),[35] which when restricted to an interface, will affect the surface free energy. This in turns allows for a switching of wettability from a hydrophobic SP to a hydrophilic MC.[26, 28] Also important to note, the merocyanine structure exists as a resonance hybrid between two forms: the charged zwitterion and a neutral quinoidal form (Figure 1.2). The zwitterionic form can bind metal ions through complexation with the phenolate anion.[17, 36-39] It is expected that the metal cation/phenolate anion can stabilize the zwitterionic form through complexation. This interaction, however, is weak enough that upon exposure to visible light, ring-closing can still occur, providing a system capable of reversible binding.

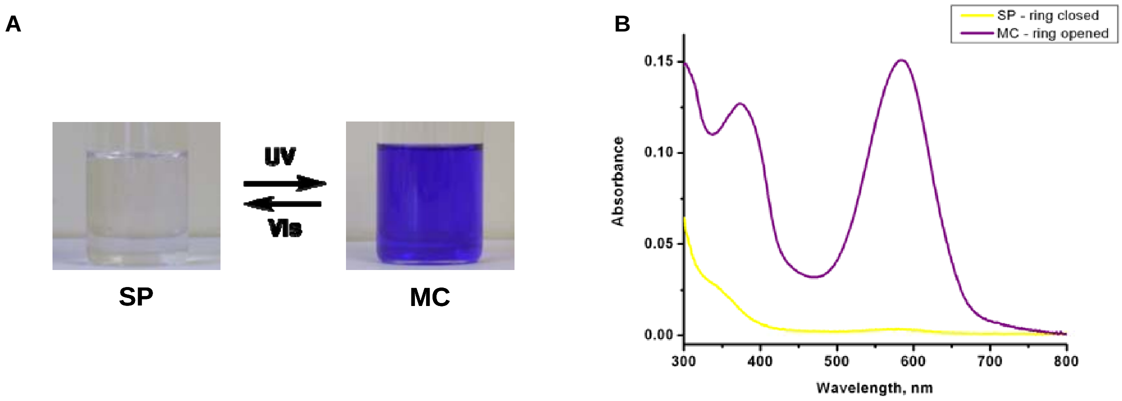

Figure 1.4. (a) The color change associated with the photoinduced conversion of spiropyran (SP) to merocyanine (MC) in a solution of dichloromethane and (b) the UV-vis absorbance spectra associated with the photoinduced conversion of SP to MC.

The chemical transformation between spiropyran and merocyanine has attracted a great deal of attention because of the drastic change in the molecular properties that occur through a basic unimolecular interaction. This has lead to research directions involving spiropyrans in the application of sensors, optical data storage, molecular switches, and other devices. Most of these applications require spiropyrans to be attached to surfaces by some method. This is significant because the microenvironment of spiropyran can dramatically affect its photoinduced properties, where the microenvironment may be composed of solvent molecules,[40, 41] substituent groups on spiropyran,[20, 39] and surface components.[41, 42]

The photochromism of spiropyran depends on the polarity of the surrounding medium (solvent or polymer matrix).[21] Nonpolar media promote the photoinduced isomerization of MC to SP. Moreover, polar media favor the formation of the zwitterionic MC form over the more neutral quinoidal form. Both of these MC forms exhibit solvatochromism, where changes in the position and intensity of the absorption bands are induced by the polarity of the surrounding medium. Specifically, the zwitterionic MC form exhibits negative solvatochromism, meaning that the absorption band undergoes a hypsochromic (blue) shift in solvents of increasing polarity.[43] This solvatochromism has been studied primarily for its use as an empirical indicator of solvent polarity.[44-46] Song *et al.* reported an in-depth study of the correlation between solvatochromism and the photochromism of spiropyran in solvents.[43] They used the transition energy for the open MC as an experimental method to measure solvent polarity and to investigate the rate of decoloration of MC to SP reversion. The results suggested that the SP form was solvated more strongly in nonpolar solvents, whereas the MC form was solvated to a greater extent in polar solvents, which is to be expected, given the zwitterionic nature of the MC form. They also reported that the rate of decay from the MC to SP form is dependent upon solvent polarity, where nonpolar solvents increase the rate constant of the reverse reaction.

The substituent groups on spiropyran can also affect the photoinduced conversion of SP to MC. It is worthwhile to mention that the MC form of 1',3',3'-trimethylspiro[chromeme-2, 2'-indoline] (BIPS) isomerizes back to SP thermally at a very high reverse rate of decoloration;[20] and therefore, the unsubstituted BIPS has no practical value in applications involving photochromism. A nitro group in the 6-position of the benzopyran moiety (R_1 = CH_3, R_2 = H, and R_3 = NO_2 in Figure 1.5) (6-NO_2-BIPS) stabilizes the MC form, thereby enhancing the photochromic activity.[20] Consequently, substituents play an important role in the photochemistry of spiropyran, and the effect of different electron-donating and electron-withdrawing groups on the reaction mechanism have been computationally studied in recent years (Figure 1.5).[20, 39]

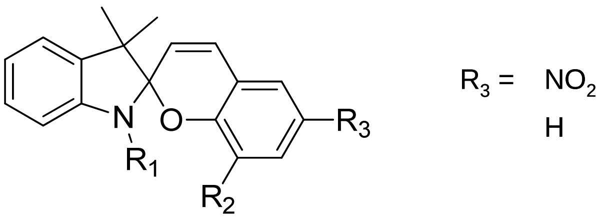

Figure 1.5. Substituted spiropyrans, where R_1 and R_2 can be a variety of functional groups, and R_3 is either NO_2 or H.

It has been previously demonstrated that, for a suitably substituted spirobenzopyran, the MC form is stabilized by complexation with certain d- and f-elements[47, 48] or alkali metal ions[49-51] through the phenolate anion. The chelating ability of MC was first observed in 1965 by Phillips,[48] but extensive research involving this interaction is still being conducted. Several groups have since reported MC binding to metal ions in solution and on surfaces.[37, 38, 52] Chibisov and Gorner first reported the use of spiropyran derivatives to complex metal ions in solution, giving rise to the potential application of SP as a metal ion sensor.[39] Complexation is accompanied by a new absorption band which is blue shifted from the λ_{max} of MC. Detailed kinetic studies were carried out to examine the formation of the merocyanine-metal ion ($MC\text{-}M^{2+}$) complex with various substituted spiropyrans. Others have synthesized a spiropyran derivative that selectively binds to Zn^{2+} in solution with 1:1 stoichiometry with respect to the Zn^{2+}:MC complex.[37] Diamond *et al.* have also reported metal ion complexation by a spiropyran derivative covalently attached to the surface.[17]

As stated above, the exploitation of spiropyrans in actual photochromic devices typically requires immobilization on a surface in such a way as to not interfere with the light-switching behavior. This has been achievable in self-assembled monolayers (SAMs) and bilayers and incorporation into polymer films and beads.[17, 26, 27, 42] The spiropyran moiety can be appended to the polymer backbone or incorporated into the main chain with quite different photochromic effects. The nature of the polymer backbone can influence the kinetics of the ring-opening and closing isomerization, the stability, or even lead to enhancement of photo degradation. Furthermore, spiropyran undergoes large changes in conformation when converting from its nonplanar, ring-closed form to a highly extended conjugated ring-open form (MC); thus, the switching of SP to MC is very sensitive to steric effects. In this respect, a significant amount of effort has been devoted to finding an environment that will allow for the maximum amount of spiropyran units to ring open. Rosario *et al.* covalently bound spiropyran to a glass surface, along with a mixture of organosilanes, in order to control the surface environment.[27] Byrne *et al.* covalently immobilized SP on a surface while varying its tether link to determine the effects of the dependence of optical switching on the environment.[17] Piech and Bell have copolymerized spiropyran with methyl methacrylate from flat surfaces and colloidal particles to study the photoinduced conversion of SP to MC in a polymer matrix.[42, 53, 54]

Optical Chemical Sensing

The field of optical chemical sensors (optodes) has been a growing research area over the last several decades.[55-57] An appropriate definition of a chemical sensor is the

"Cambridge definition,"[58] where *chemical sensors are miniaturized devices that can deliver real time and on-line information on the presence of specific compounds or ions in even complex samples*. Figure 1.6 shows a schematic of a sensor system, illustrating the three main elements; the sample (target species), transduction platform, and signal-processing. Essentially, chemical sensing comprises the following processes:[17]

1. Molecular recognition: immobilized chemo-recognition agents (ligands) that selectively bind to a target species are typically contained within the sensors and ideally do not bind with other "interfering" species that may be present in the sample matrix.
2. Transduction: the molecular binding event is transduced into an electronic or optical signal that can be observed externally. The sensor can have specific molecular transducers, such as chromophores, fluorophores, or redox agents, where they are immobilized with the recognition agent or built into the molecular structure of the recognition agent.

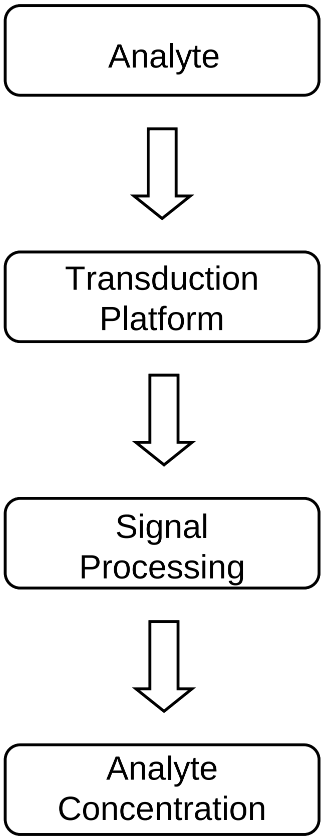

Figure 1.6. Principle stages in the operation of a sensor.

A typical optical sensor is based primarily on solid phase immobilization matrices, where organic indicator dyes are adsorbed or encapsulated in a polymer matrix that is permeable to the analyte.[59-61] Chemical sensors must have an "active" surface, incorporating sites that are pre-designed to bind with the target species in order to generate the chemically or biologically inspired signal. The interactions involved in these binding events can be very subtle, and even small changes in the surface or the environment through processes such as leaching, fouling, or binding sites becoming blocked, can have a significant effect on the output signal, influencing the overall performance of the device.[62-65] Due to these problems, optical chemical sensors experience baseline drift, variation in sensitivity, and interaction with other species that may be present in the sample. As a result, chemical sensors must be frequently calibrated, requiring the sensing surface to be periodically removed from the sample and exposed to standards, where any baseline drift or change in sensitivity is offset.[16]

There are several approaches that offer methods to simplify calibration and ultimately, improve optical chemical sensors. One such strategy is to fabricate arrays of single-use (disposable) sensors that are sequentially exposed to the sample. With current techniques, such as thin and thick film deposition, it is possible to fabricate sensors that have very predictable response characteristics, making it feasible to mass produce one-time use sensors.[66] Clinical diagnostics has already accepted this approach for single-use sensors intended for home-based diagnostic devices, where complex calibration is not possible. With disposable clinical devices, the sample (for example, blood or urine) is typically added to a strip containing the sensor, which is then introduced into the instrument by the user. After the measurement is taken, the sensor is discarded.[67] The disadvantage with this approach, however, is that the sensors potentially will be stored for long periods of time before use, which can affect the stability.

Another strategy is to fabricate lab-on-a-chip devices (miniaturized analytical instruments) that incorporate microfluidic channels which allow samples and standards to flow to a sensing region or surface, enabling calibration and analytical measurements to be performed.[68, 69] These devices are advantageous because the sensing region is not continuously exposed to the sample and very low flow rates are required (μL/min). Due to this, sample size and waste generation are small. The extended lifetime of these sensors, however, is still problematic. These microfluidic channels, which have a width and depth typically in the range of 10-500 μm, are prone to blockage and the micropumps/valves used to regulate flow rate are unreliable as they are susceptible to particulate damage. In response to these problems, some researchers have designed systems that incorporate soft polymeric pumps and valves which have many of the properties of biological materials.[70, 71] In principle, these can be fully integrated into the microfluidic manifold and can accommodate small particulates by reforming around them.

Fabrication of sensors with a switchable surface, where the surface can alter between active (sensing) and passive, is another strategy to improve upon current optical chemical sensors. This concept has been initially proposed by Byrne and Diamond.[16] In principle, this will allow the surface to be periodically activated to perform a measurement and reset to the passive state between measurements, enabling the initial response characteristics to be maintained over long periods of time while in the passive, non-reactive state.

Spiropyran is an excellent candidate to use in designing a switchable sensor. These well-known molecular switches are converted from a chemically inactive, colorless spiropyran form to the highly colored, zwitterionic merocyanine form that can bind metal ions through a negatively charged phenolate group; and furthermore, upon binding of the metal ion, the color of the MC chromophore changes. This effect has been well demonstrated in solution, but more recently has been observed in the solid phase as well.[36-39] Diamond *et al.* covalently immobilized a spiropyran derivative to a polymethacrylic acid substrate through a diamino alkyl linker.[17] The reversible switching from spiropyran to merocyanine was found to depend strongly on the distance of the spiropyran molecules from the polymer backbone, presumably due to the degree of flexibility required to facilitate the reorganization of the ring-closed SP to the ring-opened MC. They show that it is possible to fabricate a polymeric film that can be switched repeatedly from a passive to active state, simply by using light.[17] After the measurement is completed, the ion can be expelled by visible light and the film switched back to the passive state. Not surprisingly, there is considerable ongoing research into the SP-MC system to increase the sensitivity of MC to metal ions, as well as to tune the selectivity of MC to various metal ions.[18]

Spiropyran offers exciting possibilities for light control of metal ion binding for optical sensors, as it is a self-indicating, colorimetric system that is easily converted between a passive and active state using light. It provides a new approach to controlling surface binding behavior, which may in turn provide a route to developing chemical sensors with switchable surfaces where a new type of simple, low cost optical sensor is capable of long term autonomous operation.

Fabrication Methods of Polymer Thin Films

For a large number of chemical and physical processes, the bulk properties of a material, as well as the structure and composition of its surfaces, determine the performance of the entire system.[72] In order to control the interaction of a material with its environment, coatings consisting of thin polymeric films are frequently applied to the surfaces of these solids. In many cases, these coatings serve primarily as a method for protection against chemical and photochemical degradation. Thin organic coatings, however, are also applied in a large number of more high-tech applications, such as optical chemical sensors, microelectronics, and biomedical devices.[73, 74] In this context, polymeric coatings are applied to control the interactions between the material and its environment. These interfacial properties that can be controlled include friction, adhesion, adsorption of molecules from the surrounding environment, or wetting with water.[75-80] In addition, functional coatings can be applied that allow groups which interact with other molecules in their environment through specific molecular recognition processes to cover the surface. This strategy is especially important, for example, in designing optical chemical sensors that employ spiropyran.

Depending on the type of interaction between the surface and polymer coating, two methods for depositing polymer thin films can be used. In one approach, the polymers interact with the substrate by physical forces, while in the other approach, the polymers are attached to the surface through covalent bonds.[81, 82] A number of technologically important coating techniques exists which rely on physical interactions between the deposited polymers and the substrate, including painting/droplet evaporation, spray-coating, dip-coating, spin-coating, doctor blading, and Langmuir-Blodgett techniques. A commonality among all of these techniques is that the polymers are deposited from solution and the solvent evaporated during the coating process (Figure 1.7). If the deposition conditions are properly controlled, layers with well-defined thickness and good homogeneity can be generated in a simple fashion. Further, several of these techniques, such as spin-coating and dip-coating, can yield extremely thin coatings of just a few nanometers thickness to a film thickness with, effectively, no upper limit.

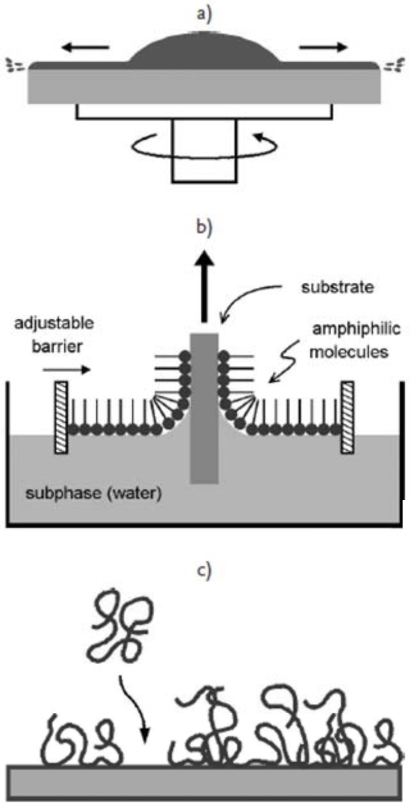

Figure 1.7. Schematic illustration of different processes used for the deposition of polymers on surfaces: (a) spin-coating, (b) Langmuir-Blodgett technique, and (c) adsorption from solution. Reprinted with permission from Reference 70. Copyright 2004, Wiley-VCH.

Spin-coating is the most common of these techniques and has been used in the microelectronics industry for the application of photoresists to silicon wafers and is involved in crucial steps in the production of DVDs and CDs.[83] This method of surface coatings has been the subject of many fundamental studies, and its use and scope has been reviewed recently.[84] This technique allows for reproducible formation of films, which are very homogenous over a large area.[83] Typically, spin-coating involves the application of a solution to a surface followed by acceleration of the substrate at a chosen rotational speed. Alternatively, the solution may be applied while the substrate is spinning. The angular velocity of the substrate results in the ejection of most of the applied liquid where only a thin film is left behind. The thickness, morphology, and surface topology of the final film are very reproducible for a particular material in a given solvent at a given concentration and are dependent upon rotational speed, viscosity, volatility, diffusivity, molecular weight, and concentration of solute.[83, 84] They depend relatively little on the amount of solution deposited, the rate of deposition, and the spinning time. The film thickness, d, can be expressed by the empirical relationship given in equation 1.1:

$$d = k\omega^{\alpha} \qquad \text{(Equation 1.1)}$$

where ω is the angular velocity, and k and α are empirical constants related to the physical properties of the solvent, solute, and substrate.[84]

Despite the advantages of spin-coating, as well as other techniques listed above, there are applications for which these methods are not useful. In all of these coating techniques, the molecules are attached to the substrate by physical interactions, and consequently, the forces holding them at the surface are weak. In unfavorable environments, the films can be ruined by four conditions:[72]

1. Desorption during solvent exposure
2. Displacement by molecules which have a stronger interaction with the surface
3. Dewetting for films above the glass transition temperature, T_g
4. Delamination for films below the T_g

Desorption and displacement are especially problematic in several applications, as coatings are usually not prepared and kept under ideal conditions. Contaminants are present on every surface and other species in the environment will compete for surface sites during or after the coating process. Dewetting, another disadvantage, occurs in all systems where the surface tension of the substrate is lower than that of the coating material, which can occur by heating the material above its T_g. Delamination arises if the films are in the glassy state and subjected to wide temperature changes, or the coating swells in the environment to which it has been exposed. Strong mechanical stress develops at the interface, and this can cause the entire film to peel off.

An alternative to coating techniques that rely on physical forces to hold the coating in place is to attach the molecule to the surface of the substrate through covalent bonds.[72] In this way, the long-term stability of the coated surface is improved. Several ways to do this exist, such as attaching self-assembled monolayers to the surface and grafting polymer brushes to and from a surface. Self-assembled monolayers (SAMs) involve attaching a small molecule with a reactive head group to a corresponding chemical moiety on the surface of the substrate (Figure 1.8, left).[85] This process is self-limiting, in that the surface attachment stops when all of the reactive surface groups have been consumed or are no longer accessible. In this way, surface coatings can be obtained which are very stable and can have a strong degree of orientational order. If molecules are assembled that carry at their tail end a specific chemical moiety, it is possible to obtain a more or less strict 2D arrangement of these functionalities.[86]

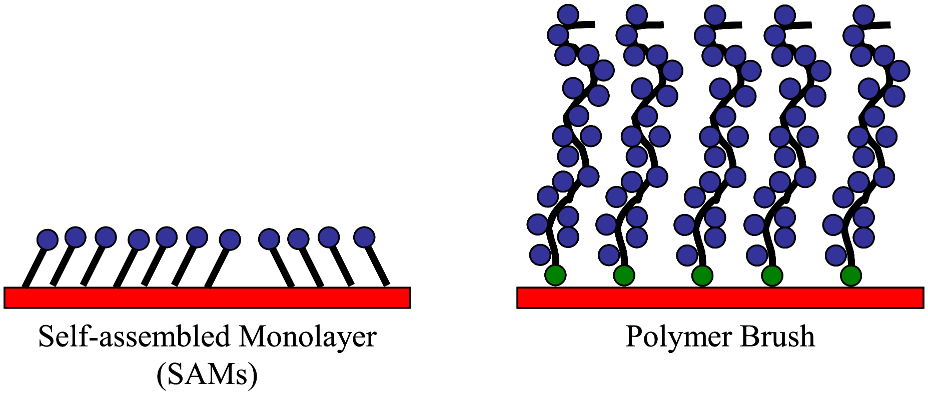

Figure 1.8. Schematic illustration of a self-assembled monolayer (left) and a polymer brush (right).

A disadvantage to using SAMs is that the maximal surface density of the functional moieties is limited by the surface area cross-section of the assembled unit.[72] The density of functional groups can be even lower as the arrangement of each individual SAM in such high packing densities can lead to the blocking of active sites. A solution to this problem is the extension into the third dimension by using polymers carrying the functional groups along the polymer backbone, generating higher cross-sectional densities of these groups and simultaneously guaranteeing good accessibility.

Polymer chain ends that are covalently tethered to a surface with a density high enough to alter the unperturbed solution dimensions of the chains are known as polymer brushes.[87] Figure 1.8 shows a schematic illustration of a polymer brush as compared to a SAM. Films generated from polymer chains in extended conformations exhibit surface phenomena that are often times different than polymers deposited onto a substrate from solution. These unique properties of polymer brushes over other thin polymer films are dictated by the ordered, extended chains that are perpendicular to the surface. The ordered chains are extended on the densely grafted surface, balancing two opposing energies: the entropic energy gained by a random walk configuration of the polymer chains and the energetic favorability of the chains to be highly solvated and non-overlapping.[88] In addition, the extended conformation provides a greater surface area of the polymer thin film, which allows for more functional groups per unit area. With increased side chain functionality, the polymer brush is able to influence the interfacial chemistry more effectively. In contrast, thin polymer films are coiled and intercalated at the surface, which leads to buried functional groups within the film layers.

Polymer brushes can be formed in a “grafting to” or “grafting from” approach. Figure 1.9 illustrates a schematic of a “grafting to” and “grafting from” polymerization. The “grafting to” method involves synthesizing a polymer in solution with a reactive functional group at one end of the chain, which is covalently attached to a complimentary functional group on the surface (Figure 1.9, top).[89, 90] The main problem with this approach is that it is diffusion limited, yielding a low polymer brush grafting density and limiting the degree to which the chains extend from the surface. The polymer chains remain in a somewhat coiled configuration, effectively blocking the surrounding reaction sites. These non-interacting random coils are referred to as the “mushroom regime,” which in good solvents have a thickness proportional to their degree of polymerization.

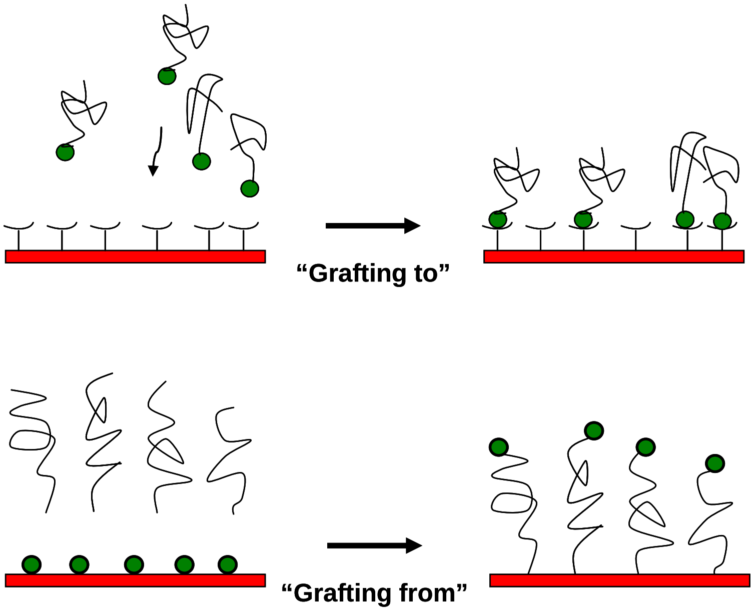

Figure 1.9. Schematic illustration of a "grafting to" (top) and "grafting from" (bottom) polymerization. Green circles represent reactive groups (initiator or covalent linker).

Polymer brushes are also synthesized in a "grafting from" approach (Figure 1.9, bottom) by direct polymerization from an immobilized initiator species on the surface (also known as surface-initiated polymerization). This approach to fabricating polymer brushes leads to surfaces with higher grafting density, where the distance between grafted polymer chains is much less than the size of the polymer coil.[91] Due to excluded volume effects, the polymer chain will forcibly grow in a more extended conformation as the polymerization proceeds. This configuration is known as the "brush regime," where the brush thickness is proportional to $N\sigma^{1/3}$, where N is the degree of polymerization and σ is the grafting density.[92] The polymer chains in this regime interact collectively and can have a much greater affect on the interfacial chemistry than the chains formed in a "grafting to" approach. In this geometry, selective control of the polymer brush microenvironment, brought about by conformational changes using stimuli such as temperature, light, or solvent, can dramatically alter film properties such as thickness and morphology. These properties are vital and can be used to generate and control nanostructures.[93]

Polymer brushes that are generated through “living” or controlled polymerization techniques are especially attractive due to low polydispersity and precise control over molecular weight. These techniques include atom transfer radical polymerization (ATRP), ring opening metathesis polymerization (ROMP), nitroxide mediated polymerization (NMP), and Kumada-type polymerization (KCTP) reactions.[94-100] Living polymerizations lead to extended polymer chains that have a very small molecular weight distribution, providing a further degree of control over surface morphology. This in turn makes for a more homogenous, collective polymer response.

Atom Transfer Radical Polymerization

Atom transfer radical polymerization (ATRP) is a controlled polymerization technique that recently has attracted commercial interest because of its easy experimental set-up, use of inexpensive and readily accessible catalyst components, and simple, commercially available or readily synthesized initiators. As seen in Figure 1.10, mechanistically, ATRP is based on an inner sphere electron transfer process, which involves a reversible homolytic (pseudo)halogen transfer between a dormant species, an added initiator or dormant propagating chain end (R-X or R-P_n-X), and a transition metal complex (usually Cu coordinated by various N-based ligands) in the lower oxidation state (Mt^n/ligand). This reaction results in the formation of propagating radicals ($R^\bullet$) and the metal complex in the higher oxidation state with a coordinated halide ligand (e.g. X-

Mt^{n+1}/ligand).[101] The active radicals form with a rate constant of activation, k_{act}, and subsequently do one of three things: 1) propagate with a rate constant, k_p, 2) reversibly deactivate, k_{deact}, or 3) terminate with a rate constant, k_t. As the reaction progresses radical termination is reduced as a result of the persistent radical effect (PRE),[102, 103] increased chain length, conversion, and viscosity.[104] As a result, the equilibrium is strongly shifted towards the dormant species ($k_{act} << k_{deact}$).[103]

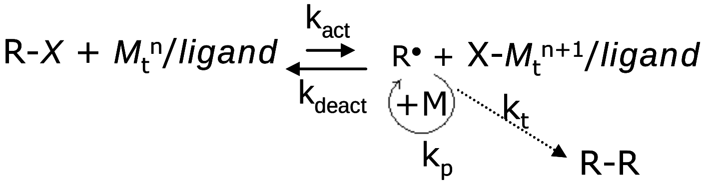

Figure 1.10. Reaction mechanism of atom transfer radical polymerization.

The higher oxidation state transition metal (complex), which in ATRP is the equivalent of the persistent radical, can be added directly to a reaction prior to initiation. In this way, the efficiency of initiation is increased by reducing the fraction of low molecular weight termination reactions initially required to generate the PRE.[105] Addition of the persistent radical, (Mt^{n+1} in the case of ATRP) is particularly useful when conducting a "grafting from" reaction with a multifunctional initiator or when ATRP is carried out in protic solvents.[106]

With ATRP, the polymerization process includes one or more (co)monomers, a transition metal complex in two or more oxidation states, which can comprise various counterions and ligands, an initiator with one or more radically transferable atoms, and a solvent. All of the components present in the reaction can affect the ATRP equilibrium.[107, 108] Due to this, it is very important to carefully select the appropriate catalyst/ligand/solvent combination. A combination that provides well-controlled polymers for one monomer may not be appropriate for another. The Matyjaszewski group has done a significant amount of research on appropriate combinations of catalyst, ligand, and solvent for various commercially available and commonly used monomers.[103, 105, 107, 108]

Chemometrics

Chemometrics is the field of extracting information from multivariate chemical data using tools of statistics and mathematics. It is typically used for one or more of three primary purposes:[109, 110]

1. to explore patterns of association in data
2. to track properties of materials on a continuous basis
3. to prepare and use multivariate classification models

The algorithms most commonly used in the field have demonstrated a significant capacity for analyzing and modeling a wide assortment of data types for an even more diverse set of applications.

Exploratory data analysis is used when pattern associations exist in the dataset, but the relationship between samples is difficult to discover due to a very large data matrix.[109] It reveals hidden patterns in complex data by reducing the information to a more comprehensible form. Such chemometric analysis can expose outliers and indicate whether there are patterns or trends in the data. Exploratory algorithms, such as principal component analysis and hierarchical cluster analysis, are designed to reduce large, complex datasets into a series of optimized and interpretable views. These views emphasize the natural groupings in the data and show which variables most strongly influence those patterns.

The goal of chemometric regression analysis, which aids in tracking properties of materials on a continuous basis, is to develop a calibration model which correlates the information in the set of known measurements to the desired property.[109] Chemometric algorithms for performing regression analysis, such as partial least squares regression analysis and principal component regression analysis, are designed to avoid problems associated with noise and correlations in the data. Because the regression algorithms used are based in factor analysis, the entire group of known measurements is considered simultaneously, and information about correlations among the variables is automatically built into the calibration model.

Many applications require that samples be assigned to predefined categories, or "classes," which generally involve predicting an unknown sample as belonging to one of several distinct groups. A classification model is used to predict a sample's class by comparing the sample to a previously analyzed training set, in which categories are already known. Partial least squares-discriminant analysis, k-nearest neighbor, and soft independent modeling of class analogy are common methods used for classification. When these techniques are used to create a classification model, the answers provided are more reliable and include the ability to reveal unusual samples in the data. In this manner, a chemometric system can be built that is objective, thereby standardizing the data evaluation process.

Principal Component Analysis

Principal component analysis (PCA) is a multivariate pattern recognition approach in an unsupervised format, where there is no *a priori* knowledge of class membership. It is a variable reduction procedure, and the aims of performing PCA on multivariate data are two-fold.[109, 111] First, PCA involves rotating and transforming the original, *n*, axes, each representing an original variable into new axes. This transformation is performed in such a way so that the new axes lie along the directions of maximum variance of the data with the constraint that the axes are orthogonal (i.e. the new variables are not correlated). It is usually the case that the number of new variables, *p*, needed to describe most of the sample data variance is less than *n*. Thus, PCA affords a method that reduces the dimensionality of the parameter space. The second goal of PCA is to reveal those variables, or combinations of variables, that describe some inherent structure in the data, and these may be interpreted in chemical or physico-chemical terms.

With PCA, the interest lies in the linear combinations of variables, with the goal of determining that combination which best summarizes the *n*-dimensional distribution of data.[110] It searches for the linear combination with the largest variance, with normalized coefficients applied to the variables used in the linear combination. This axis is called the *principal axis* or first *principal component*. Once this is determined, the search then proceeds to find a second normalized linear combination that has most of the remaining variance and is uncorrelated with the first principal component. This procedure is continued until all of the principal components have been calculated. Figure 1.11 shows a schematic diagram of new axes which describe the maximum amount of variance and are drawn orthogonal to each other.

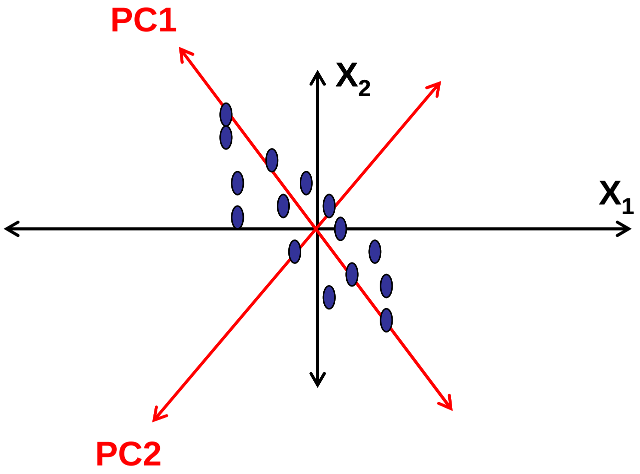

Figure 1.11. Schematic diagram of the new axes, PC1 and PC2, which describe the maximum variance and are drawn orthogonal from each other.

The power of principal component analysis is in providing a mathematical transformation of data into a form with reduced dimensionality. From the results, the similarity and difference between objects and samples can be better accessed, and this makes the technique of prime importance in chemometrics.

Partial Least Squares Regression Analysis

Partial least squares (PLS) regression analysis is a technique that generalizes and combines features from principal component analysis and multiple regression.[110] It is particularly useful when it is necessary to predict a set of dependent variables from a large set of independent variables (predictors). The goal of PLS is to predict Y from X and to describe their common structure. Specifically, the method searches for a set of components (latent vectors) that performs a simultaneous decomposition of X and Y with the constraint that these components explain as much as possible of the covariance between X and Y. It is followed by a regression step where the decomposition of X is used to predict Y.

Partial Least Squares-Discriminant Analysis

Partial least squares-discriminant analysis (PLS-DA) is a supervised method for pattern recognition requiring a training set of data in which the sample identity is known *a priori*. Unlike PCA, which identifies gross variability in the dataset, the supervised nature of PLS-DA functions to minimize within group variability and maximize among group variability.[112] PLS-DA consists in a classical PLS regression where the response variable is a categorical one (replaced by a set of dummy variables describing the categories), expressing the class membership of the statistical units; therefore, PLS-DA does not allow for other response variables than the one for defining the groups of individuals. As a consequence, all measured variables play the same role with respect to the class assignment. The sensitivity (rate of false negatives) and specificity (rate of false positives) can be reported for a PLS-DA model.

Objective and Outline of this Dissertation

The objectives of this dissertation are as follows: 1) to fabricate spiropyran-containing copolymer thin films to complex to metal ions, 2) to use these thin films as a colorimetric sensor that can selectively and quantitatively distinguish different divalent metal ions, 3) to use FT-IR and UV-vis spectroscopy to elucidate the binding interaction between merocyanine and metal ions, and 4) to synthesize spiropyran derivatives with different chelating groups and copolymerize these SP-derivatives with different polymers to tune these materials to selectively identify different metal ions.

The rest of this dissertation is organized into five chapters. Chapter 2 describes the synthesis and characterization of spiropyran-containing copolymer brushes that were used as reversible, photoswitchable optical sensors that show selectivity for different divalent metal ions and drastic changes in surface wettability. Using ATRP, the composition of spiropyran contained in the polymer backbone was varied from 10-100 mol% to investigate the influence of free volume and sterics on the photochromic response. We show that with the polymer brushes complexed to different metal ions, static contact angle changes as large as 70° are observed. Parts of this chapter were published in *Chemical Communications*, **2008**, 6288-6290.

Chapter 3 demonstrates spiropyran-containing ultrathin films that generate a unique and colorimetric response for different divalent metal ions. The main goal is to elucidate the binding interaction between merocyanine and the metal ions. FT-IR spectroscopy was used to characterize the merocyanine-metal ion (MC-M^{2+}) interaction and was analyzed using principal component analysis to elucidate the chemical binding environment. UV-vis spectroscopy was also used to characterize the MC-M^{2+} complex, and these results were analyzed using chemometric methods to show quantitative identification of divalent metal ions. This chapter was published in *Analytical Chemistry* **2010**, *82*, 3306-3314.

Chapter 4 describes these spiropyran-containing thin films as sensors that can be used to selectively identify two metal ions simultaneously. The binding affinity of merocyanine to each metal ion was also studied, and it was demonstrated that quantitative determination of each metal ion depends on the relative binding preference of merocyanine to each metal ion.

Chapter 5 describes the synthesis and characterization of spiropyran-containing copolymers that were used to study the influence of a second chelating group on the nitro ring of the chromophore on the metal ion complexation. The comonomer with which spiropyran was polymerized was also varied between methyl methacrylate and 2, 2, 2-trifluoroethyl methacrylate to study the effect of a more hydrophobic copolymer on the binding of merocyanine to metal ions. FT-IR spectroscopy was used to characterize the MC-M^{2+} complex, and principal component analysis was again used to elucidate the chemical binding environment between MC and the different metal ions.

Finally, Chapter 7 provides a general summary of all of the different photochromic polymers and thin film devices and an outlook on future studies.

References

1. Durr, H.B.-L., H., ed. *Photochromism Molecules and Systems*. 1990, Elsevier: Amsterdam.
2. Fisher, E.H., Y., *J. Chem. Soc.*, **1952**: p. 4522.
3. Irie, M., *Photoreactive Materials for Ultrahigh-Density Optical Memory*, ed. M. Irie. 1994, Amsterdam: Elsevier.
4. Brown, C.H., ed. *Photochromism*. 1971, Wiley-Interscience: New York.
5. Irie, m., *Functionality of Molecular Systems 2*, ed. K. Honda. 1999, Tokyo: Springer-Verlag.
6. Dvornikov, A.S., J. Malkin and P.M. Rentzepis, *J. Phys. Chem.*, **1994**. *98*(27): p. 6746.
7. Parthenopoulos, D.A. and P.M. Rentzepis, *Science*, **1989**. *245*(4920): p. 843.
8. Irie, M. and M. Mohri, *J. Org. Chem.*, **1988**. *53*(4): p. 803.
9. Toriumi, A., S. Kawata and M. Gu, *Opt. Lett.*, **1998**. *23*(24): p. 1924.
10. Ishikawa, M., Y. Kawata, C. Egami, O. Sugihara, N. Okamoto, M. Tsuchimori and O. Watanabe, *Opt. Lett.*, **1998**. *23*(22): p. 1781.
11. Kawata, S. and Y. Kawata, *Chem. Rev.*, **2000**. *100*(5): p. 1777.
12. Xie, S., A. Natansohn and P. Rochon, *Chem. Mater.*, **1993**. *5*(4): p. 403.
13. Dumont, M. and A. El Osman, *Chem. Phys.*, **1999**. *245*(1-3): p. 437.
14. Natansohn, A., P. Rochon, C. Barrett and A. Hay, *Chem. Mater.*, **1995**. *7*(9): p. 1612.
15. Delaire, J.A. and K. Nakatani, *Chem. Rev.*, **2000**. *100*(5): p. 1817.
16. Byrne, R. and D. Diamond, *Nat. Mater.*, **2006**. *5*(6): p. 421.

17. Byrne, R.J., S.E. Stitzel and D. Diamond, *J. Mater. Chem.*, **2006**. *16*(14): p. 1332.

18. Shao, N., Y. Zhang, S. Cheung, R. Yang, W. Chan, T. Mo, K. Li and F. Liu, *Anal. Chem.*, **2005**. *77*(22): p. 7294.

19. Hirshberg, Y., *J. Am. Chem. Soc.*, **1956**. *78*(10): p. 2304.

20. Sheng, Y., J. Leszczynski, A.A. Garcia, R. Rosario, D. Gust and J. Springer, *J. Phys. Chem. B*, **2004**. *108*(41): p. 16233.

21. Rosario, R., D. Gust, M. Hayes, J. Springer and A.A. Garcia, *Langmuir*, **2003**. *19*(21): p. 8801.

22. Osborne, E.A., B.R. Jarrett, C. Tu and A.Y. Louie, *J. Am. Chem. Soc.*, **2010**. *132*(17): p. 5934.

23. Willner, I., E. Katz, B. Willner, R. Blonder, V. Heleg-Shabtai and A.F. Bückmann, *Biosens. Bioelectron.*, **1997**. *12*(4): p. 337.

24. Willner, I. and R. Blonder, *Thin Solid Films*, **1995**. *266*(2): p. 254.

25. Willner, I., *Acc. Chem. Res.*, **1997**. *30*(9): p. 347.

26. Samanta, S. and J. Locklin, *Langmuir*, **2008**. *24*(17): p. 9558.

27. Rosario, R., D. Gust, M. Hayes, F. Jahnke, J. Springer and A.A. Garcia, *Langmuir*, **2002**. *18*(21): p. 8062.

28. Rosario, R., D. Gust, A.A. Garcia, M. Hayes, J.L. Taraci, T. Clement, J.W. Dailey and S.T. Picraux, *J. Phys. Chem. B*, **2004**. *108*(34): p. 12640.

29. Vlassiouk, I., C.-D. Park, S.A. Vail, D. Gust and S. Smirnov, *Nano Lett.*, **2006**. *6*(5): p. 1013.

30. Yang, D., M. Piech, N.S. Bell, D. Gust, S. Vail, A.A. Garcia, J. Schneider, C.-D. Park, M.A. Hayes and S.T. Picraux, *Langmuir*, **2007**. *23*(21): p. 10864.

31. Saragi, T.P.I., T. Spehr, A. Siebert, T. Fuhrmann-Lieker and J. Salbeck, *Chem. Rev.*, **2007**. *107*(4): p. 1011.

32. Görner, H., L.S. Atabekyan and A.K. Chibisov, *Chem. Phys. Lett.*, **1996**. *260*(1-2): p. 59.

33. Chibisov, A.K. and H. Görner, *J. Phys. Chem. A*, **1997**. *101*(24): p. 4305.

34. Takahashi, H., K. Yoda, H. Isaka, T. Ohzeki and Y. Sakaino, *Chem. Phys. Lett.*, **1987**. *140*(1): p. 90.

35. Bletz, M., U. Pfeifer-Fukumura, U. Kolb and W. Baumann, *J. Phys. Chem. A*, **2002**. *106*(10): p. 2232.

36. Winkler, J.D., K. Deshayesk and B. Shao, *J. Am. Chem. Soc.*, **1989**. *111*: p. 769.

37. Stauffer, M.T. and S.G. Weber, *Anal. Chem.*, **1999**. *71*(6): p. 1146.

38. Suzuki, T., Y. Kawata, S. Kahata and T. Kato, *Chem. Commun.*, **2003**(16): p. 2004.

39. Chibisov, A.K. and H. Görner, *Chem. Phys.*, **1998**. *237*(3): p. 425.

40. Tagaya, H., T. Nagaoka, T. Kuwahara, M. Karasu, J.-i. Kadokawa and K. Chiba, *Microporous Mesoporous Mater.*, **1998**. *21*(4-6): p. 395.

41. Hori, T., H. Tagaya, T. Nagaoka, J. Kadokawa and K. Chiba, *Appl. Surf. Sci.*, **1997**. *121-122*: p. 530.

42. Piech, M. and N.S. Bell, *Macromolecules*, **2006**. *39*(3): p. 915.

43. Song, X., J. Zhou, Y. Li and Y. Tang, *J. Photochem. Photobiol., A*, **1995**. *92*(1-2): p. 99.

44. Botrel, A., B. Aboab, F. Corre and F. Tonnard, *Chem. Phys.*, **1995**. *194*(1): p. 101.

45. Flannery, J.B., *J. Am. Chem. Soc.*, **1968**. *90*(21): p. 5660.

46. Keum, S.-R., Y.-K. Choi, M.-J. Lee and S.-H. Kim, *Dyes Pigm.*, **2001**. *50*(3): p. 171.

47. Shao, N., J.Y. Jin, H. Wang, Y. Zhang, R.H. Yang and W.H. Chan, *Anal. Chem.*, **2008**. *80*(9): p. 3466.

48. Phillips, J.P., A. Mueller and F. Przystal, *J. Am. Chem. Soc.*, **1965**. *87*(17): p. 4020.

49. Inouye, M., M. Ueno, T. Kitao and K. Tsuchiya, *J. Am. Chem. Soc.*, **1990**. *112*(24): p. 8977.

50. Kimura, K., M. Kaneshige, T. Yamashita and M. Yokoyama, *J. Org. Chem.*, **1994**. *59*(6): p. 1251.

51. Kimura, K., T. Utsumi, T. Teranishi, M. Yokoyama, H. Sakamoto, M. Okamoto, R. Arakawa, H. Moriguchi and Y. Miyaji, *Angew. Chem. Int. Ed.*, **1997**. *36*(22): p. 2452.

52. Evans, L., G.E. Collins, R.E. Shaffer, V. Michelet and J.D. Winkler, *Anal. Chem.*, **1999**. *71*(23): p. 5322.

53. Bell, N.S. and M. Piech, *Langmuir*, **2006**. *22*(4): p. 1420.

54. Piech, M., M.C. George, N.S. Bell and P.V. Braun, *Langmuir*, **2006**. *22*(4): p. 1379.

55. Wolfbeis, O.S., *Fibre Optic Chemical Sensors and Biosensors*. Vol. 1 and 2. 1991, Boca Raton: CRC Press.

56. Narayanaswamy, R. and O. Wolfbeis, *Optical Sensors: Industrial, Environmental, and Diagnostic Applications*. 2004, Berlin, Germany: Springer.

57. Eggins, B.R., *Chemical Sensors and Biosensors*. 2002, West Sussex, UK: John Wiley and Sons Ltd.

58. Cammann, G.G.G., E. A.; Hal, H.; Kellner, R.; Wolfbeis, O. S., *The Cambridge Definition of Chemical Sensors, Cambridge Workshop on Chemical Sensors and Biosensors*. 1996, New York: Cambridge University Press.

59. Nolan, E.M. and S.J. Lippard, *Chem. Rev.*, **2008**. *108*(9): p. 3443.

60. Buhlmann, P., E. Pretsch and E. Bakker, *Chem. Rev.*, **1998**. *98*(4): p. 1593.

61. Prodi, L., F. Bolletta, M. Montalti and N. Zaccheroni, *Coord. Chem. Rev.*, **2000**. *205*(1): p. 59.

62. Plaschke, M., R. Czolk and H.J. Ache, *Anal. Chim. Acta*, **1995**. *304*(1): p. 107.

63. Oehme, I., S. Prattes, O.S. Wolfbeis and G.J. Mohr, *Talanta*, **1998**. *47*(3): p. 595.

64. Zhang, X.-B., C.-C. Guo, Z.-Z. Li, G.-L. Shen and R.-Q. Yu, *Anal. Chem.*, **2002**. *74*(4): p. 821.

65. Rosatzin, T., P. Holy, K. Seiler, B. Rusterholz and W. Simon, *Anal. Chem.*, **2002**. *64*(18): p. 2029.

66. Lin, J.Z., D. M.; Hocevar, S. B.; McAdams, E. T.; Ogorevc, B.; Xueji Zhang, X., *Front. Biosci.*, **2003**. *10*: p. 483.

67. Meas, T., P. Taboulet, E. Sobngwi and J.F. Gautier, *Diabetes & Metabolism*, **2005**. *31*(3): p. 299.

68. Dempsey, E., D. Diamond, M.R. Smyth, G. Urban, G. Jobst, I. Moser, E.M.J. Verpoorte, A. Manz, H. Michael Widmer, K. Rabenstein and R. Freaney, *Anal. Chim. Acta*, **1997**. *346*(3): p. 341.

69. Boone, T.D., Z.H. Fan, H.H. Hooper, A.J. Ricco, H. Tan and S.J. Williams, *Anal. Chem.*, **2002**. *74*(3): p. 78 A.

70. Boncheva, M.W., G. M., in *Enyclopedia of Nanoscience and Nanotechnology*, J.A.C. Schwarz, C. I.; and Putyerak, K., Editor. 2004, Taylor and Francis: New York. p. 287.

71. Grzybowski, B.A., M. Radkowski, C.J. Campbell, J.N. Lee and G.M. Whitesides, *Appl. Phys. Lett.*, **2004**. *84*(10): p. 1798.

72. Rühe, J., *Overview: Polymer Brushes: On the Way to Tailor-Made Surfaces*, in *Polymer Brushes*, R.C. Advincula, Editor. 2004, Wiley-VCH Weinheim.

73. Thompson, L.F.W., C. G.; Bowden, M. J., ed. *Introduction to Microlithography*. 2nd Edition ed. 1994, American Chemical Society: Washington, D.C.

74. Tirrell, M., E. Kokkoli and M. Biesalski, *Surf. Sci.*, **2002**. *500*(1-3): p. 61.

75. Grest, G.S., *Polymers in Confined Environments*. 1999. p. 149.

76. Klein, J., E. Kumacheva, D. Mahalu, D. Perahia and L.J. Fetters, *Nature*, **1994**. *370*(6491): p. 634.

77. Grest, G.S., *Curr. Opin. Colloid In.*, **1997**. *2*(3): p. 271.

78. Grest, G.S., *Phys. Rev. Lett.*, **1996**. *76*(26): p. 4979.

79. Klein, J., *Colloids Surf., A*, **1994**. *86*: p. 63.

80. Klein, J., E. Kumacheva, D. Perahia, D. Mahalu and S. Warburg, *Faraday Discuss.*, **1994**. *98*: p. 173.

81. Jones, R.A.L.a.R., R. W., *Polymers at Surfaces and Interfaces*. 1999, Cambridge: Cambridge University Press.

82. Fleer, G.J.S., A. C.; Scheutjens, J. M. H. M.; Cosgrove, T.; Vincent, B., *Polymers at Interfaces*. 1993, London: Chapman.

83. Krebs, F.C., *Sol. Energy Mater. Sol. Cells*, **2009**. *93*: p. 394.

84. Norrman, K.G.-S., A.; Larsen, N. B.; , *Annu. Rep. Prog. Chem. Sect C.*, **2005**. *101*: p. 174.

85. Ulman, A., *An Introduction to Ultrathin Organic Films*. 1991, New York: Academic Press.

86. Xia, Y. and G.M. Whitesides, *Angew. Chem. Int. Ed.*, **1998**. *37*(5): p. 550.

87. Brittain, W.J. and S. Minko, *J. Polym. Sci., Part A: Polym. Chem.*, **2007**. *45*(16): p. 3505.

88. MILNER, S.T., *Science*, **1991**. *251*(4996): p. 905.

89. Ionov, L., B. Zdyrko, A. Sidorenko, S. Minko, V. Klep, I. Luzinov and M. Stamm, *Macromol. Rapid Commun.*, **2004**. *25*(1): p. 360.

90. Minko, S., S. Patil, V. Datsyuk, F. Simon, K.-J. Eichhorn, M. Motornov, D. Usov, I. Tokarev and M. Stamm, *Langmuir*, **2002**. *18*(1): p. 289.

91. Michailidou, V.N., B. Loppinet, O. Prucker, J. Rühe and G. Fytas, *Macromolecules*, **2005**. *38*(21): p. 8960.

92. Zhou, F. and W.T.S. Huck, *Phys. Chem. Chem. Phys.*, **2006**. *8*(33): p. 3815.

93. Orski, S.V., K.H. Fries, S.K. Sontag and J. Locklin, *J. Mater. Chem.*, **2011**.

94. Barbey, R., L. Lavanant, D. Paripovic, N. Schüwer, C. Sugnaux, S. Tugulu and H.-A. Klok, *Chem. Rev.*, **2009**. *109*(11): p. 5437.

95. Edmondson, S., V.L. Osborne and W.T.S. Huck, *Chem. Soc. Rev.*, **2004**. *33*(1): p. 14.

96. Liu, X., S. Guo and C.A. Mirkin, *Angew. Chem. Int. Ed.*, **2003**. *42*(39): p. 4785.

97. Senkovskyy, V., N. Khanduyeva, H. Komber, U. Oertel, M. Stamm, D. Kuckling and A. Kiriy, *J. Am. Chem. Soc.*, **2007**. *129*(20): p. 6626.

98. Sontag, S.K., N. Marshall and J. Locklin, *Chem. Commun.*, **2009**(23): p. 3354.

99. Tomlinson, M.R. and J. Genzer, *Chem. Commun.*, **2003**(12): p. 1350.

100. Wang, X., H. Tu, P.V. Braun and P.W. Bohn, *Langmuir*, **2005**. *22*(2): p. 817.

101. Singleton, D.A., D.T. Nowlan, N. Jahed and K. Matyjaszewski, *Macromolecules*, **2003**. *36*(23): p. 8609.

102. Fischer, H., *Chem. Rev.*, **2001**. *101*(12): p. 3581.

103. Tang, W., N.V. Tsarevsky and K. Matyjaszewski, *J. Am. Chem. Soc.*, **2006**. *128*(5): p. 1598.

104. Vana, P., T.P. Davis and C. Barner-Kowollik, *Macromol. Rapid Commun.*, **2002**. *23*(16): p. 952.

105. Matyjaszewski, K., A.K. Nanda and W. Tang, *Macromolecules*, **2005**. *38*(5): p. 2015.

106. Tsarevsky, N.V., T. Pintauer and K. Matyjaszewski, *Macromolecules*, **2004**. *37*(26): p. 9768.

107. Matyjaszewski, K., S. Coca, S.G. Gaynor, M. Wei and B.E. Woodworth, *Macromolecules*, **1998**. *31*(17): p. 5967.

108. Tang, W., Y. Kwak, W. Braunecker, N.V. Tsarevsky, M.L. Coote and K. Matyjaszewski, *J. Am. Chem. Soc.*, **2008**. *130*(32): p. 10702.

109. Adams, M.J., *Chemometrics in Analytical Spectroscopy*. RSC Analytical Spectroscopy Monographs, ed. N.W. Barnett. 2004, Cambridge: The Royal Society of Chemistry.

110. Elving, P.J.W., J. D.; Kolthoff, I. M., ed. *Chemometrics*. Chemical Analysis: A Series of Monographs on Analytical Chemistry and its Applications. Vol. 82. 1986, John Wiley & Sons: New York.

111. Beebe, K.R.P., R. J.; Seasholtz, M. B., *Chemometrics: A Practical Guide*. 1998, New York: John WIley & Sons.

112. Barker, M. and W. Rayens, *J. Chemom.*, **2003**. *17*(3): p. 166.

CHAPTER 2

REVERSIBLE COLORIMETRIC ION SENSORS BASED ON SURFACE-INITIATED POLYMERIZATION OF PHOTOCHROMIC POLYMERS[1]

---

[1] Fries, K. H.; Samanta, S.; Orski, S. V.; and Locklin, J. *Chemical Communications,* **2008**, 6288-6290. Reprinted with permission from The Royal Society of Chemistry, pubs.rsc.org.

Abstract

In this article, we describe the synthesis and characterization of spiropyran-containing polymer brushes that were used as reversible, photoswitchable optical sensors that show selectivity for different metal ions and drastic changes in surface wettability. Spiropyran methacrylate was polymerized with various methacrylates and acrylates to study the effect of the comonomer on the photoinduced conversion of spiropyran (SP) to merocyanine (MC). The composition of SP contained in the polymer backbone was varied from 10-100 mol% to investigate the influence of free volume and sterics on the photochromic response. Contact angle measurements were taken to show the changes in surface energy upon irradiation with UV light and that as the concentration of SP in the polymer backbone is increased, the change in contact angle decreases. We also show that with merocyanine complexed to different metal ions, static contact angle changes as large as 70° are observed. Through UV-vis spectroscopy, we demonstrate that each metal ion gives rise to a unique colorimetric response and that this blue shift in absorbance maxima correlates with the amount of static contact angle change on the surface in the presence of the different metal ions.

Introduction

Chemical sensors are molecules that are able to bind selectively and reversibly to an analyte of interest with a simultaneous change in one or more physical properties of the system, such as absorption, fluorescence, or electrochemical potential. Specifically, colorimetric chemical sensors based on organic polymeric thin films (optodes) have been investigated extensively in the last decade.[1-3] In a typical sensor configuration, organic indicator dyes are immobilized in some host polymer matrix through either chemi- or physisorption. Depending on the type of immobilization, several problems can occur that limit the sensor stability, such as leaching of the indicator,[4-6] inaccessibility of the dye after functionalization due to steric constraints, and/or diffusion of the analyte through the polymer matrix.[7, 8] Also, immobilized indicator often prohibits a reversible response of analyte because of very strong binding interactions. With increased usage, fouling, which leads to sensor drift, is unavoidable.

Recently, Byrne and Diamond have proposed the use of molecular switches that can adopt active or passive forms using external control as a way to improve sensor lifetime.[9] A switchable sensor would also simplify any method of calibration that might be necessary due to drift in the sensor response with time. In this context, they have used a photochromic spiropyran self-assembled monolayer, tethered to a poly(methyl methacrylate) support through alkyl diamine spacers, to reversibly bind cobalt(II) ions in solution.[10]

Spiropyrans are a group of photo-switchable organic molecules whose photochromism involves light induced cleavage of the spiro C-O bond. This allows reversible switching between a colorless, closed form and a strongly colored, open form.[11, 12] The photoinduced geometry change between the ring-closed spiropyran (SP) and the ring-opened merocyanine (MC) form (Figure 2.1) is accompanied by a large change in dipole moment. If confined to an interface, the change in dipole moment affects the surface free energy, which in turn, gives rise to a switching of wettability. We and others have exploited this change to generate surfaces that can be switched from hydrophobic to hydrophilic using light of the appropriate wavelength.[13-17]

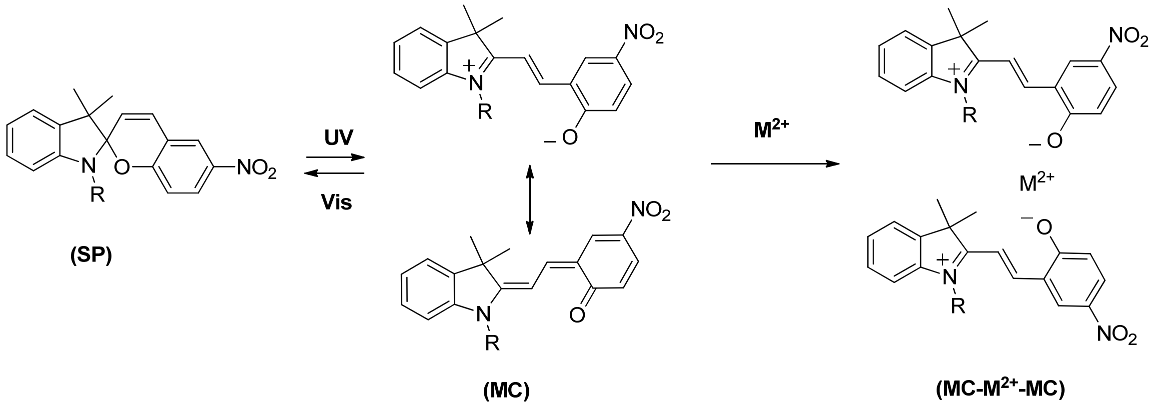

Figure 2.1. Isomeric structures of spiropyran (SP) and two canonical forms of merocyanine (MC). The dimeric complex of MC with metal ions is also shown.

The ring-opened merocyanine (MC) form exists as a resonance hybrid between two canonical forms: the charged zwitterion and a neutral quinoidal structure (Figure 2.1). It has been known for some time that the merocyanine (MC) zwitterion can bind metal ions through complexation with the phenolate anion.[11, 18, 19] This interaction is weak enough to allow dissociation of the ion and ring-closing to occur upon irradiation with visible light, which provides a system capable of reversible binding.

In this work, we have synthesized polymer brushes containing spiropyran moieties using atom transfer radical polymerization (ATRP) and free radical polymerization. Through a grafting-from approach, the number of functional groups present at a surface can be greatly enhanced through the three-dimensional arrangement of tethered polymer chains. This allows for a brush-like morphology, with extended chain conformations and high density of molecules in a limited area.[20] The increased functionality can also be used to amplify the stimuli responsive nature of the polymer coating at a surface. These brushes were used as reversible, photoswitchable optical sensors that show selectivity for different metal ions. Different metal complexation was also used to create surfaces with drastic changes in wettability. Covalently bound polymer chains allow for an increase in sensor stability, impart a rapid response to analyte, and provide reversible, switchable sensor surfaces with longer lifetimes.

Experimental Section

Materials

Silicon wafers, purchased from Silicon Quest, and BK7 microscope slides (RI = 1.514), purchased from VWR, were cut into 2 x 1 cm pieces and used as substrates for polymerization. All metal salts were purchased from either TCI or Alfa Aesar and used as received. 4-dimethylamino pyridine (DMAP), N-N'-dicyclohexylcarbodiimide (DCC), and allyl alcohol were purchased from either TCI or Alfa Aesar and used as received. Ethanol, toluene, and N, N-dimethylformamide (DMF) were purchased from

EMD and used as received. Methyl methacrylate (MMA), purchased from Alfa Aesar, and tert-butyl acrylate (tBA), purchased from TCI, were passed through a column of basic alumina to remove inhibitor and degassed before polymerization. Acrylic acid (AA) was purchased from TCI and passed through a plug of neutral alumina to remove inhibitor and degassed prior to polymerization. 2, 2, 2-trifluoroethyl methacrylate (TFEMA) and 4, 4'-azobis(4-cyanovaleric acid) were purchased from Sigma Aldrich and used as received. Tetrahydrofuran (THF), purchased from BDH, was distilled from sodium ketyl. Methylene chloride, purchased from EMD, was distilled from calcium hydride. N, N, N', N'', N''-pentamethyldiethylenetriamine (PMDETA), and ethyl-2-bromoisobutyrate (Et2BriB) were purchased from either TCI or Alfa Aesar and degassed prior to polymerization.

Initiator Synthesis and Monolayer Self-Assembly for ATRP

10-undecen-1-yl-2-bromo-2-methylpropionate and (11-(2-bromo-2-methyl)propionyloxy)undecyltrichlorosilane were synthesized according to published procedure.[1] Silicon wafers were sonicated in acetone, ethanol, and 18.2 MΩ deionized water for 5 minutes each. The wafers were then dried in a nitrogen stream and oxidized in a UV/ozone chamber for 5 minutes. The substrates were then transferred to a glove box and placed into a 3 mM solution of the synthesized trichlorosilane initiator and degassed toluene. The samples stood in this solution of 16 hours, after which they were rinsed with toluene and dried under a stream of nitrogen. When not in use, they were stored in toluene.

Initiator Synthesis for Free Radical Polymerization

Cyanovaleric acid (3.0 g, 11 mmol), allyl alcohol (1.28 g, 22 mmol) and 4-dimethylamino pyridine (DMAP) (0.27 g, 1.29 mmol) were dissolved in 20 mL of anhydrous methylene chloride. The solution stirred for 10 min and was then cooled to 0 °C with an ice bath. N-N'-dicyclohexylcarbodiimide (DCC) (2.96 g, 24.2 mmol) was dissolved in an additional 5 mL of methylene chloride and was added dropwise to the reaction mixture. The solution was left to stir overnight. For workup, the precipitate was filtered and the solvent removed via rotary evaporation. Methylene chloride was added and extracted with sodium bicarbonate and water. The organic layer was dried with $MgSO_4$, filtered, and solvent removed by rotary evaporation. Yield: 1.0 g (25%).

The resulting product (2.16 mmol) was added to 25 mL of anhydrous methylene chloride. Trichlorosilane (2.93 g, 21.6 mmol) was then added. About 5 mg of $PtCl_6 \bullet 6H_2O$ was added, and the solution was then left to stir overnight. For workup, the methylene chloride and excess trichlorosilane were removed by high vacuum. The resulting yellow oil was used without further purification.

Monolayer Self-Assembly for Free Radical Polymerization

Silicon wafers were sonicated in acetone, ethanol, and 18.2 MΩ deionized water for 5 minutes each. The wafers were then dried in a nitrogen stream and oxidized in a UV/ozone chamber for 5 minutes. The substrates were then transferred to a glove box and placed into a 3 mM solution of the synthesized trichlorosilane initiator and degassed toluene. The samples stood in this solution of 16 hours, after which they were rinsed with toluene and dried under a stream of nitrogen. When not in use, they were stored in toluene.

Monomer Synthesis

$1^{/}$-(2-Hydroxyethyl)-$3^{/}$-dimethyl-6-nitrospiro(2H-1-benzopyran-2,$2^{/}$-indole) (SP alcohol)[2] was subsequently coupled to methacrylic acid following standard procedures to synthesize spiropyran methacrylate (SPMA).[3]

Synthesis of Poly(MMA_{90}-co-$SPMA_{10}$)

SPMA (0.381 g, 0.906 mmol), MMA (0.816 g, 8.15 mmol), and CuBr (0.005 g, 0.035 mmol) were added to a dry, 25 mL schlenk flask containing the substrate with covalently attached initiator for ATRP. Anhydrous THF (5 mL) was then added, and the solution was degassed under Ar for 1 h. After degassing, PMDETA (0.060 g, 0.346 mmol), which was also degassed under Ar for 1 h, was added to the reaction mixture. The rubber septum on the schlenk flask was then replaced with a glass stopper while still under Ar to avoid any possible oxygen poisoning. The reaction was placed in an oil bath for 16 h at 65 ºC. The flask was then opened and exposed to air. Upon removal from the solution, the samples were immediately washed thoroughly with THF and DMF. The samples were stored in the dark when not in use.

Synthesis of Poly(MMA_{80}-co-$SPMA_{20}$)

SPMA (0.381 g, 0.906 mmol), MMA (0.363 g, 3.63 mmol), and CuBr (0.005 g, 0.035 mmol) were added to a dry, 25 mL schlenk flask containing the substrate with covalently attached initiator for ATRP. Anhydrous THF (5 mL) was then added, and the solution was degassed under Ar for 1 h. After degassing, PMDETA (0.060 g, 0.346 mmol), which was also degassed under Ar for 1 h, was added to the reaction mixture. The rubber septum on the schlenk flask was then replaced with a glass stopper while still under Ar to avoid any possible oxygen poisoning. The reaction was placed in an oil bath for 16 h at 65 ºC. The flask was then opened and exposed to air. Upon removal from the solution, the samples were immediately washed thoroughly with THF and DMF. The samples were stored in the dark when not in use.

Synthesis of Poly(MMA$_{75}$-co-SPMA$_{25}$)

SPMA (0.381 g, 0.906 mmol), MMA (0.272 g, 2.72 mmol), and CuBr (0.005 g, 0.035 mmol) were added to a dry, 25 mL schlenk flask containing the substrate with covalently attached initiator for ATRP. Anhydrous THF (5 mL) was then added, and the solution was degassed under Ar for 1 h. After degassing, PMDETA (0.060 g, 0.346 mmol), which was also degassed under Ar for 1 h, was added to the reaction mixture. The rubber septum on the schlenk flask was then replaced with a glass stopper while still under Ar to avoid any possible oxygen poisoning. The reaction was placed in an oil bath for 16 h at 65 ºC. The flask was then opened and exposed to air. Upon removal from the solution, the samples were immediately washed thoroughly with THF and DMF. The samples were stored in the dark when not in use.

Synthesis of Poly(tBA$_{92}$-co-SPMA$_{8}$)

SPMA (0.381 g, 0.906 mmol), tBA (1.41 g, 11.00 mmol), and CuBr (0.005 g, 0.035 mmol) were added to a dry, 25 mL schlenk flask containing the substrate with covalently attached initiator for ATRP. Anhydrous THF (5 mL) was then added, and the solution was degassed under Ar for 1 h. After degassing, PMDETA (0.060 g, 0.346 mmol), which was also degassed under Ar for 1 h, was added to the reaction mixture. The rubber septum on the schlenk flask was then replaced with a glass stopper while still under Ar to avoid any possible oxygen poisoning. The reaction was placed in an oil bath for 16 h at 65 ºC. The flask was then opened and exposed to air. Upon removal from the solution, the samples were immediately washed thoroughly with THF and DMF. The samples were stored in the dark when not in use.

Synthesis of Poly(tBA$_{85}$-co-SPMA$_{15}$)

SPMA (0.381 g, 0.906 mmol), tBA (0.629 g, 4.91 mmol), and CuBr (0.005 g, 0.035 mmol) were added to a dry, 25 mL schlenk flask containing the substrate with covalently attached initiator for ATRP. Anhydrous THF (5 mL) was then added, and the solution was degassed under Ar for 1 h. After degassing, PMDETA (0.060 g, 0.346 mmol), which was also degassed under Ar for 1 h, was added to the reaction mixture. The rubber septum on the schlenk flask was then replaced with a glass stopper while still under Ar to avoid any possible oxygen poisoning. The reaction was placed in an oil bath for 16 h at 65 ºC. The flask was then opened and exposed to air. Upon removal from the solution, the samples were immediately washed thoroughly with THF and DMF. The samples were stored in the dark when not in use.

Synthesis of Poly(tBA$_{80}$-co-SPMA$_{20}$)

SPMA (0.381 g, 0.906 mmol), tBA (0.472 g, 3.68 mmol), and CuBr (0.005 g, 0.035 mmol) were added to a dry, 25 mL schlenk flask containing the substrate with covalently attached initiator for ATRP. Anhydrous THF (5 mL) was then added, and the solution was degassed under Ar for 1 h. After degassing, PMDETA (0.060 g, 0.346 mmol), which was also degassed under Ar for 1 h, was added to the reaction mixture. The rubber septum on the schlenk flask was then replaced with a glass stopper while still under Ar to avoid any possible oxygen poisoning. The reaction was placed in an oil bath for 16 h at 65 ºC. The flask was then opened and exposed to air. Upon removal from the solution, the samples were immediately washed thoroughly with THF and DMF. The samples were stored in the dark when not in use.

Synthesis of Poly(AA$_{90}$-co-SPMA$_{10}$)

SPMA (0.381 g, 0.906 mmol) and AA (0.588 g, 8.16 mmol) were added to a dry, 25 mL schlenk flask containing the substrate with covalently attached initiator for free radical polymerization. Anhydrous THF (5 mL) was then added, and the solution was degassed under Ar for 1 h. The rubber septum on the schlenk flask was then replaced with a glass stopper while still under Ar to avoid any possible oxygen poisoning. The reaction was placed in an oil bath for 16 h at 65 ºC. The flask was then opened and exposed to air. Upon removal from the solution, the samples were immediately washed thoroughly with THF and DMF. The samples were stored in the dark when not in use.

Synthesis of Poly(TFEMA$_{90}$-co-SPMA$_{10}$)

SPMA (0.381 g, 0.906 mmol) and TFEMA (1.37 g, 8.16 mmol) were added to a dry, 25 mL schlenk flask containing the substrate with covalently attached initiator for free radical polymerization. Anhydrous THF (5 mL) was then added, and the solution was degassed under Ar for 1 h. The rubber septum on the schlenk flask was then replaced with a glass stopper while still under Ar to avoid any possible oxygen poisoning. The reaction was placed in an oil bath for 16 h at 65 ºC. The flask was then opened and exposed to air. Upon removal from the solution, the samples were immediately washed thoroughly with THF and DMF. The samples were stored in the dark when not in use.

Synthesis of Poly(TFEMA$_{80}$-co-SPMA$_{20}$)

SPMA (0.381 g, 0.906 mmol) and TFEMA (0.609 g, 3.62 mmol) were added to a dry, 25 mL schlenk flask containing the substrate with covalently attached initiator for free radical polymerization. Anhydrous THF (5 mL) was then added, and the solution was degassed under Ar for 1 h. The rubber septum on the schlenk flask was then replaced with a glass stopper while still under Ar to avoid any possible oxygen poisoning. The reaction was placed in an oil bath for 16 h at 65 ºC. The flask was then opened and exposed to air. Upon removal from the solution, the samples were immediately washed thoroughly with THF and DMF. The samples were stored in the dark when not in use.

Synthesis of Poly(SPMA)

SPMA (1.47 g, 3.49 mmol) and CuBr (0.005 g, 0.035 mmol), were added to a dry, 25 mL schlenk flask containing the substrate with covalently attached initiator for ATRP. Anhydrous THF was then added, and the solution was degassed under Ar for 1 h. After degassing, PMDETA (0.060 g, 0.346 mmol), which was also degassed under Ar for 1 h, was added to the reaction mixture. The rubber septum on the schlenk flask was then replaced with a glass stopper while still under Ar to avoid any possible oxygen poisoning. The reaction was then placed in a 65 ºC oil bath for 16 h. The flask was then opened and exposed to air. Upon removal from the solution, the samples were immediately washed thoroughly with THF and DMF. The samples were stored in the dark when not in use.

Measurements

Null ellipsometry was performed on a Multiskop (Optrel GbR) with a 638.2 nm He-Ne laser. Both δ and ψ value thickness data were measured and calculated by integrated specialized software. At least three measurements were taken for each wafer and the average thickness recorded. This same Multiskop was used to measure water contact angles by using a white light source and replacing the photodiode with a CCD camera. A contour tracing algorithm that distinguishes the drop from its mirror image was used to evaluate the contour of the drop and fit it to the Young-Laplace equation. At least three drops were measured and the average of these measurements reported. UV-vis spectra of the polymer films were obtained using a Shimadzu UV-1700 spectrophotometer using UV Probe software (version 2.21).

Light Source

An OmniCure, series 1000 with 365 nm wavelength light, was used as the UV light source. The substrates were held 2 cm from the source and irradiated at a power of 30 mW/cm^2. The visible light source was a Fiber-Lite Model with a 30 W quartz halogen fiber optic illuminator.

Merocyanine-Metal Ion Complexation Experiments

An initial UV-vis spectrum was recorded of the polymer brush before UV irradiation. The sample was then irradiated with 365 nm light for 2 minutes and a UV-vis spectrum was recorded. The sample was then immersed in a 25 mM solution of metal salt in ethanol for 3 minutes, blown dry with air for 15 seconds, and a UV-vis spectrum recorded. To reverse the complexation, the sample was washed with ethanol and then irradiated with white light for 10 minutes while immersed in toluene.

Water Contact Angle Experiments

Contact angle measurements were taken on the sample before irradiating with UV light. The sample was then irradiated with 365 nm light while immersed in a 10 mM solution of metal salt and ethanol for 2 minutes. The sample was blown dry with air and contact angle measurements were taken. To show reversibility, the sample was irradiated for 10 minutes with visible light while immersed in toluene. For samples irradiated in

DMF, the same procedure was followed with the exception that the sample was irradiated with UV light while immersed in DMF instead of the metal salt solution.

Results and Discussion

Synthesis of Polymer Brushes

Under similar conditions as reported by Piech and Bell,[21, 22] we attempted to copolymerize SPMA with either methyl methacrylate (MMA) or tert-butyl acrylate (tBA) in varying ratios using atom transfer radical polymerization, and thicknesses up to 60 nm were possible under controlled conditions with high graft density. The copolymerization of SPMA with MMA is shown in Figure 2.2. When homopolymerization was attempted, no brushes with a thickness larger than 4 nm were possible under different catalyst/ligand/solvent combinations, presumably due to the steric bulk of the SPMA monomer. We also copolymerized SPMA with either acrylic acid (AA) or 2, 2, 2-trifluoroethyl methacrylate (TFEMA) in varying ratios using free radical polymerization. The final film thickness decreased with increasing mol% of SPMA regardless of the copolymer in the brush. Table 2.1 summarizes the results. Overall, brush thicknesses were much larger with MMA as the copolymer, and for sensing experiments, the MMA-SPMA copolymer brushes were used.

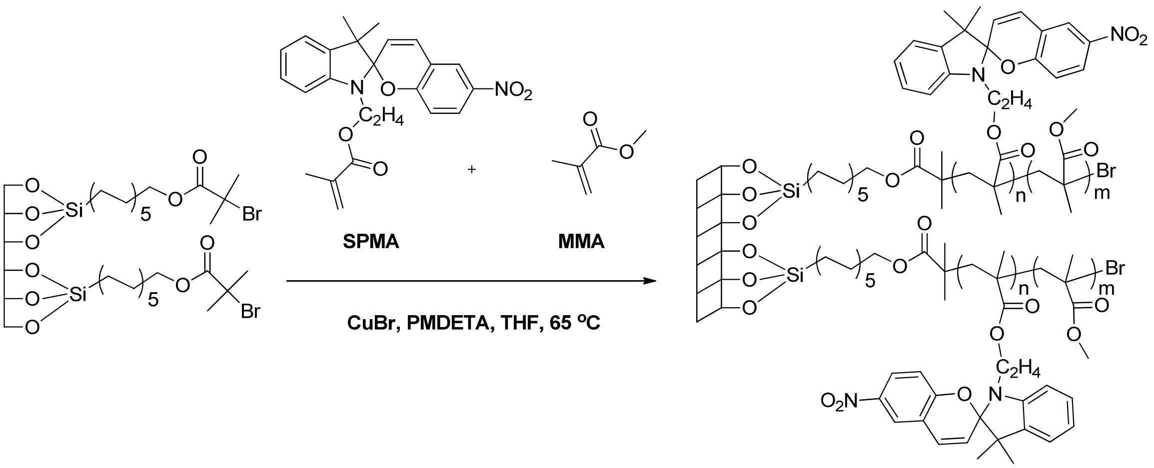

Figure 2.2. Surface-initiated copolymerization of a spiropyran methacrylate derivative (SPMA) and methyl methacrylate (MMA).

Table 2.1. Concentration of spiropyran in copolymerization with MMA, tBA, TFEMA, or AA and the resulting brush thicknesses.

Polymer	Content of SPMA in monomer feed (mol %)	Brush Thickness (nm)
Poly(MMA$_{90}$-*co*-SPMA$_{10}$)	10	60 ± 1.9
Poly(MMA$_{80}$-*co*-SPMA$_{20}$)	20	28 ± 1.1
Poly(MMA$_{75}$-co-SPMA$_{25}$)	25	22 ± 1.7
Poly(tBA$_{92}$-*co*-SPMA$_{8}$)	8	17 ± 0.5
Poly(tBA$_{85}$-*co*-SPMA$_{15}$)	15	12 ± 1.0
Poly(tBA$_{80}$-*co*-SPMA$_{20}$)	20	9 ± 0.6
Poly(TFEMA$_{90}$-*co*-SPMA$_{10}$)	10	21 ± 2.1
Poly(TFEMA$_{80}$-*co*-SPMA$_{20}$)	20	9 ± 0.3
Poly(AA$_{90}$-*co*-SPMA$_{10}$)	10	28 ± 2.0
Poly(SPMA)	100	4 ± 0.8

Photochromism of SP-Containing Polymer Brushes

The optical switching of the spiropyran moiety has been studied extensively, and its photochromic reaction between the ring-closed spiropyran (SP) and the ring-opened merocyanine (MC) is depicted in Figure 2.3. Upon UV irradiation, the neutral, colorless SP undergoes reversible photocleavage of the spiro C-O bond to form the polar, highly colored MC. The reverse process is facilitated by visible light or heat. This reaction is accompanied by characteristic changes in the UV-vis absorption spectra, which strongly depend on the microenvironment surrounding the

SP moiety. In this respect, UV-vis spectroscopy was used to characterize the photoinduced conversion of SP to MC in the SP-containing copolymer brushes, copolymerized with MMA, AA, or TFEMA. Figures 2.3a-c show the absorbance spectra of a 60 nm thick polymer brush of poly(MMA_{90}-*co*-$SPMA_{10}$), a 28 nm thick polymer brush of poly(AA_{90}-*co*-$SPMA_{10}$), and a 21 nm thick polymer brush of poly($TFEMA_{90}$-*co*-$SPMA_{10}$) with different UV exposure times, respectively. In all three brushes, the concentration of the ring-opened MC form increases with increasing UV exposure time and reaches a maxima, which is the photostationary state. The photoinduced conversion is also reversible for all three polymer brushes. When irradiated in toluene, a better solvent for the non-polar SP form, the reverse reaction occurs in minutes. For poly(MMA_{90}-*co*-$SPMA_{10}$) (Figure 2.3a), the colorless SP form has no characteristic absorbance (0 s UV exposure) in the visible region, whereas the zwitterionic, ring-opened MC form displays an intense absorbance band centered at λ_{max} = 584 nm, with a second band around 374 nm. The main peak at 584 nm can be ascribed to the ring-opened MC in the all-trans form around the double bond.[23, 24]

For poly(AA_{90}-*co*-$SPMA_{10}$), the MC is characterized by a significant hyspochromic shift (blue) in λ_{max} (557 nm) (Figure 2.3b) relative to the poly(MMA_{90}-*co*-$SPMA_{10}$) brush, which is indicative of a more polar microenvironment.[25] Careful scrutiny of the UV-vis absorbance spectra of the poly($TFEMA_{90}$-*co*-$SPMA_{10}$) brush (Figure 2.3c) indicates that the MC band is characterized by a red shift in absorbance maxima (λ_{max} = 590 nm) relative to the poly(MMA_{90}-*co*-$SPMA_{10}$) brush, with a small shoulder around 565 nm. Upon increasing the concentration of SPMA in the polymer backbone, this shoulder becomes much more visible. Figure 2.4 shows the poly(TFEMA$_{80}$-*co*-SPMA$_{20}$) brush with the MC band characterized by a bathsochromic shift in λ_{max} (590 nm) and a shoulder near 560 nm. This shoulder is most likely due to the formation of H-aggregates, characterized by antiparallel alignment of alternate MC dipoles.[26, 27] Presumably, these H-aggregates are seen more prominently in the 20 mol% SPMA copolymer brush because there are more SP moieties that can interact with each other and align in some fashion.

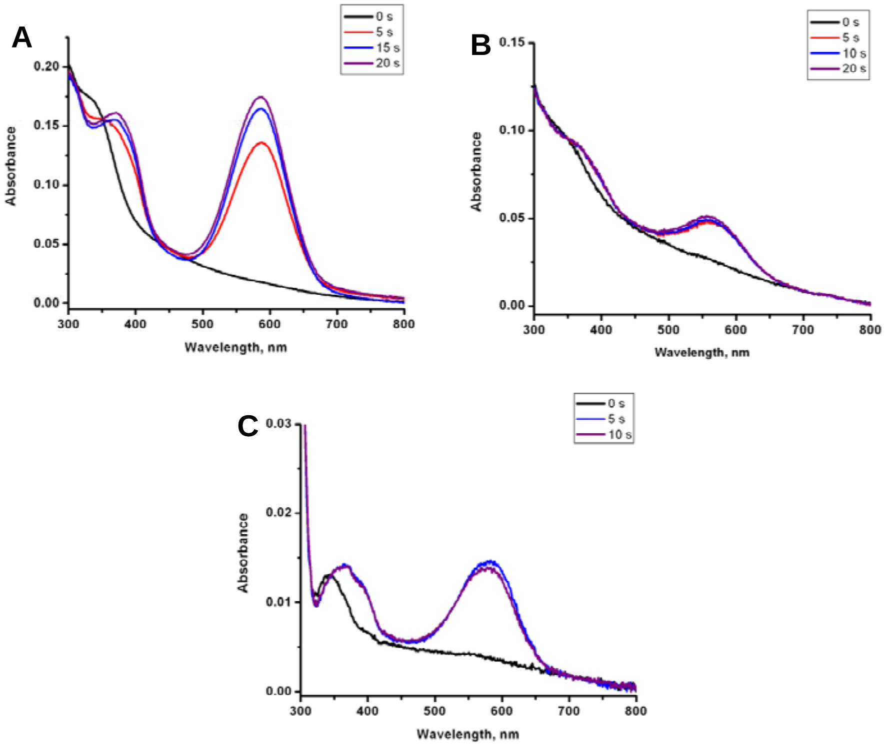

Figure 2.3. Change in UV-vis absorbance spectra of (a) poly(MMA$_{90}$-*co*-SPMA$_{10}$), (b) poly(AA$_{90}$-*co*-SPMA$_{10}$), and (c) poly(TFEMA$_{90}$-*co*-SPMA$_{10}$) with different UV exposure times.

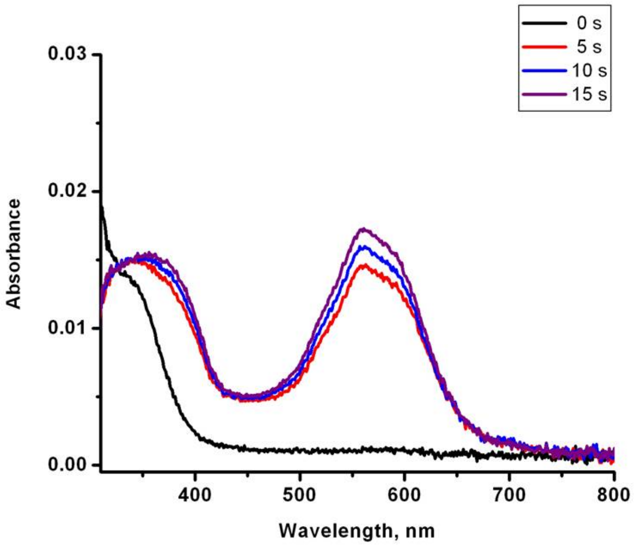

Figure 2.4. Change in UV-vis absorbance spectra of poly(TFEMA$_{80}$-*co*-SPMA$_{20}$) with different UV exposure times.

Light-Induced Contact Angle Changes

The photoinduced geometry change between the ring-closed SP and the ring-opened MC is accompanied by a large change in dipole moment, which if confined to a surface, can affect the surface free energy. This change in surface free energy can give rise to a switching of wettability. We measured the reversible changes in surface free energy of copolymer brushes using water contact angle experiments. In a typical experiment, the contact angle of the SP-containing copolymer brush was measured prior to UV irradiation. The brush was then irradiated with UV light for one minute while immersed in DMF; after which, the substrate was removed from the solution, blown dry with a stream of nitrogen, and contact angle measurements taken again. Contact angle measurements before and after UV irradiation for each of the copolymer brushes are shown in Table 2.2. Figure 2.5a shows representative images of water droplets wetting the polymer brush surface before and after UV irradiation in DMF (poly(MMA_{90}-*co*-$SPMA_{10}$) is shown). After irradiation with 365 nm light, the surface energy increases, resulting in a decrease of water contact angle. This change in contact angle was completely reversible when the substrates were irradiated with visble light in non-polar solvents. The contact angle change accompanying UV irradiation decreased with increasing concentration of SPMA, presumably due to the steric bulk of SP. As the concentration of SP is increased in the polymer backbone, it becomes more sterically hindered and has less free volume to spatially rearrange into the zwitterionic MC form.

Contact angle measurements were also taken before and after UV irradiation in DMF for the poly(AA_{90}-*co*-$SPMA_{10}$) brush and both of the TFEMA-SPMA copolymer brushes. With acrylic acid as the copolymer, the microenvironment is much more hydrophillic and the contact angle before UV irradiation is only 78°. After irradiation with UV light in DMF, the contact angle decreased to 62°, yielding a 17° change. Interestingly, with poly($TFEMA_{90}$-*co*-$SPMA_{10}$), there is no contact angle change upon UV irradiation. As the concentration is increased to 20 mol% SPMA, the contact angle change increased to 10°. This change is comparable to the 20 mol% SPMA copolymerized with 80 mol% MMA. Overall, a copolymer of 90 mol% MMA and 10 mol% SPMA yielded the largest contact angle changes, and as such, was the only copolymer used for further experiments.

Table 2.2. Equilibrium water contact angle measurements of polymer brushes before and after UV irradiation.

Polymer Brush	CA before UV irradiation	CA after UV irradiation	CA change
Poly(MMA_{90}-*co*-$SPMA_{10}$)	104°	85°	19°
Poly(MMA_{80}-*co*-$SPMA_{20}$)	96°	81°	15°
Poly(MMA_{75}-*co*-$SPMA_{25}$)	93°	85°	8°
Poly($TFEMA_{90}$-*co*-$SPMA_{10}$)	98°	98°	0°
Poly($TFEMA_{80}$-*co*-$SPMA_{20}$)	98°	88°	10°
Poly(AA_{90}-*co*-$SPMA_{10}$)	79°	62°	17°

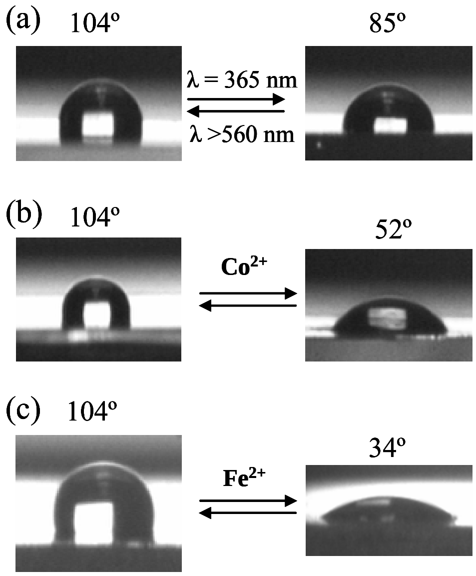

Figure 2.5. Reversible contact angle changes of poly(MMA_{90}-*co*-$SPMA_{10}$) brushes irradiated in (a) DMF, (b) 10 mM $CoCl_2$, and (c) 10 mM $FeCl_2$.

It is known that the zwitterionic MC can complex to metal ions through the negatively charged phenolate group (Figure 2.1). Byrne showed that Co^{2+} can complex with the MC form, and this complexation/decomplexation process is reversible.[10] The open merocyanine form exists as a resonance hybrid between two canonical forms: the charged, zwitterion and the neutral quinoidal structure (Figure 2.1). It is expected that the Co^{2+}/phenolate anion interaction can stabilize the zwitterionic form through complexation. Further, this interaction is weak enough to allow for the reverse, ring-closing to occur. We investigated the wettability change of a poly(MMA_{90}-*co*-$SPMA_{10}$) brush by irradiation in the presence of different divalent metal ions as a way to enhance the hydrophilic nature of the surface. A freshly prepared poly(MMA_{90}-*co*-$SPMA_{10}$) brush was immersed in a 10 mM ethanolic solution of a metal chloride and irradiated for two minutes. Figures 2.5b and c show the reversible switching of wettability changes of a droplet of water before and after irradiating with UV light while immersed in a $CoCl_2$ or $FeCl_2$ solution, respectively. Static contact angle changes as large as 70° are observed when the films are irradiated in the presence of different divalent metal ions. Table 2.3 summarizes the contact angle changes when the film is complexed to the different metal ions. Interestingly, each metal ion gives a unique contact angle change when complexed to MC, with Ni^{2+} yielding the smallest change of 50° and Fe^{2+} yielding the largest change of 70°. The change in contact angle was completely reversible when the substrates were irradiated with visible light in nonpolar solvents. The reversibility is shown in Figure 2.6, where several cycles of contact angle changes for UV and visible irradiation are shown with the polymer brush complexed to Fe^{2+}. These are the largest reversible contact angles reported for flat surfaces based on organic chromophores.

Table 2.3. Water contact angle changes of poly(MMA_{90}-*co*-$SPMA_{10}$) brushes when irradiated in the presence of divalent metal ions.

Metal Ion	CA Change
Fe^{2+}	70°
Cu^{2+}	66°
Zn^{2+}	59°
Co^{2+}	52°
Ni^{2+}	50°

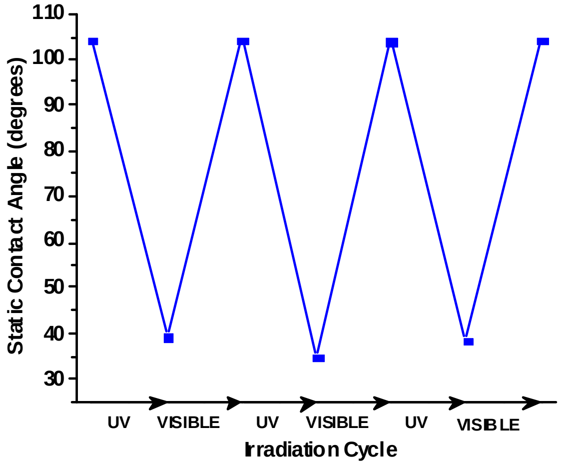

Figure 2.6. Plot of reversible contact angle changes for a poly(MMA_{90}-*co*-$SPMA_{10}$) film when irradiated in a 10 mM ethanolic solution of $FeCl_2$.

Metal Ion Complexation

The spiropyran-merocyanine optical switch is also of interest as a potential candidate for optical sensing of metal ions.[9] For sensing experiments, the films were irradiated with 365 nm light (30 mW/cm^2) in the solid state for one minute, submerged into a metal salt solution (25 mM in ethanol) for two minutes, and blown dry with air for 15 seconds. Chloride salts of each metal were used. To decomplex the metal, the films were irradiated in toluene for 10 min with visible light (30 W quartz halogen fiber optic illuminator, 2 cm from the source).

Figure 2.7 shows the UV-vis absorbance spectra of the surface-initiated SPMA copolymers in response to different metal ions. The thickness of the films used for metal ion sensing was set at 25 nm (16 hr polymerization time). As can be seen from Figure 2.7, the as-synthesized SPMA copolymer brush is transparent to the visible, with an absorption tail below 400 nm. When irradiated with UV light, the SP chromophores are converted to the MC form, which is characterized by an intense absorption band centered at 584 nm and a second band at approximately 374 nm. Upon complexation with different metal ions, there is a decrease in absorbance along with a significant blue shift in absorbance maxima, which is metal ion dependent. With Zn^{2+}, Co^{2+}, and Ni^{2+}, the spectral response is similar, with a decrease in the long wavelength absorption band at 584 nm, along with a significant hypsochromic shift in absorbance maxima. Nickel(II) yields the smallest blue shift of only 25 nm (λ_{max} = 559 nm), while Co^{2+} and Zn^{2+} give hyspochromic shifts of 53 nm (λ_{max} = 531 nm) and 91 nm (λ_{max} = 493 nm), respectively. With Cu^{2+}, the long wavelength absorption band splits with two partially overlapping absorbances at 513 nm and 420 nm, and in the case of Fe^{2+}, the long wavelength absorption band broadens with a shoulder observed at 550 nm and 440 nm.

Interestingly, the blue shift in absorbance maxima for the SPMA copolymer brushes complexed with each metal ion correlates with the amount of static contact angle change of the polymer brush in the presence of the different ions. Copper(II) and Fe^{2+} yield the largest blue shift in absorbance maxima and give the largest contact angle change upon irradiation with UV light, while Co^{2+} and Ni^{2+} yield the smallest blue shift in λ_{max} and the smallest contact angle changes. Due to such large changes in the spectral response for each metal ion, the ion selectivity can easily be discriminated with the naked eye for most metal ions, as shown in the polymer coated glass substrates in Figure 2.8. For better color contrast, the substrates were spin-coated films (80 nm) of the same polymer synthesized in solution. There was no difference in the UV-vis spectrum between polymer/metal complexes of the spin-coated film and polymer brush, except that the films would delaminate upon rinsing with toluene.

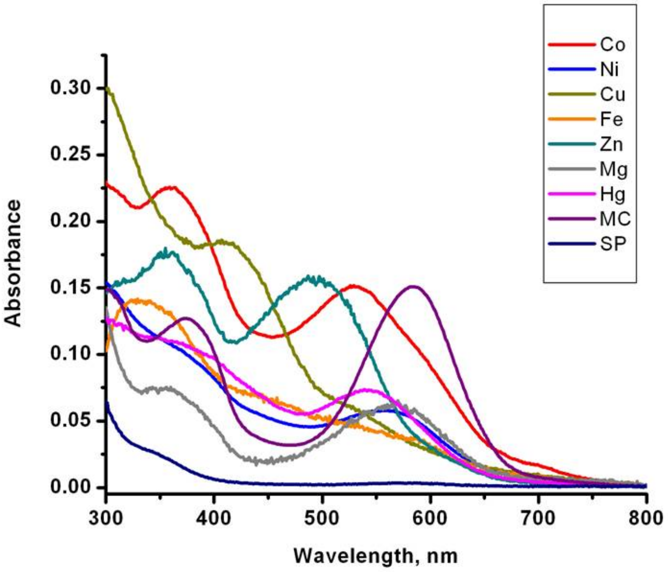

Figure 2.7. UV-vis absorbance spectra of the poly(MMA$_{90}$-*co*-SPMA$_{10}$) brush in the presence of different divalent metal ions.

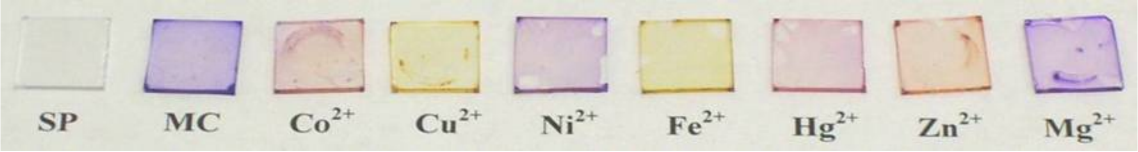

Figure 2.8. Polymer coated glass substrates after UV irradiation and complexation with different divalent metal ions. For better color contrast, the substrates were spin-coated films (80 nm) of the same polymer synthesized in solution.

The SPMA/metal complex is stable, even under irradiaton in visible light for several hours in the solid state. The metal decomplexation reaction is reversible when the films are irradiated with visible light in nonpolar solvents. Using toluene, the reverse reaction occurs in minutes. The colorimetric response of the films is identical after repeating several cycles of complexation/decomplexation.

The MC absorbance band of the polymer is much more sensitive than free monomer in the presence of the different ions due to the confined microenvironment of the pendant chromophores present in the film. The free monomer in solution does bind to each metal ion in a 2:1 merocyanine-metal ion complex (Figure 2.9), but the shift in absorbance maximum is not sensitive for metal ions other than Fe^{2+} and Cu^{2+}. We are currently investigating the influence of different microenvironments by fabricating copolymer brushes of methacrylates with differing steric bulk.

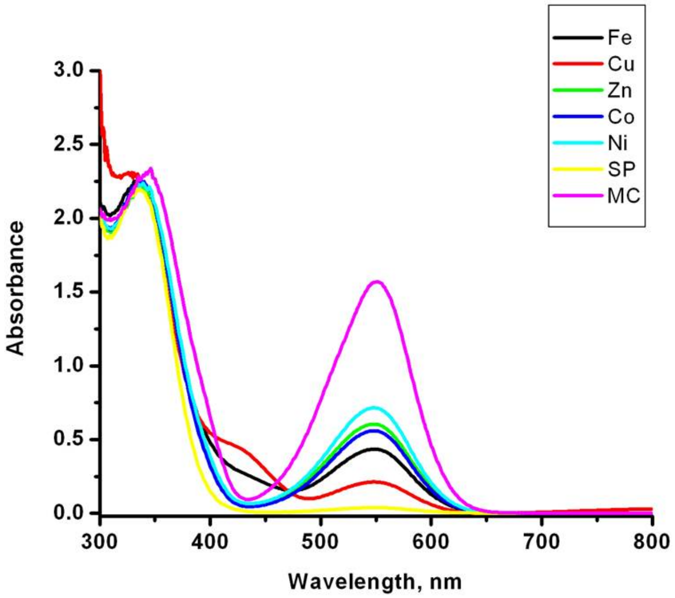

Figure 2.9. UV-vis absorbance spectra of SPMA monomer bound to metal ions in a 2:1 MC-M^{2+} complex.

Conclusions

In summary, we have developed a reversible ion sensor based on spiropyran-containing copolymer brushes. The confined microenvironment provides a colorimetric response that is sensitive and selective for different metal ion complexation. The sensor response to different chemical microenvironments, detection limits, and fluorescence sensitivity are currenlty under investigation in our laboratory. The metal ion complexation was also used to create surfaces with drastic changes in wettability. Reversible contact angle changes of up to 70° were observed for films grown from flat substrates, which can be amplified further by growing polymers from rough surfaces. Polymer brushes grown from surface bound initiators allow for an increase in sensor stability and high chromophore density, impart a rapid response to analyte, and provide reversible, switchable sensor surfaces with longer lifetimes.

References

1. Bühlmann, P., E. Pretsch and E. Bakker, *Chem. Rev.*, **1998**. *98*(4): p. 1593.
2. Nolan, E.M. and S.J. Lippard, *Chem. Rev.*, **2008**. *108*(9): p. 3443.
3. Prodi, L., F. Bolletta, M. Montalti and N. Zaccheroni, *Coord. Chem. Rev.*, **2000**. *205*(1): p. 59.
4. Zhang, X.-B., C.-C. Guo, Z.-Z. Li, G.-L. Shen and R.-Q. Yu, *Anal. Chem.*, **2002**. *74*(4): p. 821.
5. Oehme, I., S. Prattes, O.S. Wolfbeis and G.J. Mohr, *Talanta*, **1998**. *47*(3): p. 595.
6. Plaschke, M., R. Czolk and H.J. Ache, *Anal. Chim. Acta*, **1995**. *304*(1): p. 107.
7. Rosatzin, T., P. Holy, K. Seiler, B. Rusterholz and W. Simon, *Anal. Chem.*, **1992**. *64*(18): p. 2029.
8. Eggins, B.R., *Chemical Sensors and Biosensors*. 2002, West Sussex, UK: John Wiley and Sons Ltd.
9. Byrne, R. and D. Diamond, *Nat. Mater.*, **2006**. *5*(6): p. 421.
10. Byrne, R.J., S.E. Stitzel and D. Diamond, *J. Mater. Chem*, **2006**. *16*(14): p. 1332.
11. Hirshberg, Y., *J. Am. Chem. Soc.*, **1956**. *78*(10): p. 2304.
12. Saragi, T.P.I., T. Spehr, A. Siebert, T. Fuhrmann-Lieker and J. Salbeck, *Chem. Rev.*, **2007**. *107*(4): p. 1011.
13. Samanta, S. and J. Locklin, *Langmuir*, **2008**. *24*(17): p. 9558.
14. Rosario, R., D. Gust, M. Hayes, F. Jahnke, J. Springer and A.A. Garcia, *Langmuir*, **2002**. *18*(21): p. 8062.
15. Rosario, R., D. Gust, A.A. Garcia, M. Hayes, J.L. Taraci, T. Clement, J.W. Dailey and S.T. Picraux, *J. Phys. Chem. B*, **2004**. *108*(34): p. 12640.

16. Vlassiouk, I., C.-D. Park, S.A. Vail, D. Gust and S. Smirnov, *Nano Lett.*, **2006**. *6*(5): p. 1013.

17. Yang, D., M. Piech, N.S. Bell, D. Gust, S. Vail, A.A. Garcia, J. Schneider, C.-D. Park, M.A. Hayes and S.T. Picraux, *Langmuir*, **2007**. *23*(21): p. 10864.

18. Phillips, J.P., A. Mueller and F. Przystal, *J. Am. Chem. Soc.*, **1965**. *87*(17): p. 4020.

19. Evans, L., G.E. Collins, R.E. Shaffer, V. Michelet and J.D. Winkler, *Anal. Chem.*, **1999**. *71*(23): p. 5322.

20. R. C. Advincula, W.J.B., K. C. Caster and J. Rühe, *Polymer Brushes: Synthesis, Characterization, Applications*. 2004, Weinheim: Wiley-VCH.

21. Piech, M. and N.S. Bell, *Macromolecules*, **2006**. *39*(3): p. 915.

22. Bell, N.S. and M. Piech, *Langmuir*, **2006**. *22*(4): p. 1420.

23. Irie, M., T. Iwayanagi and Y. Taniguchi, *Macromolecules*, **1985**. *18*(12): p. 2418.

24. Kalisky, Y. and D.J. Williams, *Macromolecules*, **1984**. *17*(3): p. 292.

25. Rosario, R., D. Gust, M. Hayes, J. Springer and A.A. Garcia, *Langmuir*, **2003**. *19*(21): p. 8801.

26. Goldburt, E., F. Shvartsman, S. Fishman and V. Krongauz, *Macromolecules*, **1984**. *17*(6): p. 1225.

27. Goldburt, E. and V. Krongauz, *Macromolecules*, **1986**. *19*(1): p. 246.

CHAPTER 3

SPECTROSCOPIC ANALYSIS OF METAL ION BINDING IN SPIROPYRAN-CONTAINING COPOLYMER THIN FILMS[1]

---

[1] Fries, K. H.; Driskell, J. D.; Samanta, S.; and Locklin, J. *Analytical Chemistry*, **2010**, *82*, 3306-3314. Reprinted with permission from *Anal. Chem.* **2010**, *82*, 3306-3314. Copyright 2010 American Chemical Society.

Abstract

In this article, we describe the synthesis and characterization of a series of spiropyran-containing copolymers that were used as colorimetric sensors for a series of divalent metal ions. The composition of spiropyran contained in the polymer backbone was varied from 10-100 mol% to investigate the influence of free volume and sterics on the photochromic response. FT-IR spectroscopy was used to characterize the photoinduced conversion, as well as the merocyanine-metal ion (MC-M^{2+}) interaction. FT-IR spectra were analyzed using chemometric methods to elucidate the chemical binding environment between MC and M^{2+} and to selectively identify different metal ions bound to MC. By means of UV-vis absorption spectroscopy, we also demonstrate that each metal ion gives rise to a unique colorimetric response that is dependent upon the amount of spiropyran comonomer contained in the polymer backbone, and that by increasing the concentration of chromophore in the copolymer, the selectivity between different metal ions decreases. Using chemometric methods, UV-vis spectra can be analyzed to quantitatively identify metal ions in a concentration range from 1 μM to 100 mM.

Introduction

Chemical sensing has attracted a great deal of attention in recent years due to the increasing need for detection of clinically and environmentally relevant analytes, including small molecules and metal ions.[1, 2] Specifically, optical sensors such as optodes offer a wide variety of advantages over other sensing techniques.[3, 4] These systems are based primarily on solid phase immobilization matrices, where organic indicator dyes are adsorbed or encapsulated in a polymer matrix that is permeable to the analyte.[5-7] With these sensors, the analyte is not consumed, no reference is required, and there is minimal electrical or magnetic interference.[8-10] Optodes are amenable to miniaturization and also have the potential to be used in remote sensing applications.

With respect to metal ion sensing, the elegant synthetic design of appropriate receptor ligands leads to ion complex formation that is thermodynamically favorable, and the stability constant for the complex is typically quite large. These materials are quickly saturated, especially when a small amount of organic material indicator is adsorbed or encapsulated in a polymer matrix that is permeable to the analyte. This can be a drawback, and limits the approaches to quantitative ion determination, especially in situations where ion concentration can vary several orders of magnitude.[11] If the concentration of a given ion in solution is unknown, then multiple sensors with varying affinity for a specific ion are necessary.[5] There are several other disadvantages to using organic dyes immobilized in a polymer matrix. Reversibility is not possible because of the strong binding interactions between the analyte and the dye, and durability is often inadequate, leading to the indicator dye leaching out of the matrix.[12-14] Also, overtime, binding sites can become blocked, reducing sensor response. Other disadvantages include fouling of the surface, inaccessibility of the dye due to steric constraints,[15, 16] and the sensor is typically one time use. Reversible sensors that can switch between passive and active states have been proposed by Byrne and Diamond,[17] and would offer a solution to many of the problems that arise when using an organic indicator dye immobilized in a polymer matrix. Photochromic compounds that undergo reversible, light-induced structural changes provide a strategy to accomplish this goal.

Spiropyrans are a well known class of materials that undergo a reversible photocleavage of the spiro C-O bond, which allows switching between a ring-closed, colorless spiropyran (SP) form and a ring-opened, strongly colored merocyanine (MC) form.[18, 19] The merocyanine structure exists as a resonance hybrid between two forms: the charged zwitterion and a neutral quinoidal form. Metal ions can bind to the merocyanine through the negatively charged phenolate group of the zwitterionic form (Figure 3.1).[20, 21,22-25] This interaction, however, is weak enough that upon exposure to visible light, ring-closing can still occur, yielding a molecular system that is capable of reversible ion sensing. There have been a few reports of SP-MC binding to metal ions in solution and as a self-assembled monolayer on solid substrates.[23-26] In previous work, we have synthesized homopolymers and copolymers containing spiropyran moieties, using controlled surface-initiated polymerization techniques, that demonstrate reversible wettability changes of up to 70°.[27, 28] We also observed that these materials show distinctive, colorimetric responses for different metal ions and have great potential as metal ion sensors that can be photochemically switched between active and passive forms.[28]

In this work, we demonstrate thin films of a single photoresponsive copolymer that generate a unique and selective colorimetric response for different metal ions. The spectral responses of these ultrathin films are concentration dependent and allow for the direct quantification of ion concentration with high reproducibility. We have synthesized a series of copolymers containing spiropyran moieties with controlled molecular weight and low polydispersity using atom transfer radical polymerization (ATRP). The composition of spiropyran contained in the polymer backbone was varied from 10-100 mol% to investigate the influence of free volume and sterics on the photochromic response. Using a polymeric backbone, the stimuli responsive nature of the chromophore is not only amplified, but the microenvironment for merocyanine-divalent metal ion (MC-M^{2+}) sensing, and therefore the colorimetric response, can also be tuned by comonomer composition.

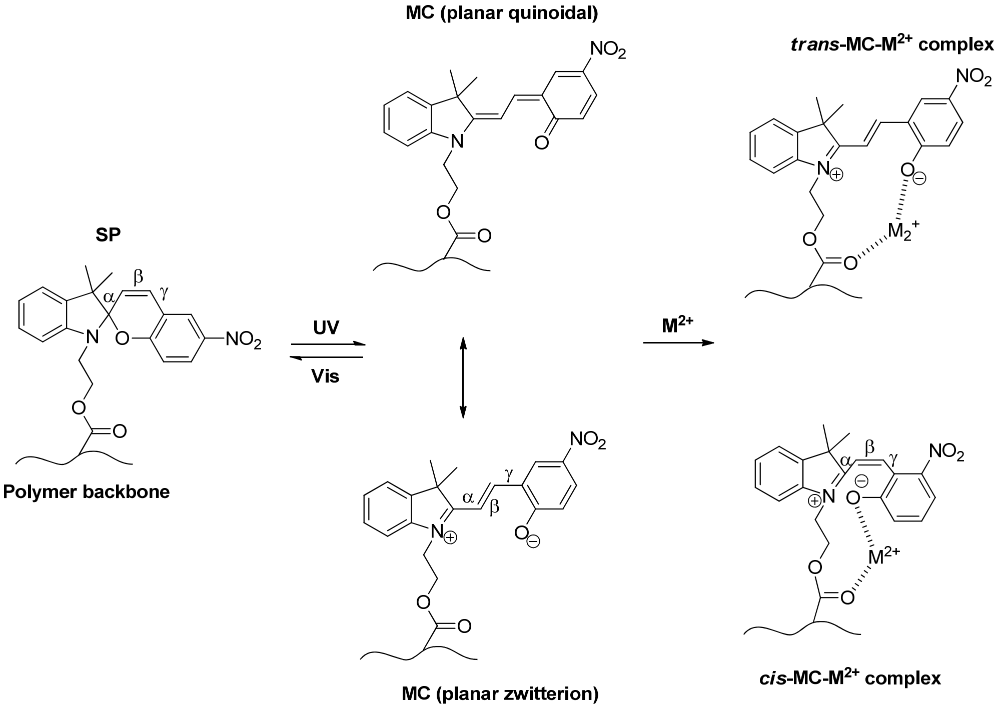

Figure 3.1. Isomeric structures of spiropyran and merocyanine and the MC-M^{2+} complex in *cis*/*trans* conformations.

Experimental Section

Materials

Silicon wafers (orientation <100>, native oxide) were purchased from University Wafer. BK7 microscope slides (RI = 1.514) were purchased from VWR. THF, purchased from BDH, was distilled from sodium-ketyl. Methyl methacrylate (MMA), purchased from Alfa Aesar, was flashed through a basic alumina column to remove inhibitor and degassed before polymerization. Ethanol was purchased from EMD, and methanol and chloroform were purchased from BDH. All metal salts were purchased from either TCI or Alfa Aesar and used as received. N, N, N’, N’’, N’’-

pentamethyldiethylenetriamine (PMDETA) and ethyl-2-bromoisobutyrate (Et2BriB) were purchased from either TCI or Alfa Aesar and degassed prior to polymerization.

Synthesis of Spiropyran Methyl Methacrylate (SPMA)

1-(2-Hydroxyethyl)-3-dimethyl-6-nitrospiro(2H-1-benzopyran-2,2-indole) (SP alcohol)[19] was subsequently coupled to methacrylic acid following standard procedures.[29]

Synthesis of Poly(MMA_{90}-co-$SPMA_{10}$)

SPMA (0.381 g, 0.906 mmol), MMA (0.816 g, 8.15 mmol), CuBr (0.005 g, 0.035 mmol), and Et2BriB (0.007 g, 0.035 mmol) were added to a dry, 25 mL schlenk flask. Anhydrous THF (5 mL) was then added, and the solution was degassed under Ar for 1 h. After degassing, PMDETA (0.060 g, 0.346 mmol), which was also degassed under Ar for 1 h, was added to the reaction mixture. The rubber septum on the schlenk flask was then replaced with a glass stopper while still under Ar to avoid any possible oxygen poisoning. The reaction was then placed in an oil bath for 16 h at 65 ºC. The flask was then opened and exposed to air. The solution was precipitated in approximately 50 mL of cold methanol, and the precipitate was filtered through a medium frit funnel. The polymer was re-dissolved in THF and the precipitation repeated. A pink powder was collected (M_w = 39,148 kDa, M_n = 37,010 kDa, M_w/M_n = 1.058, as obtained by gel permeation chromatography). ^1H NMR (500 MHz, $CDCl_3$) δ (ppm): 8.03 (s, 0.2H); 7.21 (s, 0.1H); 7.11 (s, 0.1H); 6.91 (s, 0.2H); 6.75 (d, 0.2H); 5.89 (m, 0.1H); 4.08 (s, 0.2H); 3.55 (m, 2.6H); 1.81; 1.30 (m, 0.3H); 1.20 (m, 0.3H); 1.02 (s, 0.1H); 0.83 (s, 1.6H).

Synthesis of Poly(MMA_{50}-co-$SPMA_{50}$)

SPMA (0.73 g, 1.74 mmol), MMA (0.18 g, 1.74 mmol), CuBr (0.005 g, 0.035 mmol), and Et2BriB (0.007 g, 0.035 mmol) were added to a dry, 25 mL schlenk flask. Anhydrous THF (5 mL) was then added, and the solution was degassed under Ar for 1 h.

After degassing, PMDETA (0.060 g, 0.346 mmol), which was also degassed under Ar for 1 h, was added to the reaction mixture. The rubber septum on the schlenk flask was then replaced with a glass stopper while still under Ar to avoid any possible oxygen poisoning. The reaction was then placed in an oil bath for 16 h at 65 ºC. The flask was then opened and exposed to air. The solution was precipitated in approximately 50 mL of cold methanol, and the precipitate was filtered through a medium frit funnel. The polymer was re-dissolved in THF and the precipitation repeated. A pink powder was collected (M_w = 84,871 kDa, M_n = 70,126 kDa, M_w/M_n = 1.210, as obtained by gel permeation chromatography). ^{1}H NMR (500 MHz, $CDCl_3$) δ (ppm): 7.99 (s, 1H); 7.10 (s, 1H); 6.89 (s, 1H); 6.70 (s, 1H); 5.87 (s, 0.5H); 4.03 (s, 1H); 3.48 (s, 2.5H); 1.77 (s, 2.6H); 1.16 – 1.27 (d, 2H); 0.78 (s, 3H).

Synthesis of Poly(SPMA)

SPMA (1.47 g, 3.49 mmol), CuBr (0.005 g, 0.035 mmol), and Et2BriB (0.007 g, 0.035 mmol) were added to a dry, 25 mL schlenk flask. Anhydrous THF was then added, and the solution was degassed under Ar for 1 h. After degassing, PMDETA (0.060 g, 0.346 mmol), which was also degassed under Ar for 1 h, was added to the reaction mixture. The rubber septum on the schlenk flask was then replaced with a glass stopper while still under Ar to avoid any possible oxygen poisoning. The reaction was then placed in a 65 ºC oil bath for 16 h. The flask was then opened and exposed to air. The solution was precipitated in approximately 50 mL of cold methanol. Precipitate was filtered through a medium frit funnel. It was then re-dissolved in THF and the procedure was repeated. A pink powder was collected (M_w = 42,562 kDa, M_n = 38,592 kDa, M_w/M_n = 1.103, as obtained by gel permeation chromatography).

Characterization

Fourier transform-infrared (FT-IR) measurements were taken with a Nicolet model 6700 instrument with a grazing angle attenuated total reflectance accessory (GATR, Harrick Scientific) at 264 scans with 4 cm^{-1} resolution. UV-vis spectroscopy was performed on a Cary 50 spectrophotometer (Varian). Number and weight average molecular weights of all polymers were estimated using gel permeation chromatography (Viscotek, Malvern Inc.) with two high molecular weight columns (I-MBHMW-3078) and one low molecular weight column (I-MBLMW-3078). Triple point detection, consisting of refractive index, light scattering, and viscometry, was used. Polystyrene standards were used to determine molecular weights from universal calibration. The film thickness was measured using null ellipsometry performed on a Multiskop (Optrel GbR) with a 632.8 nm He-Ne laser beam as the light source. Both δ and ψ value thickness data were measured and calculated by integrated specialized software. At least three measurements were taken for each wafer and the average thickness recorded.

Light Source

An OmniCure, series 1000 (EXFO, Inc.) with 365 nm wavelength light, was used as the UV light source. The substrates were held 2 cm from the source and irradiated at a power of 30 mW/cm^2. The visible light source was a Fiber-Lite Model with a 30 W quartz halogen fiber optic illuminator.

Spin-Coating Polymer Films on Silicon and Glass Substrates

Silicon wafers and glass substrates were cut into approximately 1 x 1 cm^2 squares. They were sonicated in isopropanol for 5 min and blown dry with a stream of nitrogen. A solution of 15 mg of polymer in 1 mL $CHCl_3$ (filtered with a 0.2 μm poly(tetrafluoroethylene) filter) was spin-coated on the clean substrates at 1600 rpm for 30 s (Chemat Technology Spin Coater KW-4A). The thickness of the films was held constant at 80 nm for each experiment, as measured by ellipsometry.

Merocyanine-Metal Ion Complexation Experiments

Initial UV-vis spectra and GATR-FT-IR spectra were recorded for the spin-coated film before UV irradiation. The substrate was then irradiated with 365 nm light for 1 minute, and a UV-vis spectrum and GATR-FT-IR spectrum were recorded of the merocyanine form. The substrate was then immersed in a 25 mM solution of metal(II) chloride in degassed ethanol for 3 min, blown dry under a stream of nitrogen, and UV-vis and GATR-FT-IR spectra recorded.

Chemometric Data Analysis

FT-IR and UV-visible absorption spectra were analyzed using chemometric methods to aid in spectral interpretation with respect to molecular conformation, to qualitatively identify the metal ion, and to quantify the metal ion in a sample solution. Commercially available software, PLS Toolbox 4.2 (Eigen Vector Research, Inc., Wenatchee, WA), operating in the MATLAB 7.5 environment (The Mathworks, Inc., Natick, MA) was utilized for spectral pretreatment, principal component analysis (PCA), partial least squares-discriminant analysis (PLS-DA), and partial least squares (PLS) regression analysis.

Spectral Preprocessing

Several spectroscopic pretreatments were investigated to optimize qualitative and quantitative predictive models. Spectral range, baseline correction, normalization, mean centering, and combinations of these steps were explored to optimize the PCA, PLS-DA, and PLS models. Using a leave-one-out cross validation algorithm, minimization of the root-mean-square error of cross validation (RMSECV) was used as the criterion to identify the optimum preprocessing steps. Optimal preprocessing of the IR dataset consisted of analyzing the spectral range of 1000-1800 cm^{-1} by taking the 2nd derivative of each spectrum using a fifteen-point, 2nd-order polynomial Savitzky-Golay algorithm, followed by normalization to unit-vector length and mean centering. Optimal preprocessing of the UV-visible absorption spectra required baseline correction (MATLAB specified point, 8th order) and mean centering.

Principal Component Analysis

PCA was used as an unsupervised method to explore variation in the sample spectra and to visualize clustering of similar spectra.[30] PCA models were built using the IR data for pre- and post-UV irradiated polymer films and FT-IR spectra for the polymer films complexed to each of five metal ions. PC scores plots were constructed to search for clustering of samples according to their identity. Loadings plots for the FT-IR datasets identified the spectral bands responsible for spectral variation to aid interpretation of conformational changes due to metal ion complexation and determine differences in binding among the metal ions.

Partial Least Squares-Discriminant Analysis

PLS-DA was applied to the FT-IR dataset as a means of sample classification. PLS-DA is a supervised method requiring a training set of data in which the sample identity is known *a priori*. Unlike PCA which identifies gross variability in the dataset, the supervised nature of PLS-DA functions to minimize within group variability and maximize among group variability.[31] The classification error of the cross validation samples using leave-one-out cross validation was used to optimize the number of latent variables to be included in the PLS-DA model. The sensitivity, i.e., rate of false negatives, and specificity, i.e., rate of false positives, are reported for each PLS-DA classification model.

Partial Least Squares Regression Analysis

Polymer films coated onto glass microscope slides were exposed to varying concentrations of each of the metal ions for collection of UV-visible absorption spectra. A PLS model was built for absorption spectra of each ion to assess the quantitative information contained in the spectra. Minimization of the RMSECV using leave-one-out cross validation was used to optimize the number of latent variables to be included in the PLS model.

Results and Discussion

Solution Polymerization

The SPMA monomer was copolymerized with MMA at various concentrations using atom transfer radical polymerization (Figure 3.2). The content of SPMA in the copolymer backbone and the molecular weight of each copolymer are summarized in Table 3.1. In each polymerization, the mol% of SPMA content found in the copolymer mirrors the monomer feed composition, with the difference being no larger than 2%, as determined by integration of the NMR resonances for each monomer in the polymer backbone (Figures A-1 and A-2 in Appendix A). Table 3.1 also shows that the experimental M_n determined by gel permeation chromatography agrees well with the theoretical M_n for both copolymer ratios, as well as the homopolymer of SPMA. This combined with the low polydispersity, indicates a living polymerization.

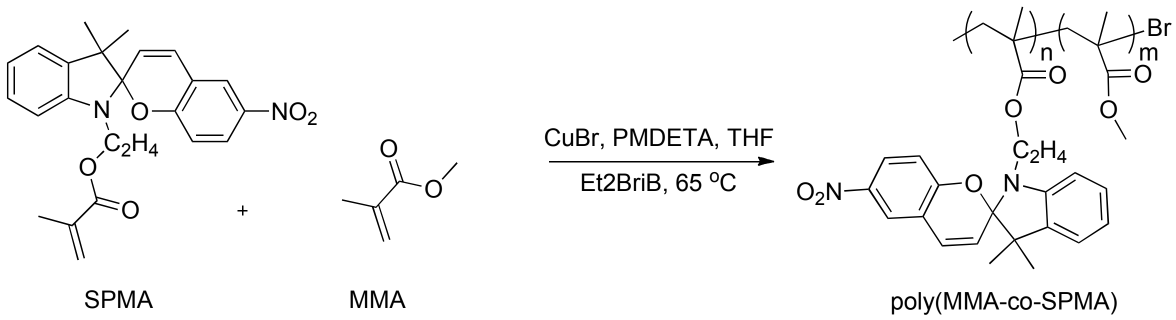

Figure 3.2. ATRP copolymerization conditions and structure of poly(MMA-*co*-SPMA).

Table 3.1. Content of SPMA unit in copolymer.

Copolymer	Content of SPMA unit in the feed (mol %)	Content of SPMA unit in copolymer (mol %)[a]	M_w[b]	M_n[b]	M_w/M_n[b]	Theoretical M_n
SPMA/MMA 1	10	10	65,159	49,701	1.311	34,296[c]
SPMA/MMA 2	50	48	84,871	70,126	1.210	67,695[d]
SPMA 1	100	100	42,562	38,592	1.103	42,048[e]

[a] Calculated from ^1H NMR (Figures A-1 and A-2 in Appendix A). [b] Average molecular weight was obtained by gel-permeation chromatography.
[c] CuBr:MMA:SPMA:PMDETA:Et2BriB 1:234:26:10:1.
[d] CuBr:MMA:SPMA:PMDETA:Et2BriB 1:50:50:10:1.
[e] CuBr:SPMA:PMDETA:Et2BriB 1:100:10:1.

In this study, we first polymerized SPMA-MMA copolymers containing different concentrations of spiropyran (Figure 3.2), as well as poly(SPMA) to investigate the effect of spiropyran concentration on the MC-M^{2+} complex. By statistical copolymerization, the ring-opening of the spiropyran moiety is less sterically hindered and free to undergo changes in conformation. It was found that a copolymer composition of MMA_{90}-*co*-$SPMA_{10}$ provided unique colorimetric responses to different metal ions as outlined below, and this polymer composition, poly(MMA_{90}-*co*-$SPMA_{10}$), was synthesized predominantly. Once purified, the polymers were spin-coated onto either glass or silicon substrates as ultrathin films to be used as sensors that can selectively identify and quantify various metal ions.

Photoinduced Conversion of SP to MC

GATR-FT-IR was used to characterize the photoinduced conversion of spiropyran to merocyanine in the polymer thin films. In order to deconvolute the MMA component from the SPMA in the polymer backbone, we initially examined the FT-IR profile of SPMA monomer that was spin-coated onto a silicon substrate before and after UV irradiation to identify pertinent peaks associated with the ring-opening process. Figure 3.3 shows the ring-closed SP and ring-opened MC form after irradiation with UV light. Complete characterization and assignments are listed in Table 3.2. Bands of particular importance are the tertiary C-N stretching band at 1337 cm^{-1}, the C-C-N bend at 1025 cm^{-1}, and the O-C-N stretching band at 955 cm^{-1}, which disappeared upon irradiation, while new bands emerged at 1592 cm^{-1}, 1428 cm^{-1}, and 1308 cm^{-1} that are assigned to the $C=N^+$, $C-O^-$, and $C-N^+$ stretches, respectively.[32-37] Also, the symmetrical stretching band of the aryl nitro group shifted to lower energy from 1517 cm^{-1} to 1508 cm^{-1} upon irradiation due to the increased conjugation brought about in the planar, merocyanine.

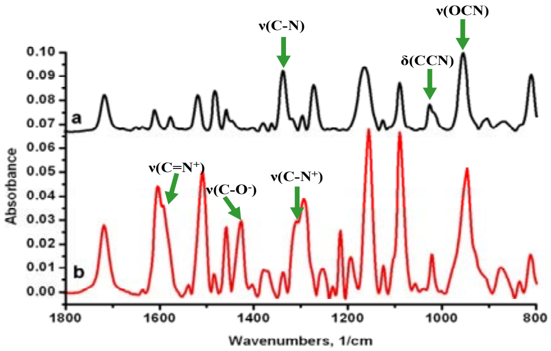

Figure 3.3. FT-IR spectra of SPMA monomer (a) before UV irradiation and (b) after UV irradiation. Peaks that indicate the photoconversion of spiropyran to merocyanine are labeled.

Table 3.2. Main FT-IR frequencies for SPMA monomer before (spiropyran) and after (merocyanine) UV irradiation.

	Spiropyran	**Merocyanine**
Assignment	**Wavenumbers (cm^{-1})**	**Wavenumbers (cm^{-1})**
C=O	1717	1717
C=C stretch	1649 and 1637	1634
$C=N^+$	—	1592
NO_2 sym stretch	1517	1508
$C-O^-$	—	1428
NO_2 asym stretch	1337	1337
C-N (3°) stretch	1337	—
$C-N^+$	—	1308
C-O-C ether sym stretch	1272	—
C-O-C ether asym stretch	1164	—
C-O ester stretch	1164	1155
C-O ester stretch	1089	1089
C-C-N bend	1025	—
O-C-N stretch	955	—
C=CH; CH out of plane deformation (cis)	955	947
C-N stretch of NO_2	903	903

Figure 3.4 shows the FT-IR spectra of poly(MMA_{90}-*co*-$SPMA_{10}$) which was spin-coated on a Si/SiO_2 wafer from $CHCl_3$. The thickness of the film was held constant at 80 nm for each experiment. With respect to the monomer characterization, several of the absorbance bands increased slightly in wavenumber upon polymerization. The symmetrical stretching band of the aryl nitro group in the ring-closed spiropyran shifted to higher energy, from 1517 cm^{-1} to 1521 cm^{-1}, and the carbonyl stretch shifted from 1717 cm^{-1} to 1730 cm^{-1}, which is a combination of absorbances for both SPMA and MMA. (Table 3.3). Also in the ring-closed form, the energy of the tertiary C-N

stretching band at 1339 cm^{-1}, the C-C-N bend at 1025 cm^{-1}, and the O-C-N stretch at 956 cm^{-1} were all either very close to or equal to the spiropyran monomer absorbances. Upon UV irradiation, the C-O^- stretching band of the phenolate increased from 1428 cm^{-1} to 1433 cm^{-1}, but this band is also masked by the CH_3 deformation associated with the MMA addition to the copolymer. The C=N^+ band and the C-N^+ band also emerged at 1593 cm^{-1} and 1311 cm^{-1}, respectively, which is consistent with the monomeric spiropyran spectrum.

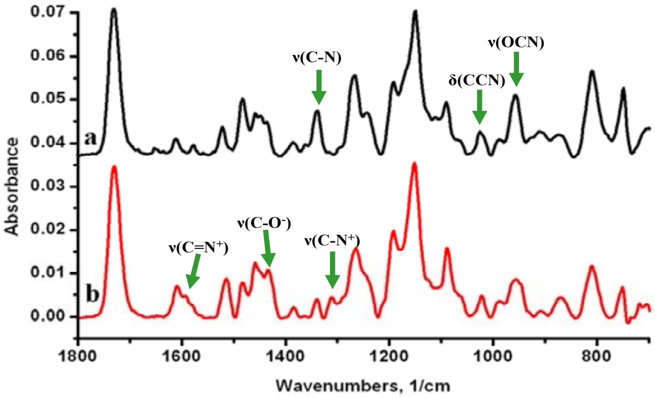

Figure 3.4. FT-IR spectra of poly(MMA_{90}-*co*-$SPMA_{10}$) (a) before UV irradiation and (b) after UV irradiation. Peaks that indicate the photoconversion of spiropyran to merocyanine are labeled.

Table 3.3. Important FT-IR frequencies for poly(MMA$_{90}$-*co*-SPMA$_{10}$) before (spiropyran) and after (merocyanine) UV irradiation.

	Spiropyran	**Merocyanine**
Assignment	**Wavenumbers (cm^{-1})**	**Wavenumbers (cm^{-1})**
C=O	1730	1730
C=N$^+$	–	1593
NO$_2$ sym stretch	1521	1513
C-O$^-$	–	1433
NO$_2$ asym stretch	1339	1339
C-N (3°) stretch	1339	–
C-N$^+$	–	1311
C-O-C ether sym stretch	1266	–
C-O-C ether asym stretch	1166	–
C-O ester stretch	1150	1151
C-O ester stretch	1089	1088
C-C-N bend	1025	–
O-C-N stretch	956	–

FT-IR spectra for multiple spin-coated films of poly(MMA$_{90}$-*co*-SPMA$_{10}$) before and after UV irradiation were analyzed with principal component analysis (PCA). PCA involves defining new axes, which are linear combinations of the original, *n*, axes each representing a wavenumber, such that the new principal component (PC) axes describe the maximum variance in the dataset.[30] PCA allows visualization of clusters of similar spectra to assess spectral reproducibility, identification of different sample types, and identification of variables responsible for spectral differences that can be interpreted with respect to chemical or physical phenomenon. For each data set, five poly(MMA$_{90}$-*co*-SPMA$_{10}$) spin-coated films were prepared, and FT-IR spectra were acquired before and after UV irradiation for each. The spectra were processed using standard methods,[30] as described above, prior to PCA. It was determined that 2nd derivative, vector normalized, and mean centered data provided the optimal PCA model. A single principal component, PC1, describes 98.88% of the spectral variance in the dataset. A plot of the scores on PC1 reveals a clear separation in the spectra obtained before and after UV irradiation (Figure 3.5). Moreover, spectra collected for the same sample type cluster tightly. This data illustrates the reproducibility in the preparation method of the copolymer films and also in the consistency of the photo-induced conversion from SP to MC that occurs upon ring-opening in the thin films.

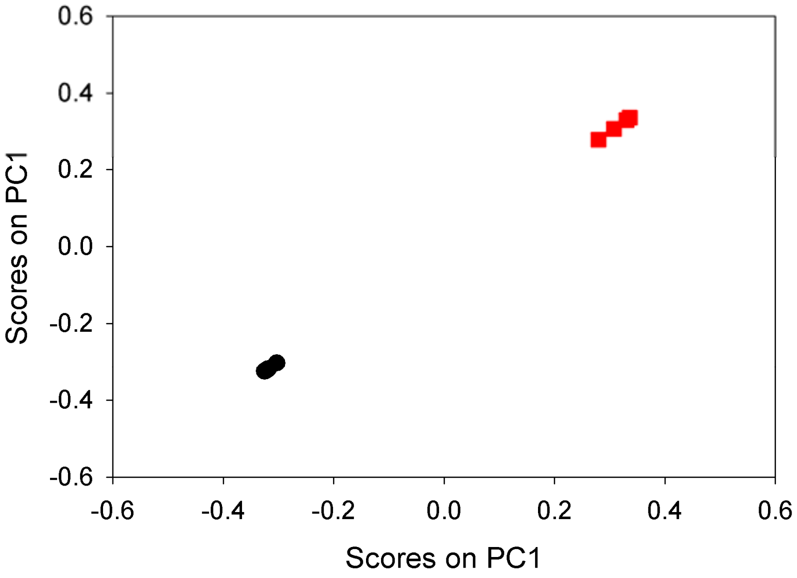

Figure 3.5. Scores plot for PC1 computed from the FT-IR spectra of poly(MMA$_{90}$-*co*-SPMA$_{10}$) before UV irradiation (black) and after UV irradiation (red) for independently prepared films.

Evaluation of the loadings on PC1 provides information regarding the contribution of each wavenumber to the newly defined PC1. Effectively, these are the wavenumbers responsible for the observed separation along PC1. A plot of the loadings for PC1 is overlaid on the average FT-IR spectra obtained for the poly(MMA$_{90}$-*co*-SPMA$_{10}$) spin-coated films before and after UV irradiation (Figure 3.6). The PC1 loadings plot identifies the bands corresponding to the symmetric nitro stretch (1521 cm^{-1}), C-N (3°) stretch (1339 cm^{-1}), symmetric C-O-C ether stretch (1266 cm^{-1}), and asymmetric C-O-C ether stretch (1166 cm^{-1}) as the most significant variation between the pre- and post-UV irradiation, although several other bands are identified. These results are consistent with the ring-opening of SP to MC and the results provided in Table 3.3 obtained through manual spectral interpretation. These results also demonstrate the power of PCA to identify spectral variation among samples for interpretation at the molecular level.

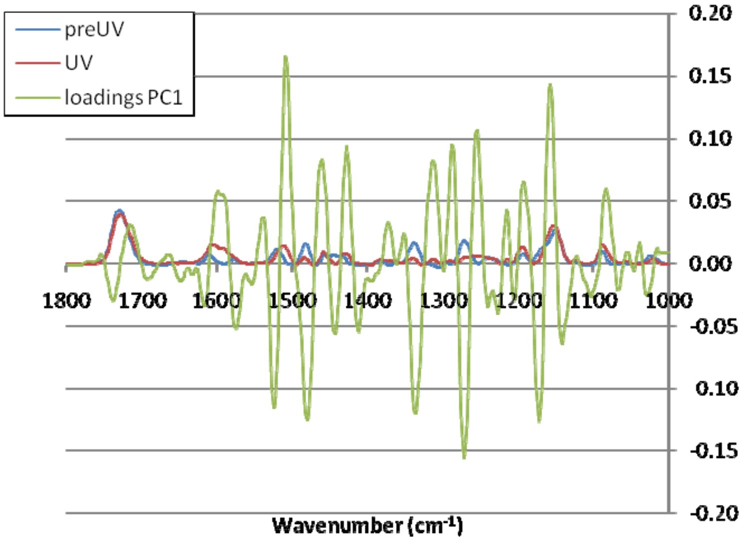

Figure 3.6. Loadings plot for PC1 computed from the FT-IR spectra of pre- and post-UV irradiated poly(MMA$_{90}$-*co*-SPMA$_{10}$) overlaid on the average FT-IR spectra for the two samples.

UV-Vis Studies of the Merocyanine-Metal Ion Complex

In order to examine the merocyanine-metal ion complex, UV-vis spectra were recorded for a spin-coated poly(MMA_{90}-*co*-SPMA_{10}) film before and after UV irradiation. The substrates were then immersed in a 25 mM solution of metal(II) chloride in ethanol for 3 minutes and blown dry with nitrogen before recording UV-vis and FT-IR spectra. Figure 3.7 shows the UV-vis absorbance spectra of the SPMA copolymer film in response to different metal ions. As can be seen from the SP trace in Figure 3.7, when spiropyran is in the ring-closed state, the SPMA copolymer is colorless, with an absorption tail below 400 nm. After the photoinduced change to the ring-opened state, the copolymer thin film in the solid state was characterized by an intense absorption band at λ_{max} = 584 nm, with a second band centered at 375 nm. It has been shown that there are eight possible conformers that correspond to different values of the three dihedral angles α, β, and γ describing the rotation about the bonds depicted in Figure 3.1.[37, 38] The conformations with a central *trans* segment ($\beta = 180^{o}$) provide the optimal conjugation of the two π-electron ring systems, the indoline and benzopyran, which give rise to the long wavelength absorption (*trans*-MC, Figure 3.1). Upon complexation with Zn^{2+}, Co^{2+}, and Ni^{2+}, there is a decrease in the long wavelength absorbance at 584 nm, along with a significant hypsochromic shift in absorbance maxima, which is dependent upon the metal ion contained in the solution. This blue shift in absorbance maxima is due to a disruption in planarity of the *trans*-MC that occurs upon complexation. With Fe^{2+}, the absorption band broadens, with a shoulder observed at 520 nm and 437 nm. In the case of Cu^{2+}, the longer wavelength absorption band splits, so that there are two partially overlapping absorbances; the first around 520 nm and the second around 410 nm. The spectra suggest that these ions may form a *cis*-MC-M^{2+} complex, through complexation with the phenolic oxygen and carbonyl of the ester sidechain. A possible structure is shown in Figure 3.1. Wojtyk *et al.* have observed complexes of a *cis*-merocyanine complex with some metal(II) ions and a monomeric spiropyran with a carboxylic acid substituent.[39] It has also recently been found that imidizolium-based ionic liquids that are strong hydrogen-bond acceptors can also complex with a *cis*-merocyanine form.[40]

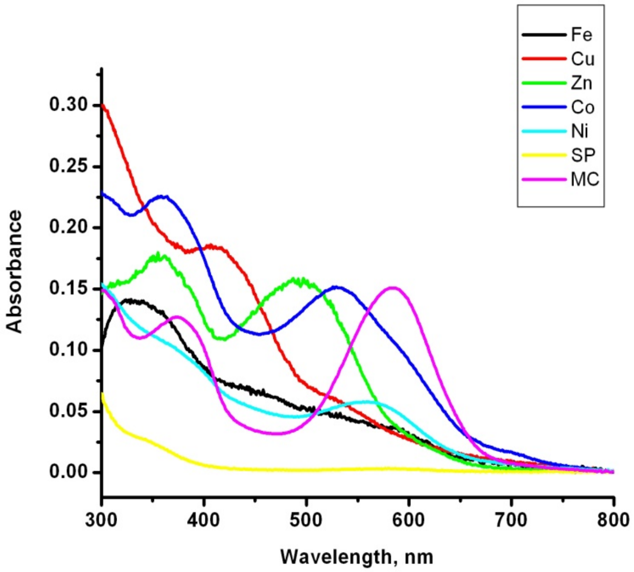

Figure 3.7. UV-vis absorbance spectra of poly(MMA$_{90}$-*co*-SPMA$_{10}$) in the presence of different divalent metal ions: Fe, Cu, Zn, Co, Ni. SP and MC refer to the absorbance spectra of the polymer thin films in the ring-opened (MC) and ring-closed (SP) state.

The spectral response of each polymer thin film to metal ion binding is drastically different than that of the monomeric SPMA in solution. Figure 3.8 shows the UV-vis spectra for SPMA monomer in ethanol. The merocyanine monomer has a λ_{max} = 551 nm, which is significantly blue shifted from the absorbance maxima of the copolymer in the solid state (λ_{max} = 584 nm). It has been well documented that solvent polarity can affect the absorption band for merocyanine, with polar solvents, such as ethanol, giving rise to a hypsochromic shift in absorbance maxima.[41, 42] For SPMA monomer, there is a decrease in intensity of absorbance maxima when different metal ions are added to solution (Figure 3.8). There is no colorimetric selectivity observed between Co^{2+}, Ni^{2+}, and Zn^{2+}. While this is inconsistent with work previously published by Gorner and Chibisov,[43] these results are still reasonable. Binding experiments for SPMA monomer were performed with metal chlorides in ethanol, where as in previous work, metal nitrates were used in acetone or acetonitrile. The counter ion,[43] as well as solvent polarity,[41, 42] can effect the absorption spectra of the MC-M^{2+} complex. Upon addition of Cu^{2+} and Fe^{2+} to the MC solution, the long energy absorbance band does not shift to higher energy as observed in the polymer thin film. The spectrum does reveal the appearance of the *cis*-MC-M^{2+} complex at λ = 427 nm with Cu^{2+}, and a broadened absorbance with a shoulder at 434 nm is observed in the case of Fe^{2+}.

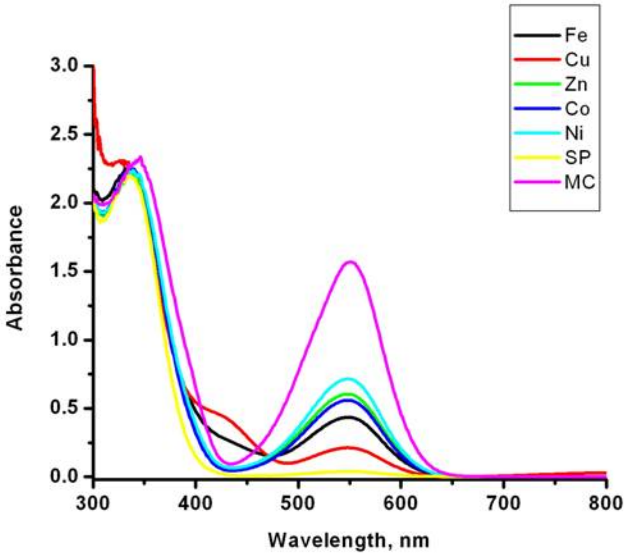

Figure 3.8. UV-vis absorbance spectra of SPMA monomer bound to metal ions in 2:1 MC-M^{2+} complex.

Because of the significant difference between the interaction of metal ions to the monomer in solution and the polymer as a thin film, we hypothesize that the large differences in the colorimetric response for each MC-M^{2+} complex is due to the local microenvironment of the chromophore in the copolymer thin film. Fabricating a copolymer that contains only 10 mol% SPMA allows for the merocyanine to be less sterically hindered and have more free volume to spatially rearrange and accommodate metal ion binding. In order to examine the influence of steric bulk, we synthesized a 50% copolymer, poly(MMA_{50}-*co*-$SPMA_{50}$), and the pure homopolymer, poly(SPMA), to confirm that upon increasing the concentration of spiropyran in the copolymer, or by polymerizing the homopolymer, the differences in absorbance for each MC-M^{2+} ion complex will decrease until there is only minimal differences between each complex in the UV-vis absorbance spectra. Figures 3.9a and b show the UV-vis absorbance spectra for poly(MMA_{50}-*co*-$SPMA_{50}$) and poly(SPMA), respectively.

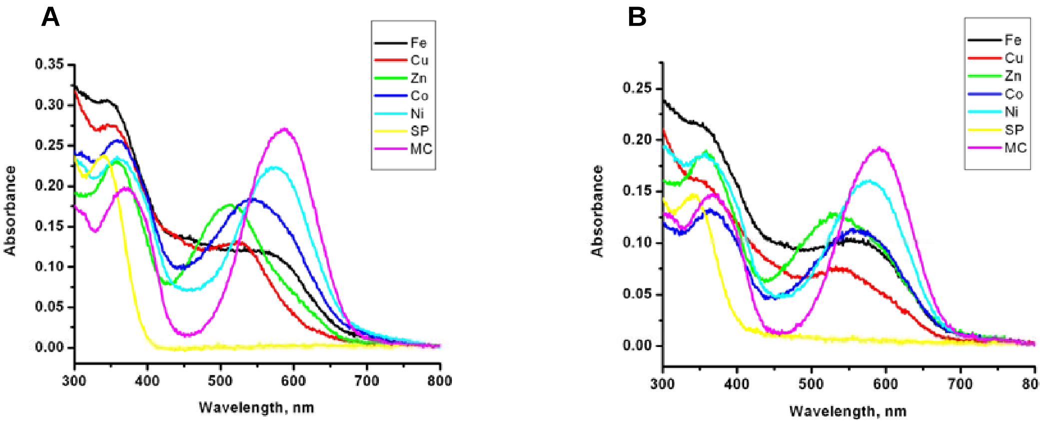

Figure 3.9. UV-vis absorbance spectra of (a) poly(MMA_{50}-*co*-$SPMA_{50}$) and (b) poly(SPMA) in the presence of different metal ions.

As can be seen for poly(MMA_{50}-*co*-$SPMA_{50}$) in Figure 3.9a, although complexation with a metal ion causes a decrease in absorbance at λ_{max} = 586 nm, there is less variation in the colorimetric response between different ions. With poly(MMA_{90}-*co*-$SPMA_{10}$), the MC-Zn^{2+} and MC-Co^{2+} complexes have a hypsochromic shift of 90 nm and 54 nm, respectively. With poly(MMA_{50}-*co*-$SPMA_{50}$), the MC-Zn^{2+} and MC-Co^{2+} complexes shift 73 nm and 43 nm, respectively. The absorbance maximum for the MC-Ni^{2+} complex in the poly(MMA_{50}-*co*-$SPMA_{50}$) shifts only slightly (11 nm), compared to a 23 nm blue shift for poly(MMA_{90}-*co*-$SPMA_{10}$). The largest differences between the two copolymers are found in the MC-Cu^{2+} and MC-Fe^{2+} complexes. In both cases, the shoulder around 400-430 nm does not appear, suggesting that poly(MMA_{50}-*co*-$SPMA_{50}$) does not form *cis*-MC-M^{2+} complexes in the presence of Cu^{2+} or Fe^{2+}.

Further increasing the concentration of SPMA in the polymer backbone leads to even less variation in the colorimetric response of the polymers to different metal ions. The MC-Zn^{2+} and MC-Co^{2+} complexes in poly(SPMA) homopolymer thin films produce a blue shift of 56 nm and 30 nm, respectively (Figure 3.9b). This represents a 50% decrease in the blue shift of absorbance maximum for these two complexes when the concentration of SPMA is increased from 10 to 100 mol% in the polymer. As with poly(MMA_{50}-*co*-$SPMA_{50}$), the MC-Cu^{2+} and MC-Fe^{2+} complexes do not give rise to the two partially overlapping absorbance bands in the homopolymer. In these cases, there is only one absorbance maxima for Cu^{2+} and Fe^{2+} at 540 nm and 576 nm, respectively, again indicating that Cu^{2+} and Fe^{2+} do not form stable *cis*-MC-M^{2+} complexes. The blue shift in absorbance maximum for the MC-Ni^{2+} complex in the homopolymer does not change significantly from what is observed with poly(MMA_{50}-*co*-$SPMA_{50}$). The lack of a large blue shift in absorbance maxima for the MC-M^{2+} complexes in poly(MMA_{50}-*co*-$SPMA_{50}$) and poly(SPMA) lends support to the hypothesis that as the concentration of spiropyran is increased in the copolymer, the chromophore is more sterically hindered and less accessible to accommodate binding to divalent metal ions. The necessity of the chromophore to be able to rearrange sufficiently enough to allow for metal ion binding is supported by Byrne *et al.*[20] Given that there is much less spectral variation for the different MC-M^{2+} complexes in poly(MMA_{50}-*co*-$SPMA_{50}$) and poly(SPMA) thin films, poly(MMA_{90}-*co*-$SPMA_{10}$) thin films were analyzed for the FT-IR studies described below.

FT-IR Studies of the Merocyanine-Metal Ion Complex

GATR-FT-IR spectroscopy was also used to characterize the merocyanine-metal ion complex in poly(MMA$_{90}$-*co*-SPMA$_{10}$) thin films. Key differences in the FT-IR spectra of the MC-M^{2+} complex (Figure 3.10) exist, revealing important insights into their binding interactions within the copolymer system. While the phenolate anion band (1433 cm^{-1}) is partially obscured by the MMA in the copolymer film, changes in the shape of the peak when the merocyanine is bound to a metal ion still allow for inferences to be made. As can be seen in Figure 3.10, the phenolate anion band at 1433 cm^{-1} decreases in intensity for Cu^{2+}, Fe^{2+}, and to some extent Zn^{2+}, while the shape and intensity remain identical to the UV irradiated polymer in the case of Co^{2+} and Ni^{2+}. Also of importance, the symmetrical stretching band of the aryl nitro group shifted from 1514 cm^{-1} for the UV irradiated merocyanine to higher energy for each metal complex, the magnitude of which is metal ion dependent (Table 3.4). The metal ions that shift the UV-vis absorbance to higher energy, such as Fe^{2+} Cu^{2+}, and Zn^{2+} (Figure 3.7), have bands for the symmetrical stretching of the aryl nitro group at 1524 cm^{-1}, 1523 cm^{-1}, and 1521 cm^{-1} respectively, while the nitro group stretching bands for Co^{2+} and Ni^{2+} are much closer to the nonbinding merocyanine band. As the metal ions interact with the phenolate anion, electron density is drawn away from the aromatic ring and the nitro group, shifting the symmetrical stretching bands of the aryl nitro group to higher energy. Cobalt(II) and Ni^{2+}, which have a weaker interaction with the phenolate anion, do not afford this same shift to higher energy for the nitro stretching band.

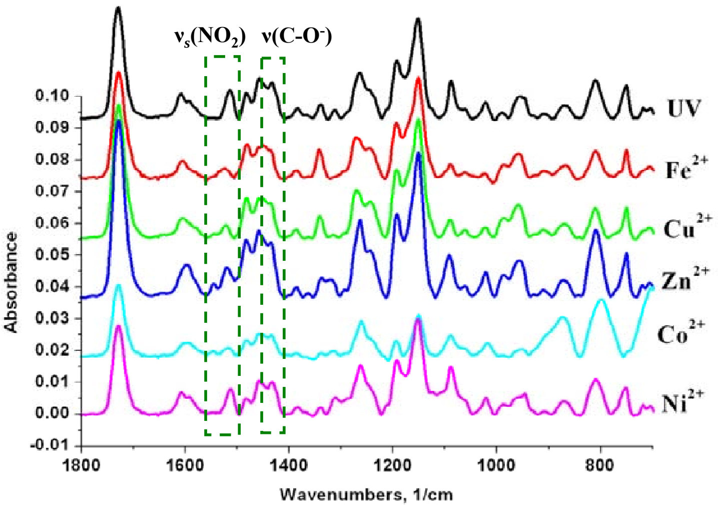

Figure 3.10. FT-IR spectra of poly(MMA_{90}-*co*-$SPMA_{10}$) after UV irradiation, (b) after binding to Fe^{2+}, (c) after binding to Cu^{2+}, (d) after binding to Zn^{2+}, (e) after binding to Co^{2+}, and (f) after binding to Ni^{2+}. The dashed green boxes highlight the major differences in the various merocyanine-metal ion complexes.

Table 3.4. Important FT-IR assignments of the MC-M^{2+} complex.

	Fe^{2+} (cm^{-1})	**Cu^{2+} (cm^{-1})**	**Zn^{2+} (cm^{-1})**	**Co^{2+} (cm^{-1})**	**Ni^{2+} (cm^{-1})**
C=O	1728	1728	1728	1728	1728
NO_2 sym stretch	1524	1523	1521	1517	1514
$C\text{-}O^-$	—	—	—	—	1432
NO_2 asym stretch	1342	1342	1337	1339	1340
C-N (3°) stretch	—	—	—	—	—
$C\text{-}N^+$	—	1315	1319	1314	1312

In order to assess the reproducibility of the spectra and elucidate the binding interaction for each metal ion, PCA was performed on the spectra after metal ion complexation. PCA scores plots for PC1, PC2, and PC3 are shown in Figures 3.11a and

b. It is obvious from the plot of the scores on PC2 versus PC1 that spectra for each of the metal ion complexes tightly cluster, signifying the reproducibility of the spectral collection (Figure 3.11a). Moreover, clusters for each of the metal ion complexes are easily resolved, with the exception of Fe^{2+} and Cu^{2+}, which facilitates the distinction between most of the metal ions. While the clustering is less precise and the degree of separation less significant, the Fe^{2+} and Cu^{2+} complexes can be differentiated by the scores on PC3 (Figure 3.11b). Interestingly, the scores on PC1 directly correlate with the binding strength of the metal ion to merocyanine as determined by interpretation of the UV-visible absorption spectra. Close examination of scores on PC1 for each sample reveals: UV irradiated film results (absence of M^{2+} complexation) $\ll Ni^{2+} < Co^{2+} < Zn^{2+} < Cu^{2+} = Fe^{2+}$. Thus, this PCA model can potentially be used to determine the interaction strength of other metal ions to merocyanine relative to these five ions. The peaks that contribute to the differences between the clusters, as identified by the loadings on PC1, are assigned to the phenolate anion stretch (1433 cm^{-1}) and the symmetrical (1521 cm^{-1}) and asymmetrical (1339 cm^{-1}) stretching of the aryl nitro group (Figure 3.12a). As PC3 can be used to differentiate Cu^{2+} from Fe^{2+}, the loadings on PC3 suggest that these two ions differ most significantly in their binding to the carbonyl and ester based on the change in intensity of the carbonyl stretching region (1730 cm^{-1}) and ester C-O stretch (1150 cm^{-1}) (Figure 3.12b).

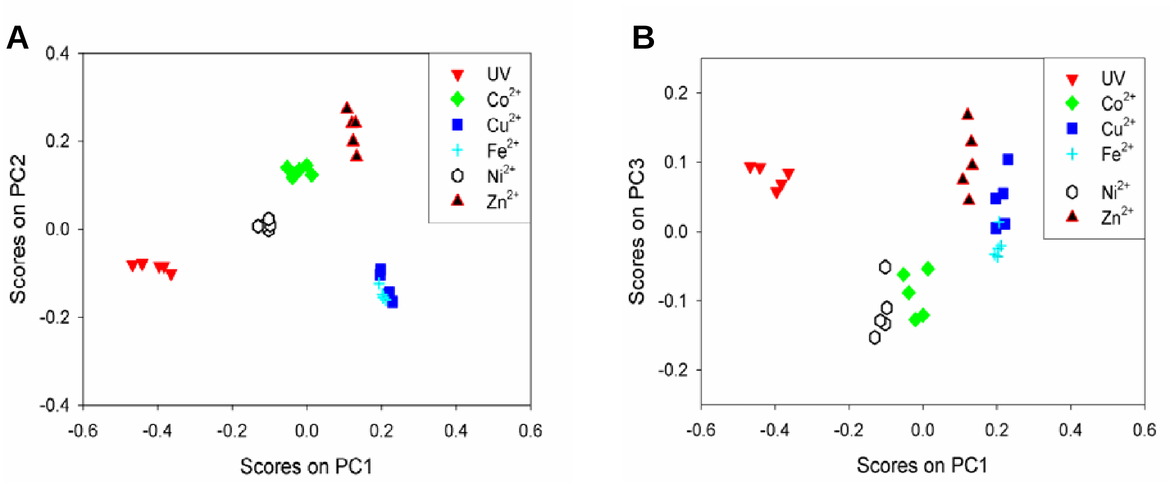

Figure 3.11. Scores plots of (a) PC2 versus PC1 and (b) PC3 versus PC1 for the PCA model computed from the FT-IR spectra of poly(MMA$_{90}$-*co*-SPMA$_{10}$) after UV irradiation, after binding to Fe^{2+}, after binding to Cu^{2+}, after binding to Zn^{2+}, after binding to Co^{2+}, and after binding to Ni^{2+}.

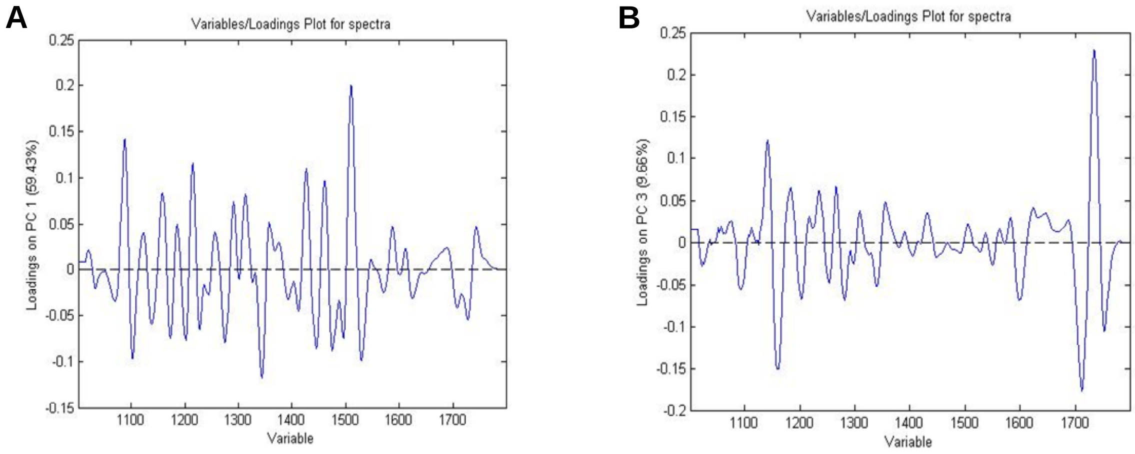

Figure 3.12. Loadings plots for (a) PC1 and (b) PC3 computed from the PCA model built using FT-IR spectra of poly(MMA$_{90}$-*co*-SPMA$_{10}$) after UV irradiation, after binding to Fe^{2+}, after binding to Cu^{2+}, after binding to Zn^{2+}, after binding Co^{2+}, and after binding to Ni^{2+}.

Metal Ion Sensing

Qualitative Identification of M^{2+}

By using UV-vis and GATR-FT-IR spectroscopy, it has been shown that each metal ion uniquely interacts with poly(MMA$_{90}$-*co*-SPMA$_{10}$) thin films which can be spectroscopically probed. We exploit this property, in conjunction with discriminant analysis, to identify the ion bound to the merocyanine copolymer film and assess its potential as a selective ion sensor. Specifically, partial least squares-discriminant analysis (PLS-DA) was used to identify the metal ion bound to merocyanine based on the FT-IR spectra. PLS-DA builds a classification model based on a calibration dataset consisting of spectra for known metal ion complexes. PLS-DA functions to maximize the importance of FT-IR frequencies that differ among the metal ions and minimize the importance of the frequencies which vary among spectra collected for the same metal ion.[31] FT-IR spectra were collected for a spin-coated film of the SPMA copolymer after UV irradiation and after exposure to a constant concentration, 25 mM, of the metal ions. Each ion was exposed to five independently prepared polymer films to generate a total of 30 spectra. After spectral preprocessing (2nd derivative, vector normalization, mean centering) a PLS-DA model was generated. The PLS-DA model was optimized and assessed based on the classification performance of the cross validated samples (leave-one-out). The optimized model utilized eight latent variables. Results for both the calibration and cross validation samples are provided in Table 3.5. The model achieves 100% sensitivity and > 97% specificity for the cross validation samples, where sensitivity is defined as the number of samples assigned to the class divided by the actual number of samples belonging to that class, and specificity is defined as the number of samples not assigned to that class divided by the actual number of samples not belonging to that class. Overall, only a single sample was misclassified (1/30), and it is likely that a larger dataset would improve the model performance.

Table 3.5. Results of PLS-DA classification of metal ions based on UV-vis absorbance spectra.

	MC	**Co**	**Fe**	**Ni**	**Cu**	**Zn**
Sensitivity (Cal):	1.00	1.00	1.00	1.00	1.00	1.00
Specificity (Cal):	1.00	1.00	1.00	1.00	1.00	1.00
Sensitivity (CV):	1.00	1.00	1.00	1.00	1.00	1.00
Specificity (CV):	1.00	0.97	1.00	1.00	1.00	1.00

Quantitative Determination of M^{2+}

A poly(MMA_{90}-*co*-$SPMA_{10}$) thin film was used to bind to Cu^{2+} ions in various concentrations of Cu(II) chloride in ethanolic solutions (Figure 3.13). As illustrated in the figure, the UV-visible absorption spectra of MC-Cu^{2+} are influenced by the concentration of Cu^{2+} in solution. As the concentration of Cu^{2+} is increased from 1 μM to about 10 mM, the absorbance maximum at λ_{max} = 584 nm decreases. Once the concentration of Cu^{2+} is increased to about 25 mM, along with the decrease in absorbance, a small blue shift in absorbance maxima is seen. As the concentration of Cu^{2+} is increased from 25 mM to 100 mM, the blue shift in absorbance maxima continues to increase. The largest blue shift in absorbance maxima occurs at a concentration of 100 mM. Concentrations exceeding 100 mM do not produce a larger shift to higher energy. A similar trend is observed for Fe^{2+}, Zn^{2+}, Co^{2+}, and Ni^{2+} as well (Figures 3.14-3.17, respectively).

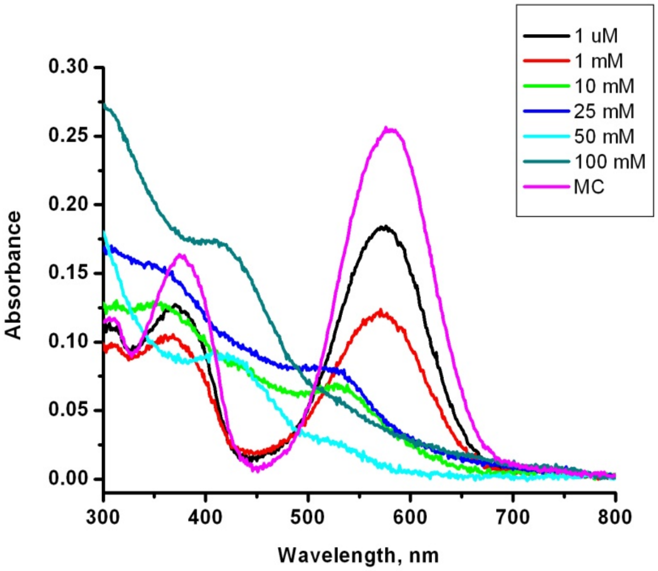

Figure 3.13. UV-vis absorbance spectra of merocyanine bound to Cu^{2+} at various concentrations of $CuCl_2$ solution.

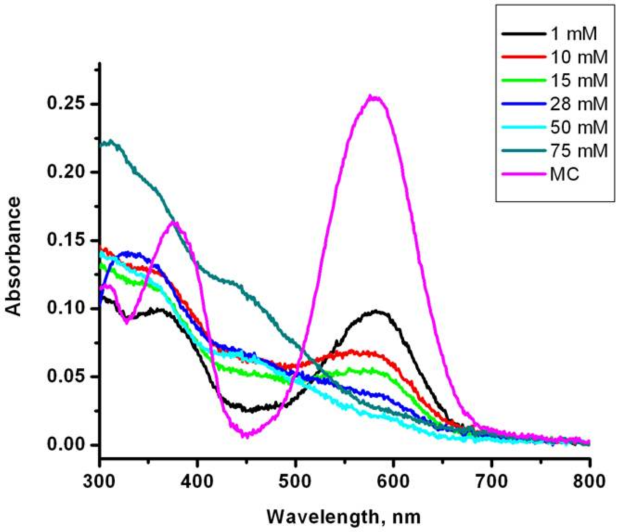

Figure 3.14. UV-vis absorbance spectra of merocyanine bound to Fe^{2+} at various concentrations of $FeCl_2$ solution.

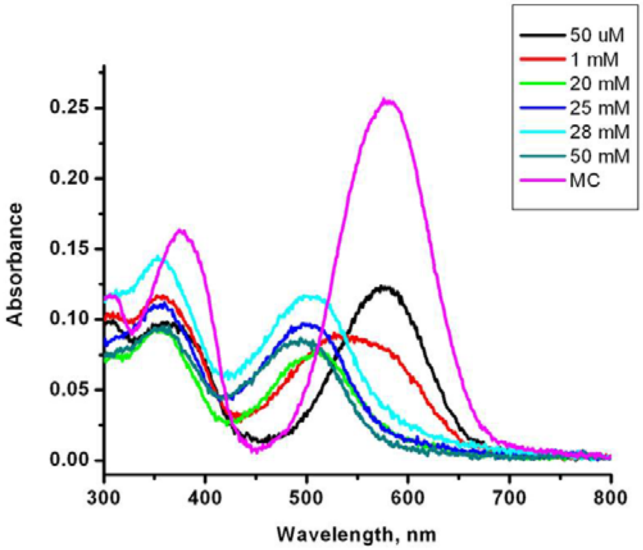

Figure 3.15. UV-vis absorbance spectra of merocyanine bound to Zn^{2+} at various concentrations of $ZnCl_2$ solution.

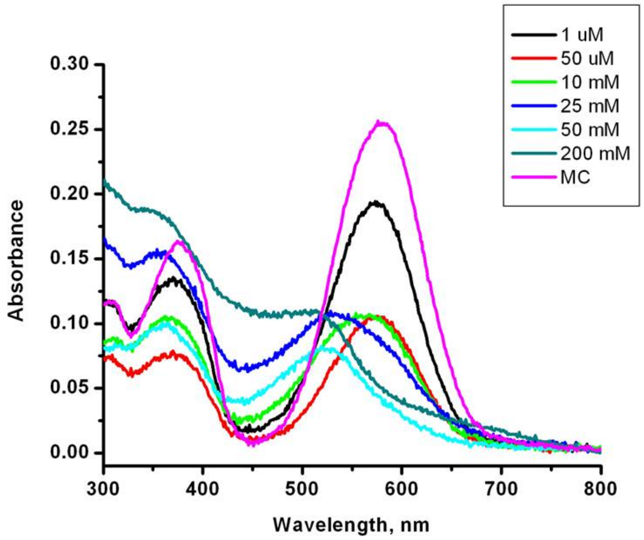

Figure 3.16. UV-vis absorbance spectra of merocyanine bound to Co^{2+} at various concentrations of $CoCl_2$ solution.

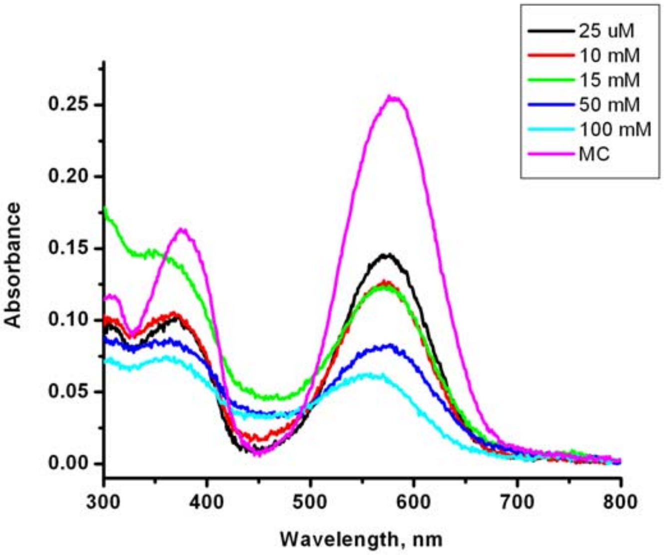

Figure 3.17. UV-vis absorbance spectra of merocyanine bound to Ni^{2+} at various concentrations of $NiCl_2$ solution.

As can be seen from Figure 3.13, a single absorbance band is not observed to increase or decrease in response to the Cu^{2+} concentration, which does not allow straightforward univariate quantitative analysis. Instead, bands are shifted and new bands are observed due to concentration dependent conformational changes. As a result, a multivariate means of quantitative analysis, such as partial least squares regression analysis (PLS), which considers the entire spectrum for calibration is required for quantitative analysis. A PLS model was generated using the preprocessed UV-visible spectra (see Experimental Section) for MC films exposed to various concentrations of Cu^{2+}. Each concentration was exposed to five independently prepared films. The root-mean-square error for cross validation (RMSECV), using the leave-one-out algorithm, was analyzed to determine the optimum rank for the PLS model. A plot of the predicted concentration for the cross validation samples versus the true concentration for the Cu^{2+}

samples is given in Figure 3.18. This model only included one latent variable and resulted in an RMSECV of 9.8 mM; inclusion of additional LVs had minimal effect on the RMSECV and would likely result in over-fitting the data and lead to poor quantification of test samples. The results of the optimized PLS models and analytical performances for each of the M^{2+} ions are presented in Table 3.6.

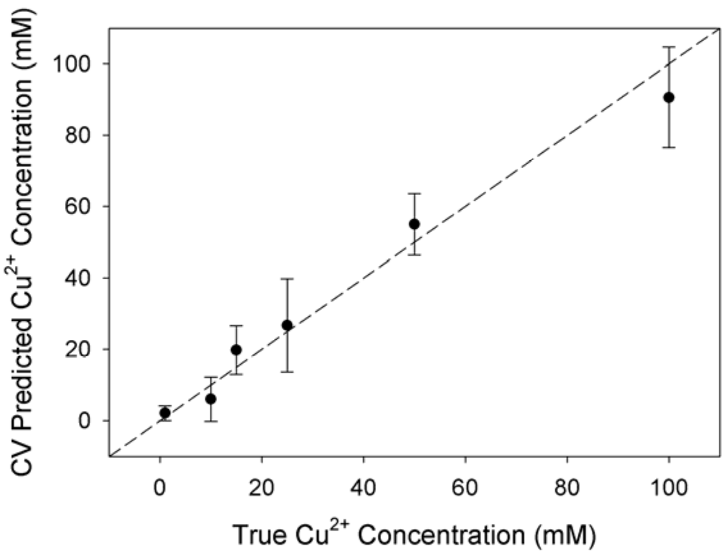

Figure 3.18. Plot of PLS regression cross validation predicted versus true concentration of Cu^{2+} for the UV-visible absorption data. Error bars represent one standard deviation. Solid line is a plot of $x = y$, to serve as a guide.

Table 3.6. The RMSECV for the optimized PLS regression model for each M^{2+} based on UV-vis absorbance spectra.

	Co	**Fe**	**Ni**	**Cu**	**Zn**
RMSECV (mM)	12.9	10.9	16.8	9.8	13.5

These polymer thin films, along with spectral analysis, offer a means to quantitative sensing of metal ions in the micromolar to millimolar range. To our knowledge, this has not been observed with a single chromophore and is typically only possible with an array of different compounds. The weakness of the interaction between the MC-M^{2+} complex limits the lower limit of detection, but also gives rise to quantitative sensing of metal ion concentration in the 1 μM to the 100 mM range with reasonable accuracy (Table 3.6).

Conclusions

In summary, we have synthesized a series of spiropyran-containing copolymers that were used as colorimetric sensors for the divalent ions, Cu^{2+}, Fe^{2+}, Zn^{2+}, Co^{2+}, and Ni^{2+}. These polymers also exhibit unique responses to some monovalent and trivalent ions, which are under further investigation in our laboratory. FT-IR spectroscopy was used to characterize the photoinduced conversion of spiropyran to merocyanine, as well as the MC-M^{2+} complexes. FT-IR spectra were analyzed using chemometric methods to elucidate the binding interaction between MC and M^{2+} and to selectively identify the metal ions bound to MC. By means of UV-vis absorption spectroscopy, we have also shown that each metal ion gives rise to a unique colorimetric response that is dependent upon the amount of spiropyran comonomer contained in the polymer backbone, and that by increasing the concentration of SPMA in the copolymers, the selectivity between different metal ions decreases. Using chemometric methods, UV-vis spectra can be analyzed to quantitatively identify metal ions in a concentration range from 1 μM to 100 mM. With poly(MMA_{90}-*co*-$SPMA_{10}$) thin films, the uniqueness of each MC-M^{2+}

complex allows one to fabricate sensors out of a single polymer that can selectively and quantitatively distinguish different metal ions.

References

1. Oehme, I. and O. Wolfbeis, *Microchim. Acta*, **1997**. *126*(3): p. 177.
2. Janata, J., M. Josowicz, P. Vanysek and D.M. DeVaney, *Anal. Chem.*, **1998**. *70*(12): p. 179.
3. McDonagh, C., C.S. Burke and B.D. MacCraith, *Chem. Rev.*, **2008**. *108*(2): p. 400.
4. Narayanaswamy, R. and O. Wolfbeis, *Optical sensors: industrial, environmental and diagnostic applications*. 2004: Springer Berlin.
5. Nolan, E.M. and S.J. Lippard, *Chem. Rev.*, **2008**. *108*(9): p. 3443.
6. Buhlmann, P., E. Pretsch and E. Bakker, *Chem. Rev.*, **1998**. *98*(4): p. 1593.
7. Prodi, L., F. Bolletta, M. Montalti and N. Zaccheroni, *Coord. Chem. Rev.*, **2000**. *205*(1): p. 59.
8. He, X. and G.A. Rechnitz, *Anal. Chem.*, **1995**. *67*(13): p. 2264.
9. Choi, M.M.F. and D. Xiao, *Anal. Chim. Acta.*, **1999**. *387*(2): p. 197.
10. Gabor, G., S. Chadha and D.R. Walt, *Anal. Chim. Acta.*, **1995**. *313*(1-2): p. 131.
11. Rodman, D., H. Pan, C. Clavier, X. Feng and Z. Xue, *Anal. Chem.*, **2005**. *77*(10): p. 3231.
12. Plaschke, M., R. Czolk and H.J. Ache, *Anal. Chim. Acta.*, **1995**. *304*(1): p. 107.
13. Oehme, I., S. Prattes, O.S. Wolfbeis and G.J. Mohr, *Talanta*, **1998**. *47*(3): p. 595.
14. Zhang, X.-B., C.-C. Guo, Z.-Z. Li, G.-L. Shen and R.-Q. Yu, *Anal. Chem.*, **2002**. *74*(4): p. 821.
15. Rosatzin, T., P. Holy, K. Seiler, B. Rusterholz and W. Simon, *Anal. Chem.*, **2002**. *64*(18): p. 2029.

16. Eggins, B.R., *Chemical Sensors and Biosensors*. 2002, West Sussex, UK: John Wiley and Sons Ltd.

17. Byrne, R. and D. Diamond, *Nat. Mater.*, **2006**. *5*(6): p. 421.

18. Saragi, T.P.I., T. Spehr, A. Siebert, T. Fuhrmann-Lieker and J. Salbeck, *Chem. Rev.*, **2007**. *107*(4): p. 1011.

19. Hirshberg, Y., *J. Am. Chem. Soc.*, **1956**. *78*(10): p. 2304.

20. Byrne, R.J., S.E. Stitzel and D. Diamond, *J. Mater. Chem*, **2006**. *16*(14): p. 1332.

21. Little, J.C., *J. Am. Chem. Soc.*, **1965**. *87*(17): p. 4020.

22. Winkler, J.D., K. Deshayes and B. Shao, *J. Am. Chem. Soc.*, **1989**. *111*(2): p. 769.

23. Stauffer, M.T. and S.G. Weber, *Anal. Chem.*, **1999**. *71*(6): p. 1146.

24. Suzuki, T., Y. Kawata, S. Kahata and T. Kato, *Chem. Commun.*, **2003**(16): p. 2004.

25. Chibisov, A.K. and H. Görner, *Chem. Phys.*, **1998**. *237*(3): p. 425.

26. Evans, L., G.E. Collins, R.E. Shaffer, V. Michelet and J.D. Winkler, *Anal. Chem.*, **1999**. *71*(23): p. 5322.

27. Samanta, S. and J. Locklin, *Langmuir*, **2008**. *24*(17): p. 9558.

28. Fries, K., S. Samanta, S. Orski and J. Locklin, *Chem. Commun.*, **2008**(47): p. 6288.

29. Dong-June Chung, Y.I., Yukio Imanishi, *J. Appl. Polym. Sci.*, **1994**. *51*: p. 2027.

30. Beebe, K.R., R.J. Pell and M.B. Seasholtz, *Chemometrics: A Practical Guide*. 1998, New York: John Wiley & Sons. 348.

31. Barker, M. and W. Rayens, *J. Chemom*, **2003**. *17*(3): p. 166.

32. Uznanski, P., *Langmuir*, **2003**. *19*(6): p. 1919.

33. Dattilo, D., L. Armelao, G. Fois, G. Mistura and M. Maggini, *Langmuir*, **2007**. *23*(26): p. 12945.

34. Delgado-Macuil, R., M. Rojas-López, V.L. Gayou, A. Orduña-Díaz and J. Díaz-Reyes, *Mater. Charact. 58*(8-9): p. 771.

35. R Delgado Macuil, M.R.L., A Orduña Díaz and V Camacho Pernas *J. Phys.: Conf. Ser.*, **2009**. *167*.

36. Futami, Y., M.L.S. Chin, S. Kudoh, M. Takayanagi and M. Nakata, *Chem. Phys. Lett.*, **2003**. *370*(3-4): p. 460.

37. Cottone, G., R. Noto, G. La Manna and S.L. Fornili, *Chem. Phys. Lett.*, **2000**. *319*(1-2): p. 51.

38. Ernsting, N.P. and T. Arthen-Engeland, *J. Phys. Chem*, **1991**. *95*(14): p. 5502.

39. Wojtyk, J.T.C., P.M. Kazmaier and E. Buncel, *Chem. Mater.*, **2001**. *13*(8): p. 2547.

40. Wu, Y., T. Sasaki, K. Kazushi, T. Seo and K. Sakurai, *J. of Phys. Chem. B*, **2008**. *112*(25): p. 7530.

41. Byrne, R., K.J. Fraser, E. Izgorodina, D.R. MacFarlane, M. Forsyth and D. Diamond, *Phys. Chem. Chem. Phys.*, **2008**. *10*(38): p. 5919.

42. Scarmagnani, S., Z. Walsh, C. Slater, N. Alhashimy, B. Paull, M. Macka and D. Diamond, *J. Mater. Chem*, **2008**. *18*(42): p. 5063.

43. Chibisov, H.G.a.A.K., *J. Chem. Soc., Faraday Trans.*, **1998**. *94*(17): p. 2557.

CHAPTER 4

FABRICATION OF SPIROPYRAN-CONTAINING THIN FILM SENSORS USED FOR SIMULTANEOUS IDENTIFICATION OF MULTIPLE METAL IONS[1]

---

[1] Fries, K. H.; Driskell, J. D.; Sheppard, G. R.; Locklin, J. To be submitted to *Langmuir*.

Abstract

In this article, a methacrylate-based spiropyran-containing copolymer was used as a colorimetric sensor to simultaneously identify multiple metal ions. Through UV-vis absorption spectroscopy, the relative binding affinity of merocyanine to each metal ion was investigated by displacement studies of a bound metal ion with a second metal ion of higher binding affinity. We also show that because each metal ion gives rise to a distinct spectral response, partial least squares-discriminant analysis (PLS-DA) can be used to analyze the UV-vis absorbance spectra to identify the two metal ions that are present in solution at varying concentrations simply by dipping a coated polymer substrate into solution after irradiation. Partial least squares regression analysis (PLS) was used to quantitatively determine the metal ions in solution for several binary mixtures. We also demonstrate that quantitative determination depends on the relative binding preference of merocyanine to each metal ion.

Introduction

Real-time analysis of metal ions is important for chemical monitoring, as well as environmental and clinical applications.[1, 2] Considerable research has recently been directed toward the development of rapid and reliable methods for simultaneous determination of multiple metal ions.[3-7] Optical sensors, which are based on immobilization strategies where organic indicator dyes are encapsulated in a polymer matrix that is permeable to the analyte, offer a wide variety of advantages over other sensing techniques.[8, 9] These advantages include minimal electrical or magnetic interference, no need for a reference, and no consumption of analyte.[10-12]

With respect to the simultaneous detection of multiple metal ions, however, challenges still exist. Finding a set of conditions under which all target metal ions can be detected, as well as determining a method which produces distinguishable signals for each metal ion detected is quite difficult.[3, 13] A common approach currently under development utilizes an array of sensing elements, each displaying cross-reactivities for all or some of the target analytes, in order to individually detect metal ions in mixtures.[14-17] In general, computational pattern analysis processes are used to evaluate the results produced from these arrays.[15-17] Two major disadvantages to this sensing method, however, are the lack of recognition of some of the metal ions by the chelators and by the overall uniformity of the individual sensor responses. To circumvent this, one group designed a panel of azo dye chelators which were capable of binding to a variety of heavy metal ions and producing diverse optical responses upon chelation.[4] While these metal-ligand complexes showed substantial diversity in their UV-vis absorbance spectra, multiple ligands had to be synthesized to detect each metal ion, which can often be difficult and time-consuming.

A single material that is capable of simultaneously binding multiple metal ions and giving a unique spectral response to each metal ion-ligand complex would make for a more simple and cost-effective sensor. Spiropyrans are a class of materials that could not only be used for the concurrent detection of multiple metal ions,[18, 19] but also as a reversible sensor that can switch between passive and active states,[20] which would aid in extending the lifetime of the sensor. Spiropyrans are a well-known class of photochromic compounds that undergo reversible, photocleavage of the spiro C-O bond, which allows switching between a ring-closed, colorless spiropyran (SP) form and a ring-opened, highly colored merocyanine (MC) form.[21, 22] The merocyanine structure exists as a resonance hybrid between two forms: the charged zwitterionic form and a neutral quinoidal form. It is known that metal ions can bind to merocyanine through the negatively charged phenolate group of the zwitterionic form (Figure 4.1).[23-29] In previous work, we prepared thin films of a single, photoresponsive copolymer that generate a unique and selective colorimetric response to different divalent metal ions.[30, 31] We found that by attaching a photochromophore to the polymeric backbone, the stimuli responsive nature of the chromophore is not only enhanced, but the microenvironment for the merocyanine-metal ion (MC-M^{2+}) complex, and therefore the colorimetric response, can be tuned by co-monomer composition.[31]

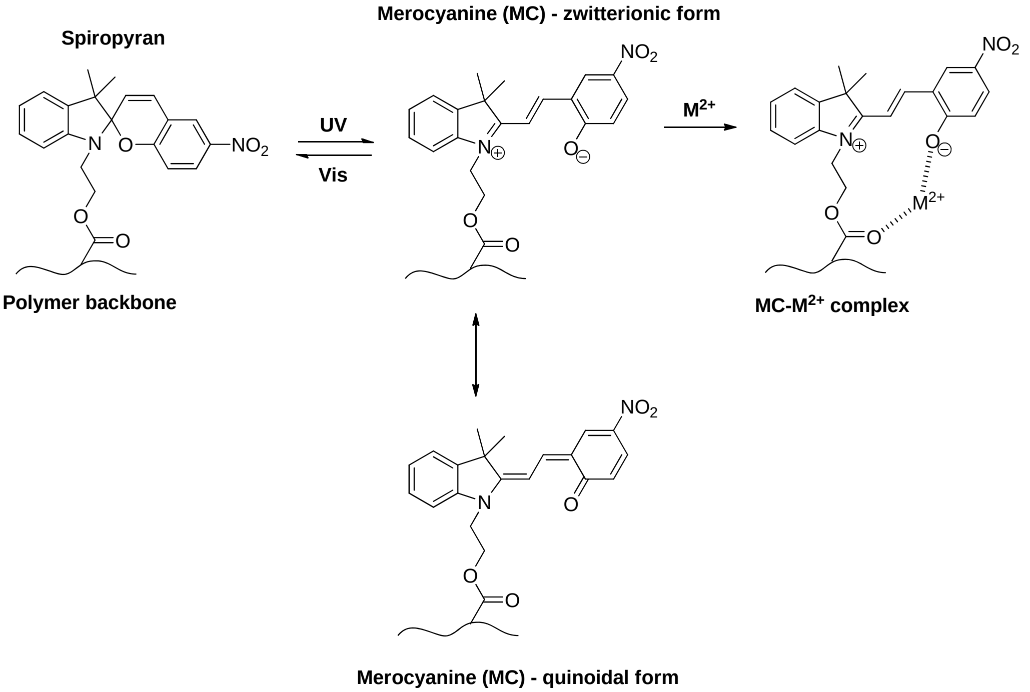

Figure 4.1. Isomeric structures of spiropyran (SP) and merocyanine (MC) and the MC-M^{2+} complex.

In this work, we used the unique spectral response of poly(MMA_{90}-*co*-$SPMA_{10}$) thin films to different divalent metal ions to simultaneously identify multiple metal ions from binary solutions. We investigated the relative affinity of MC to each metal ion by binding MC to one ion and attempting to displace it with an ion of higher binding affinity. With the results obtained from these experiments, a better understanding of the binding preference of MC to each metal ion was obtained. It is these differences in binding affinity that allow for the fabrication of a spiropyran-containing thin film sensor that can simultaneously identify both metal ions in a binary mixture. In addition, for several binary ion combinations, it is possible to quantitatively determine both metal ions in the solution.

Experimental Section

Materials

Silicon wafers (orientation <100>, native oxide) were purchased from University Wafer. BK7 microscope slides (RI = 1.514) were purchased from VWR. THF, purchased from BDH, was distilled from sodium-ketyl. Methyl methacrylate (MMA), purchased from Alfa Aesar, was flashed through a basic alumina column to remove inhibitor and degassed before polymerization. Ethanol was purchased from EMD, and methanol and chloroform were purchased from BDH. All metal salts were purchased from either TCI or Alfa Aesar and used as received. N, N, N', N'', N''-pentamethyldiethylenetriamine (PMDETA) and ethyl-2-bromoisobutyrate (Et2BriB) were purchased from either TCI or Alfa Aesar and degassed prior to polymerization.

Synthesis of Spiropyran Methyl Methacrylate (SPMA)

1-(2-Hydroxyethyl)-3-dimethyl-6-nitrospiro(2H-1-benzopyran-2,2-indole) (SP alcohol)[22] was subsequently coupled to methacrylic acid following standard procedures.[32]

Synthesis of Poly(MMA$_{90}$-co-SPMA$_{10}$)

SPMA (0.381 g, 0.906 mmol), MMA (0.816 g, 8.15 mmol), CuBr (0.005 g, 0.035 mmol), and Et2BriB (0.007 g, 0.035 mmol) were added to a dry, 25 mL schlenk flask. Anhydrous THF (5 mL) was then added, and the solution was degassed under Ar for 1 h. After degassing, PMDETA (0.060 g, 0.346 mmol), which was also degassed under Ar for 1 h, was added to the reaction mixture. The rubber septum on the schlenk flask was then replaced with a glass stopper while still under Ar to avoid any possible oxygen poisoning. The reaction was then placed in an oil bath for 16 h at 65 ºC. The flask was then opened and exposed to air. The solution was precipitated in approximately 50 mL of cold methanol, and the precipitate was filtered through a medium frit funnel. The polymer was re-dissolved in THF and the precipitation repeated. A pink powder was collected (M_w = 39,148 kDa, M_n = 37,010 kDa, M_w/M_n = 1.058, as obtained by gel permeation chromatography). ^{1}H NMR (500 MHz, $CDCl_3$) δ (ppm): 8.03 (s, 0.2H); 7.21 (s, 0.1H); 7.11 (s, 0.1H); 6.91 (s, 0.2H); 6.75 (d, 0.2H); 5.89 (m, 0.1H); 4.08 (s, 0.2H); 3.55 (m, 2.6H); 1.81; 1.30 (m, 0.3H); 1.20 (m, 0.3H); 1.02 (s, 0.1H); 0.83 (s, 1.6H).

Characterization

UV-vis spectroscopy was performed on a Cary 50 spectrophotometer (Varian). Number and weight average molecular weights of the copolymer were estimated using gel permeation chromatography (Viscotek, Malvern Inc.) with two high molecular weight columns (I-MBHMW-3078) and one low molecular weight column (I-MBLMW-3078). Triple point detection, consisting of refractive index, light scattering, and viscometry, was used. Polystyrene standards were used to determine the molecular weight from universal calibration. The film thickness was measured using null ellipsometry performed on a Multiskop (Optrel GbR) with a 632.8 nm He-Ne laser beam as the light source. Both δ and ψ value thickness data were measured and calculated by integrated specialized software. At least three measurements were taken for each wafer, and the average thickness recorded.

Light Source

An OmniCure, series 1000 (EXFO, Inc.) with 365 nm wavelength light, was used as the UV light source. The substrates were held 2 cm from the source and irradiated at a power of 30 mW/cm^2.

Spin-Coating Polymer Films on Silicon and Glass Substrates

Silicon wafers and glass substrates were cut into approximately 1 x 1 cm^2 squares. They were sonicated in isopropanol for 5 min and blown dry with a stream of nitrogen. A solution of 15 mg of polymer in 1 mL $CHCl_3$ (filtered with a 0.2 μm poly(tetrafluoroethylene) filter) was spin-coated on the clean substrates at 1600 rpm for 30 s (Chemat Technology Spin Coater KW-4A). The thickness of the films was held constant at 80 nm for each experiment, as measured by ellipsometry.

Merocyanine-Metal Ion Complexation Experiments

Initial UV-vis spectra were recorded for the spin-coated film before UV irradiation. The substrate was then irradiated with 365 nm light for one minute and a UV-vis spectrum of the merocyanine form was taken. The substrate was then immersed in a 25 mM solution of metal(II) chloride in ethanol for one minute, blown dry under a stream of nitrogen, and UV-vis spectra recorded.

Displacement Experiments

The spin-coated poly(MMA_{90}-*co*-$SPMA_{10}$) thin film was irradiated with 365 nm light for one minute and then immersed in a 25 mM ethanolic solution of metal(II) chloride for one minute. The substrate was blown dry with a nitrogen stream, and a UV-vis spectrum was recorded. The substrate was then immersed in another 25 mM solution of a different metal(II) chloride in ethanol for one minute, blown dry with nitrogen gas, and a UV-vis spectrum subsequently recorded.

Selectivity Experiments

The spin-coated poly(MMA_{90}-*co*-$SPMA_{10}$) thin film was irradiated with 365 nm light for one minute and then immersed in an ethanolic solution containing two metal(II) chloride salts in varying concentration combinations. Various combinations of 225 mM and 25 mM were used. The substrate was removed from the solution and blown dry under a stream of nitrogen gas. UV-vis spectra were recorded.

Chemometric Data Analysis

Chemometric methods were used to analyze UV-vis absorption spectra to aid in spectral interpretation with respect to identifying and quantifying the concentration of two metal ions in a solution. Commercially available software, PLS Toolbox 4.2 (Eigenvector Research, Inc., Wenatchee, WA), operating in MATLAB 7.5 (The Mathworks, Inc., Natick MA) was used for spectral pretreatment, partial least squares-discriminant analysis (PLS-DA), and partial least squares (PLS) regression analysis.

Spectral Preprocessing

Several spectroscopic preprocessing steps were explored to optimize PLS-DA and PLS models. Spectral range, baseline correction, normalization, mean centering, and combinations of these steps were examined to optimize the models. A leave-one-out cross validation algorithm and minimization of the root-mean-square error of cross validation (RMSECV) were used as measures to identify the optimum preprocessing steps. To build the PLS-DA model, optimal preprocessing of the UV-vis absorption spectra required baseline correction (OPUS Version 6.5, Bruker Optics), followed by taking the first derivative of each spectrum using a 15-point second order polynomial Savitzky-Golay algorithm, and normalization to unit-vector length. To build the PLS model, optimal preprocessing of the UV-vis absorption spectra required rubber band baseline correction (OPUS Version 6.5, Bruker Optics).

Partial Least Squares-Discriminant Analysis

PLS-DA was applied to the UV-vis absorption spectra as a means of sample classification. PLS-DA is a supervised method requiring a training set of data in which the sample identity is known *a priori*. It functions to minimize within class variance and maximize between class variance.[33] The classification error of the cross validation samples using leave-one-out cross validation was used to optimize the number of latent variables to be included in the PLS-DA model. The sensitivity (rate of false negatives) and the specificity (rate of false positives) are reported for each PLS-DA classification model.

Partial Least Squares Regression Analysis

A PLS model was built for UV-vis absorption spectra to assess the quantitative information contained in the spectra. Minimization of the RMSECV using leave-one-out cross validation was used to optimize the number of latent variables to be included in the PLS model.

Results and Discussion

Merocyanine-Metal Ion Complex

In previous work, we have shown that using the unique spectral response of each merocyanine-metal ion complex, poly(MMA_{90}-*co*-$SPMA_{10}$) thin films can be used to fabricate sensors that can selectively and quantitatively distinguish different metal ions.[31] Figure 4.2 shows the UV-vis absorbance spectra of a SPMA copolymer film, with a thickness of 80 nm, in response to a 25 mM concentration of divalent metal ions, Sn^{2+}, Cu^{2+}, Fe^{2+}, Zn^{2+}, Co^{2+}, and Ni^{2+}. As can be seen from the figure, the colorless, ring-closed spiropyran (SP trace) is characterized by an absorption tail below 400 nm. After the photoinduced change to the ring-opened merocyanine, the copolymer is characterized by an intense absorption band at λ_{max} = 584 nm, with a second band centered around 375 nm. Upon complexation with Zn^{2+}, Co^{2+}, and Ni^{2+}, the spectral response is similar, with a decrease in the long wavelength absorption band at 584 nm, along with a significant hypsochromic shift in absorbance maxima, which is metal ion dependent. The MC-Ni^{2+} complex yields the smallest blue shift of only 25 nm (λ_{max} = 559 nm), while the MC-Co^{2+} and MC-Zn^{2+} complexes give blue shifts of 53 nm (λ_{max} = 531 nm) and 91 nm (λ_{max} = 493 nm), respectively. This shift to higher energy accompanying binding is attributed to the disruption of planarity of the *trans*-MC that occurs upon complexation.[31]

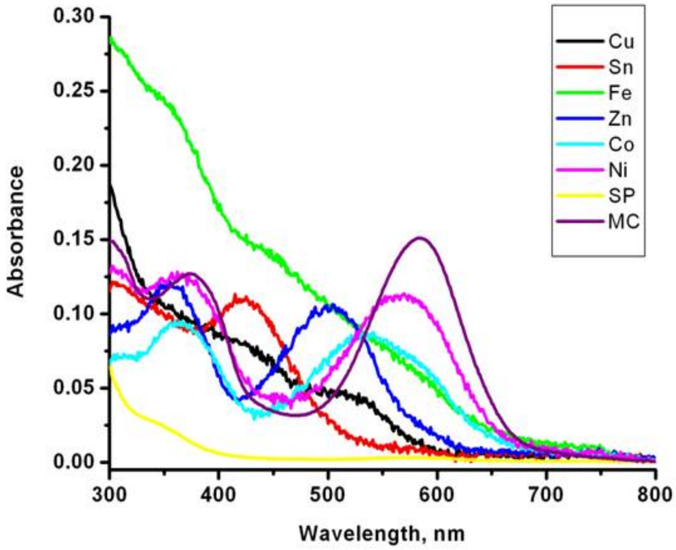

Figure 4.2. UV-vis absorbance spectra of poly(MMA_{90}-*co*-$SPMA_{10}$) in the presence of different divalent metal ions: Cu, Sn, Fe, Zn, Co, Ni. SP and MC refer to the absorbance spectra of the polymer thin films in the ring-closed (SP) and ring-opened (MC) state.

With Cu^{2+}, the long wavelength absorption band splits with two partially overlapping absorbances at 513 nm and 420 nm. In the case of Fe^{2+}, the long wavelength absorption band broadens with a shoulder observed at 550 nm and 440 nm. These spectra and subsequent GATR-FT-IR analysis suggest that Cu^{2+} and Fe^{2+} may form a *cis*-MC-M^{2+} complex, through complexation with the phenolate anion and the carbonyl of the ester side chain.[31] The MC-Sn^{2+} complex shows only one absorption band with a λ_{max} = 423 nm, also indicative of a *cis*-MC-M^{2+} complex. These considerable differences in the spectral response of merocyanine to each metal ion can be used to fabricate a sensor with a single copolymer capable of binding simultaneously to multiple metal ions.

Displacement Experiments

In order to gain insight into the relative affinity of MC to each metal ion, displacement experiments were conducted. In a typical experiment, the spin-coated copolymer film was irradiated with UV light for one minute and immersed in a 25 mM solution of metal(II) chloride in ethanol for one minute. The substrate was then removed from the solution, blown dry with a stream of nitrogen gas, and a UV-vis spectrum was recorded. Next, the substrate was promptly immersed in a 25 mM solution of a different metal(II) chloride solution for one minute. Again, the substrate was removed from the solution, blown dry under a stream of nitrogen gas, and a UV-vis spectrum was recorded.

Table 4.1 summarizes the results obtained from these displacement experiments. From the results in the table, it can be seen that Sn^{2+} displaces all other divalent metal ions that are originally bound to MC. The UV-vis spectra of the films all have a single absorbance band around 425 nm, indicating the presence of only the MC-Sn^{2+} complex (Figures B-1 - B-5 in Appendix B). No absorbance band indicative of a MC-Cu^{2+}, MC-

Fe^{2+}, MC-Zn^{2+}, MC-Co^{2+}, or MC-Ni^{2+} complex, respectively, is present in any case. In addition, MC maintains its complex to Sn^{2+} when immersed into a solution of other divalent metal ions studied. The concentration of the metal ion bound to the surface is orders of magnitude smaller than the concentration of the displacing ion in solution. One would expect that the ion in solution would saturate the thin film sensor, at least partially displacing the metal ion already bound. The fact that merocyanine retains its complex to Sn^{2+} suggests that it has a strong binding affinity to Sn^{2+}.

Table 4.1. Summary of results from displacement experiments.

	Displacing Metal Ion					
Bound Metal Ion	**Sn**	**Cu**	**Fe**	**Zn**	**Co**	**Ni**
Sn	x	Sn	Both	Both	Sn	Sn
Cu	Sn	x	Both	Zn	Both	Both
Fe	Sn	Cu	x	Zn	Both	Fe
Zn	Sn	Cu	Both	x	Co	Both
Co	Sn	Cu	Fe	Zn	x	Ni
Ni	Sn	Cu	Fe	Zn	Ni	x

The metal ions listed in each box indicate the metal ions the poly(MMA_{90}-*co*-$SPMA_{10}$) thin film complexed to last. "Both" indicates the film is complexed to both metal ions simultaneously.

The merocyanine form of SPMA also has a strong preference to Cu^{2+}. As shown in Table 4.1, Cu^{2+} displaces all of the ions investigated except for Sn^{2+}. Furthermore, when MC is originally bound to Cu^{2+}, the presence of the both the MC-Cu^{2+} complex and the MC-M^{2+} complex with the displacing metal ion is seen in the UV-vis spectra for most of the displacing ions (Figures B-6 - B-8 in Appendix B). Only when Zn^{2+} and Sn^{2+} are used as the displacing ions will MC not retain its complex to Cu^{2+}.

The results in Table 4.1 also show that MC has the weakest affinity for Ni^{2+} and Co^{2+}. Merocyanine does not retain its complex with either Co^{2+} or Ni^{2+} while in the presence of any of the other metal ions investigated. Further, Co^{2+} and Ni^{2+} serve as poor displacing metal ions. The fact that Co^{2+} and Ni^{2+} cannot fully displace any ion suggests that MC has a very weak binding preference for these ions, since the displacing ion in solution is in much higher concentration than the ion already bound to the film.

Merocyanine appears to have a moderate binding preference to Zn^{2+} and Fe^{2+}. As seen in Table 4.1, MC preserves its complex to Fe^{2+} when the SPMA copolymer film is placed in the presence of some of the metal ion solutions, and Fe^{2+} can at least partially displace any of the metal ions investigated. Zinc(II) follows a similar trend. Furthermore, Zn^{2+} displaces all of the other metal ions studied with the exception of Sn^{2+}, where both ion complexes are observed in the absorbance spectra.

From these displacement studies, an order of relative affinity of MC to each metal ion can be inferred, where $Sn^{2+} > Cu^{2+} > Fe^{2+} \geq Zn^{2+} > Ni^{2+} \geq Co^{2+}$. This compares well to the trend seen in the spectral responses of the MC-M^{2+} complexes shown in Figure 4.2. Tin(II) and Cu^{2+} complexes with MC give the largest shift in absorbance maxima to higher energy, and these are also the ions to which MC has the strongest affinity. Cobalt(II) and Ni^{2+} complexes, which have the least affinity to MC, yield the smallest hypsochromic shift in absorbance maxima.

Selectivity Studies

From these displacement studies, in the case of several binary metal ion combinations, MC is capable of identifying both metal ions simultaneously. To explore this further, a series of experiments were conducted in which poly(MMA$_{90}$-*co*-SPMA$_{10}$) thin films were immersed in solutions containing a binary mixture of two different metal ions in varying concentration ratios for one minute and blown dry prior to recording UV-vis absorbance spectra. The same six metal ions were used, Sn^{2+}, Cu^{2+}, Fe^{2+}, Zn^{2+}, Co^{2+}, and Ni^{2+}, and the concentration ratios used were (1) 90% to 10% (225 mM to 25 mM) (2) 50% to 50% (25 mM to 25 mM) and (3) 10% to 90% (25 mM to 225 mM). The results are summarized in Table 4.2.

Table 4.2. Summary of the results from selectivity studies. "Both" indicates the film is complexed to both metal ions simultaneously.

Metal Ion Mixtures	**Ratios** **10-90**	 **50-50**	 **90-10**
Sn-Co	Sn	Sn	Sn
Sn-Ni	Sn	Sn	Sn
Sn-Zn	Sn	Sn	Sn
Sn-Fe	Sn	Sn	Sn
Sn-Cu	both	both	both
Ni-Zn	Zn	Zn	Zn
Ni-Fe	Fe	Fe	Fe
Cu-Co	both	both	both
Cu-Ni	both	both	both
Cu-Fe	both	both	both
Cu-Zn	both	both	both
Co-Ni	both	both	both
Zn-Fe	both	both	both
Zn-Co	both	both	both
Co-Fe	both	both	both

Detection of Only One Metal Ion

As can be seen from Table 4.2, a few metal ion combinations exist where the poly(MMA$_{90}$-*co*-SPMA$_{10}$) thin film binds exclusively to one ion and cannot detect the presence of both ions in solution. The SPMA copolymer film binds solely to Sn^{2+} at any concentration ratio with Fe^{2+}, Co^{2+}, Ni^{2+}, or Zn^{2+}, with only the MC-Sn^{2+} complex observed in all spectra (Figures B-9 - B-12 in Appendix B, respectively). Only in the case of Cu^{2+} are both ions observed in the film. At the other (low) end of the binding affinity, Ni^{2+} is only observed in the film where the other ion contained in the solution is Cu^{2+} or Co^{2+}. With mixtures of Sn-Ni, Zn-Ni, and Fe-Ni, the SPMA copolymer film always preferentially complexes to the ion that is not Ni^{2+} at any concentration ratio (Figures B-11, B-13, and B-14 in Appendix B, respectively).

These results for Sn^{2+} and Ni^{2+} follow the trends seen in the spectral responses of the individual metal ions complexed to MC (Figure 4.2) in terms of a spectral shift to higher energy and also the results obtained from the displacement experiments, where the SPMA copolymer has the strongest affinity for Sn^{2+} and weakest affinity for Ni^{2+}.

Simultaneous Identification of Multiple Metal Ions

In all cases where both ions are observed in the UV-vis spectra of the poly(MMA_{90}-*co*-$SPMA_{10}$) thin film upon complexation, simultaneous identification of multiple metal ions in solution is possible. Despite these differences in the spectral shifts in λ_{max} seen for the complexation of different metal ions, there is significant overlap of the spectra for binary mixtures, making it difficult to distinguish between the contributions of each ion. In order to deconvolute the spectra, partial least squares-discriminant analysis (PLS-DA) was used to analyze the UV-vis absorption spectra and to identify the metal ions bound to MC. PLS-DA is a classification model that is particularly complementary to applications involving a large number of highly overlapping, broad analyte signatures, such as those found in UV-vis spectroscopy.[34] It serves to maximize the importance of the wavelengths that differ among the metal ions and minimize the importance of the wavelengths which vary among spectra collected for the same binary solution. UV-vis absorbance spectra were collected for the SPMA copolymer thin film after UV irradiation and exposure to an ethanolic solution of two metal ions at various concentrations ratios: (1) 225 mM to 25 mM, (2) 25 mM to 25 mM, (3) 25 mM to 225 mM. Each binary mixture was exposed to five independently prepared

SPMA copolymer spin-coated films to generate a total of 135 spectra. After spectral preprocessing (1st derivative, vector normalization), a PLS-DA model was generated. The model was optimized and assessed based on the classification performance of the cross validated samples (leave-one-out). The optimized model utilized ten latent variables.

Results for both the calibration and the cross validation samples are provided in Table 4.3. The model achieves no less than 81% sensitivity and specificity for the cross validation samples. Sensitivity is defined as the number of samples assigned to the class divided by the actual number of samples belonging to that class (percent of true positives), and specificity is defined as the number of samples not assigned to that class divided by the actual number of samples not belonging to that class (percent of true negatives). The model was more successful in identifying Sn^{2+} and Cu^{2+} than the other ions as it achieved 100% sensitivity for Sn^{2+} and greater than 98% sensitivity for Cu^{2+}. Both ions also had greater than 96% specificity. The model was also successful in identifying Fe^{2+} (89% specificity and 91% sensitivity). The model was moderately successful in predicting Co^{2+}, Ni^{2+}, and Zn^{2+}; although, neither the sensitivity, nor the specificity, was less than 80% for any ion. The lower correct identification rate with these three ions is a result of less significant differences between the λ_{max} of each MC-M^{2+} complex. Tin(II), Cu^{2+}, and Fe^{2+} give a much more distinctive spectral response when complexed to MC than Zn^{2+}, Co^{2+} and Ni^{2+}.

Table 4.3. Results of PLS-DA classification of metal ions based on UV-vis absorbance spectra.

	Co	**Fe**	**Ni**	**Cu**	**Zn**	**Sn**
Sensitivity (Cal):	0.900	0.978	0.900	0.986	0.932	1.000
Specificity (Cal):	0.946	0.955	0.933	0.983	0.867	0.992
Sensitivity (CV):	0.833	0.889	0.833	0.986	0.818	1.000
Specificity (CV):	0.851	0.910	0.913	0.967	0.811	0.966

Simultaneous and Quantitative Determination of Multiple Metal Ions

Our previous work with poly(MMA_{90}-*co*-$SPMA_{10}$) thin films offered a means to quantitative identification of individual metal ions in a solution with concentrations from the micromolar to millimolar range.[31] Here, we examined the capability of the SPMA copolymer thin film to simultaneously determine the concentration of two metal ions in a binary mixture. A poly(MMA_{90}-*co*-$SPMA_{10}$) thin film was used to bind to Co^{2+} and Ni^{2+} simultaneously at various concentrations of $CoCl_2$ and $NiCl_2$ in ethanolic solutions. As can be seen from Figure 4.3, the UV-vis absorption spectra of MC bound to both ions are influenced by the concentration of both Co^{2+} and Ni^{2+} in solution. The difference in the spectral response of the SPMA copolymer thin film upon exposure to different concentration mixtures of Co^{2+} and Ni^{2+} is the shape of the single, broad absorption band for each binary mixture. This is seen for several of the different binary metal ion mixtures. Partial least squares regression analysis (PLS), a multivariate means of quantitative analysis, focuses on the spectral features that correlate with the parameter of interest. In other words, PLS relates a matrix of predictor variables, X (i.e., UV-vis absorption spectra), and a matrix of chemical properties, Y (i.e., concentration values), by a linear multivariate model; and therefore, can be used to analyze the UV-vis spectra of MC bound to both ions in a binary mixture at various concentrations.

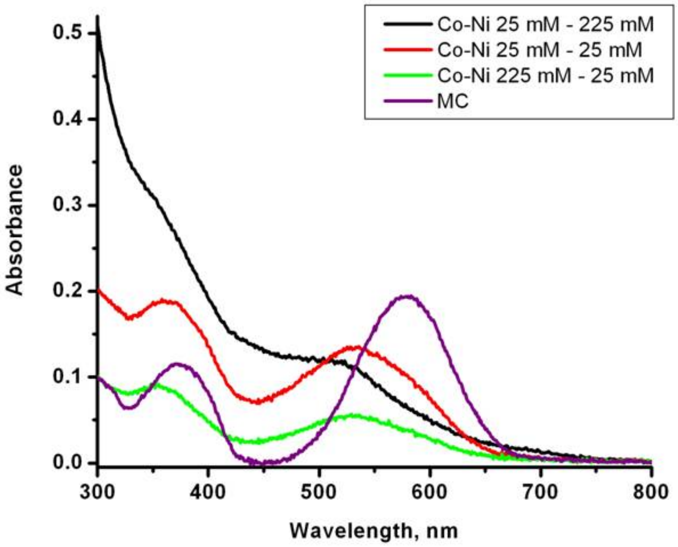

Figure 4.3. UV-vis absorbance spectra of poly(MMA_{90}-*co*-$SPMA_{10}$) in response to a solution containing 25 mM $CoCl_2$ and 225 mM $NiCl_2$ (black trace), 25 mM $CoCl_2$ and 25 mM $NiCl_2$ (red trace), and 225 mM $CoCl_2$ and 25 mM $NiCl_2$ (green trace).

In order to avoid weighting the data towards one concentration over another, two separate PLS analyses were performed using the preprocessed UV-visible absorbance spectra for SPMA copolymer films exposed to binary mixtures of metal ions in various concentrations (see Experimental Section). In one analysis, the UV-vis spectra were collected for the SPMA copolymer thin film after UV irradiation and exposure to an ethanolic solution of two metal ions at equimolar concentrations of 25 mM. Each binary mixture was exposed to five independently prepared SPMA copolymer spin-coated films to generate a total of 45 spectra. In the second analysis, the UV-vis spectra were collected for the thin film after UV irradiation and exposure to an ethanolic solution at the concentrations ratios: (1) 225 mM to 25 mM, (2) 25 mM to 225 mM. Each binary mixture was exposed to five independently prepared spin-coated films to generate a total of 90 spectra. The root-mean-square error for cross validation (RMSECV), using the leave-one-out algorithm, was analyzed to determine the optimum rank for each PLS analysis. The first analysis contained only one latent variable, while the second included nine latent variables.

Table 4.4 shows RMSECV values for each metal ion given by the model generated for the equimolar binary mixtures. For binary mixtures of varying concentration, the RMSECV values for each metal ion are reported in Table 4.5. In both cases the results show that these SPMA copolymer thin films can quantitatively determine each metal ion concentration in several of the binary mixtures with reasonable accuracy.

Table 4.4. The RMSECV for the optimized PLS regression model for the equimolar binary mixtures.

	Co	**Fe**	**Ni**	**Cu**	**Zn**	**Sn**
RMSECV (mM)	8.46	11.66	10.23	9.62	12.37	7.73

Table 4.5. The RMSECV for the optimized PLS regression model for the binary mixtures at varying concentrations.

	Co	**Fe**	**Ni**	**Cu**	**Zn**	**Sn**
RMSECV (mM)	48.64	48.03	60.20	68.36	77.11	40.55

To probe these results further, plots were produced that show the average concentration predicted for both metal ions in the solution at all measured concentration ratios. Figure 4.4a shows the plot of predicted and measured concentrations for all three concentration ratios for Co^{2+} and Ni^{2+} solutions. As can be seen from Figure 4.4a, PLS can be used to predict the concentration, within the standard deviation, of both Co^{2+} and Ni^{2+} at all three concentration ratios tested. Figures 4.4b and 4.4c show similar results for solutions that contain Co^{2+} and Fe^{2+} and solutions that contain Zn^{2+} and Co^{2+} at all three concentration ratios, respectively. In all cases, PLS can be used to sense the concentration of both metal ions in the solution.

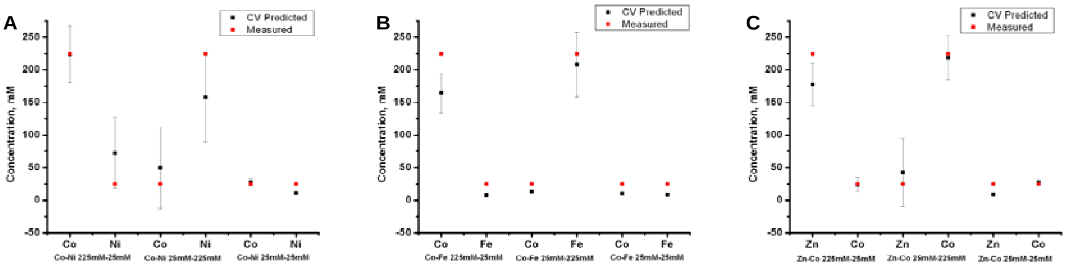

Figure 4.4. Plot of predicted and measured concentrations for (a) Co^{2+} and Ni^{2+} at (1) 225 mM $CoCl_2$ and 25 mM $NiCl_2$, (2) 25 mM $CoCl_2$ and 225 mM $NiCl_2$, and (3) 25 mM $CoCl_2$ and 25 mM $NiCl_2$, (b) Co^{2+} and Fe^{2+} at (1) 225 mM $CoCl_2$ and 25 mM $FeCl_2$, (2) 25 mM $CoCl_2$ and 225 mM $FeCl_2$, and (3) 25 mM $CoCl_2$ and 25 mM $FeCl_2$, and (c) Zn^{2+} and Co^{2+} at (1) 225 mM $ZnCl_2$ and 25 mM $CoCl_2$, (2) 25 mM $ZnCl_2$ and 225 mM $CoCl_2$, and (3) 25 mM $ZnCl_2$ and 25 mM $CoCl_2$.

While the copolymer film can quantitatively sense both metal ions in several of the metal ion mixtures studied, some mixtures exist where quantitative identification is not possible. Solutions containing one ion for which MC has a very strong affinity and one ion for which MC has a very weak affinity do not allow for quantitative sensing of either metal ion at any concentration ratio. For example, the SPMA copolymer film is not a reliable predictor of concentration for solutions of Cu^{2+} and Co^{2+} (Figure 4.5a). Solutions consisting of Cu^{2+} and Ni^{2+} show similar results (Figure 4.5b) Also, when two ions of strong binding affinity (Sn^{2+} and Cu^{2+} or Cu^{2+} and Fe^{2+}) are present in solution at different concentrations, the SPMA copolymer thin film cannot be used to quantitatively predict the concentration (Figures 4.6a and b). It is likely that the sensor is quickly saturated and unable to accurately determine concentrations. In all of these cases where *quantitative* determination fails, it is important to note that the spiropyran-containing thin film can still *qualitatively* identify the presence of both metal ions in solution.

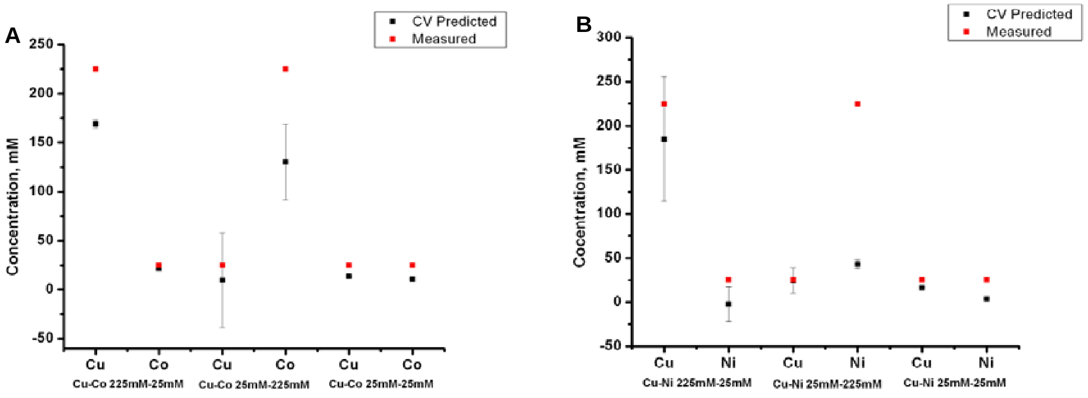

Figure 4.5. Plot of predicted and measured concentrations for (a) Cu^{2+} and Co^{2+} at (1) 225 mM $CuCl_2$ and 25 mM $CoCl_2$, (2) 25 mM $CuCl_2$ and 225 mM $CoCl_2$, and (3) 25 mM $CuCl_2$ and 25 mM $CoCl_2$ and (b) Co^{2+} and Ni^{2+} at (1) 225 mM $CoCl_2$ and 25 mM $NiCl_2$, (2) 25 mM $CoCl_2$ and 225 mM $NiCl_2$, and (3) 25 mM $CoCl_2$ and 25 mM $NiCl_2$.

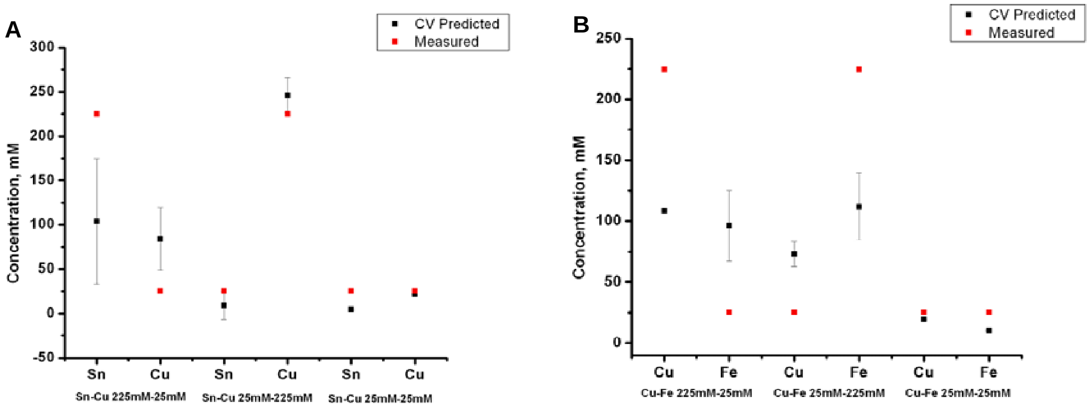

Figure 4.6. Plot of predicted and measured concentrations for (a) Sn^{2+} and Cu^{2+} at (1) 225 mM $SnCl_2$ and 25 mM $CuCl_2$, (2) 25 mM $SnCl_2$ and 225 mM $CuCl_2$, and (3) 25 mM $SnCl_2$ and 25 mM $CuCl_2$ and (b) Cu^{2+} and Fe^{2+} at (1) 225 mM $CuCl_2$ and 25 mM $FeCl_2$, (2) 25 mM $CuCl_2$ and 225 mM $FeCl_2$, and (3) 25 mM $CuCl_2$ and 25 mM $FeCl_2$.

Conclusions

In summary, we have synthesized a poly(MMA_{90}-*co*-$SPMA_{10}$) thin film that is used as a colorimetric sensor to detect multiple divalent metal ions in binary solutions. UV-vis spectroscopy was analyzed using chemometric methods to show that the SPMA copolymer thin film can simultaneously identify and quantitatively determine the concentration of various metal ion mixtures at different concentration ratios. UV-vis spectroscopy was also used to study the displacement of a bound metal ion with a second metal ion in order to investigate the relative order of binding affinity of merocyanine to each metal ion. By understanding that the binding preference plays a role in the ability of the sensor to quantitatively determine metal ion concentration, it becomes possible to design sensors with other spiropyran derivatives that have different affinities to other metal ions. In this way, one can tune the sensors through molecular design, and by using the unique spectral response of each MC-M^{2+} complex, a single sensor can be fabricated that can simultaneously detect multiple metal ions in a solution.

References

1. Oehme, I. and O.S. Wolfbeis, *Microchim. Acta*, **1997**. *126*(3): p. 177.
2. Janata, J., M. Josowicz, P. Vanýsek and D.M. DeVaney, *Anal. Chem.*, **1998**. *70*(12): p. 179.
3. Andria, S.E., C.J. Seliskar and W.R. Heineman, *Anal. Chem.*, **2010**. *82*(5): p. 1720.
4. Szurdoki, F., D. Ren and D.R. Walt, *Anal. Chem.*, **2000**. *72*(21): p. 5250.
5. Liu, J., J.H. Lee and Y. Lu, *Anal. Chem.*, **2007**. *79*(11): p. 4120.
6. Basabe-Desmonts, L., J. Beld, R.S. Zimmerman, J. Hernando, P. Mela, M.F. García Parajó, N.F. van Hulst, A. van den Berg, D.N. Reinhoudt and M. Crego-Calama, *J. Am. Chem. Soc.*, **2004**. *126*(23): p. 7293.
7. Hassan, S.S.M. and M.M. Habib, *Anal. Chem.*, **1981**. *53*(3): p. 508.
8. McDonagh, C., C.S. Burke and B.D. MacCraith, *Chem. Rev.*, **2008**. *108*(2): p. 400.
9. Narayanaswamy, R.a.W., O., *Optical Sensors: Industrial, Environmental and Diagnostic Applications*. 2004, Berlin, Germany: Springer.
10. He, X. and G.A. Rechnitz, *Anal. Chem.*, **1995**. *67*(13): p. 2264.
11. Choi, M.M.F. and D. Xiao, *Anal. Chim. Acta*, **1999**. *387*(2): p. 197.
12. Gabor, G., S. Chadha and D.R. Walt, *Anal. Chim. Acta*, **1995**. *313*(1-2): p. 131.
13. Otto, M. and W. Wegscheider, *Anal. Chem.*, **1989**. *61*(17): p. 1847.
14. Vlasov, Y., A. Legin and A. Rudnitskaya, *Sens. Actuators, B*, **1997**. *44*(1-3): p. 532.

15. Y.K. Cheung, P., L.M. Kauvar, Å.E. Engqvist-Goldstein, S.M. Ambler, A.E. Karu and L.S. Ramos, *Anal. Chim. Acta*, **1993**. *282*(1): p. 181.

16. Dickinson, T.A., J. White, J.S. Kauer and D.R. Walt, *Nature*, **1996**. *382*(6593): p. 697.

17. Lavigne, J.J., S. Savoy, M.B. Clevenger, J.E. Ritchie, B. McDoniel, S.-J. Yoo, E.V. Anslyn, J.T. McDevitt, J.B. Shear and D. Neikirk, *J. Am. Chem. Soc.*, **1998**. *120*(25): p. 6429.

18. Abdullah, A., C.J. Roxburgh and P.G. Sammes, *Dyes Pigm.*, **2008**. *76*(2): p. 319.

19. Evans, L., G.E. Collins, R.E. Shaffer, V. Michelet and J.D. Winkler, *Anal. Chem.*, **1999**. *71*(23): p. 5322.

20. Byrne, R. and D. Diamond, *Nat. Mater.*, **2006**. *5*(6): p. 421.

21. Saragi, T.P.I., T. Spehr, A. Siebert, T. Fuhrmann-Lieker and J. Salbeck, *Chem. Rev.*, **2007**. *107*(4): p. 1011.

22. Hirshberg, Y., *J. Am. Chem. Soc.*, **1956**. *78*(10): p. 2304.

23. Byrne, R.J., S.E. Stitzel and D. Diamond, *J. Mater. Chem.*, **2006**. *16*(14): p. 1332.

24. Samanta, S. and J. Locklin, *Langmuir*, **2008**. *24*(17): p. 9558.

25. Suzuki, T., Y. Kawata, S. Kahata and T. Kato, *Chem. Commun.*, **2003**(16): p. 2004.

26. Stauffer, M.T. and S.G. Weber, *Anal. Chem.*, **1999**. *71*(6): p. 1146.

27. Chibisov, A.K. and H. Görner, *Chem. Phys.*, **1998**. *237*(3): p. 425.

28. Winkler, J.D., K. Deshayes and B. Shao, *J. Am. Chem. Soc.*, **1989**. *111*(2): p. 769.

29. Phillips, J.P., A. Mueller and F. Przystal, *J. Am. Chem. Soc.*, **1965**. *87*(17): p. 4020.

30. Fries, K., S. Samanta, S. Orski and J. Locklin, *Chem. Commun.*, **2008**(47): p. 6288.

31. Fries, K.H., J.D. Driskell, S. Samanta and J. Locklin, *Anal. Chem.*, **2010**. *82*(8): p. 3306.

32. Chung, D.-J., Y. Ito and Y. Imanishi, *J. Appl. Polym. Sci.*, **1994**. *51*(12): p. 2027.

33. Barker, M. and W. Rayens, *J. Chemom.*, **2003**. *17*(3): p. 166.

34. Brown, S.D., *Appl. Spectrosc.*, **1995**. *49*: p. 14A.

CHAPTER 5

THE ROLE OF DIFFERENT CHELATING GROUPS AND COMONOMERS ON THE MEROCYANINE-METAL ION INTERACTION IN SPIROPYRAN-CONTAINING COPOLYMER THIN FILMS[1]

---

[1] Fries, K. H.; Sheppard, G. R.; Locklin, J. To be submitted to *Macromolecules*.

Abstract

In this article, we describe the synthesis and characterization of spiropyran-containing copolymers that were used to study the influence of two different spiropyran derivatives, spiropyran methacrylate (SPMA) and spiropyran methacrylate with a methoxy substituent in the 8' position of the benzopyran ring (MEO), on divalent metal ion complexation. The comonomer with which spiropyran was polymerized is also varied between methyl methacrylate (MMA) and 2, 2, 2-trifluoroethyl methacrylate (TFEMA) to study the effect of the hydrophobicity on the binding of MC to metal ions. Fourier transform-infrared (FT-IR) spectroscopy was used to characterize the photoinduced conversion of spiropyran to merocyanine, as well as the merocyanine-metal ion (MC-M^{2+}) interaction. FT-IR spectra were analyzed using principal component analysis to elucidate the chemical binding environment between MC and the different metal ions. By means of UV-vis absorption spectroscopy, we demonstrate that each metal ion gives rise to a unique colorimetric response for the various spiropyran-containing copolymers studied.

Introduction

The design and synthesis of functional molecules that can serve as molecular devices for sensors is an area of intense research with potentially huge significance. Further, the development of optical methods for the detection of clinically and environmentally relevant analytes, including small molecules and metal ions has attracted a great deal of attention in recent years.[1, 2] Currently, optical sensors, or optodes, are based largely on solid phase immobilization matrices, where organic indicator dyes are adsorbed or encapsulated in a polymer matrix that is permeable to the analyte.[3-5] With these sensors, the analyte is not consumed, no reference is required, and there is minimal electrical and magnetic interference.[6-8] Several disadvantages exist, however, such as leaching of indicator dye, binding sites becoming blocked overtime, inadequate durability, fouling of the surface, and the sensor is typically one-time use.[9-12]

Byrne and Diamond have proposed that reversible sensors, which can switch between passive and active states, would offer a solution to many of the problems associated with using an organic indicator dye immobilized in a polymer matrix.[13] Spiropyrans, which are photochromic compounds that undergo reversible, light-induced structural changes, provide a strategy to accomplish this goal. Spiropyrans undergo a reversible photocleavage of the spiro C-O bond, which allows switching between a ring-closed, colorless spiropyran form and a ring-opened, strongly colored merocyanine form.[14, 15] The merocyanine structure exists as a resonance hybrid between a charged, zwitterionic form and a neutral quinoidal form. Metal ions can bind to the merocyanine through the negatively charged phenolate group of the zwitterionic form (Figure 5.1).[16-21]

This interaction is weak enough that upon exposure to visible light, ring-closing can still occur, yielding a molecular sensor that is capable of reversible ion sensing.

Several groups have used this negatively charged phenolic oxygen in the zwitterionic form to produce a moiety that can act as an effective ligand to bind to metal ions.[18-20] It also may be possible to synthesize spiropyran derivatives that can act as sensitive receptors for metal ions through careful functionalization of spiropyran with multiple binding sites placed in strategic positions of the aromatic ring, where the interaction of different chelating groups with the metal ions can be facilitated. There have been several reports of more complex spiropyran derivatives used to bind metal ions in solution, where there is generally a second chelating group or a crown ether attached to spiropyran to aid in metal ion binding.[22-29] In these reports, however, an in depth analysis of the interaction between ligand and metal ion has not been studied for a variety of metal ions. If the binding is better understood, it will become possible to tailor spiropyran-based receptors to selectively bind to specific metal ions. In previous work, we prepared thin films of spiropyran-containing copolymers that generate a unique and selective colorimetric response to different divalent metal ions.[30, 31] We have observed that by attaching the chromophore to the polymeric backbone, the stimuli-responsive nature of spiropyran is not only enhanced, but the microenvironment for the MC-M^{2+} complex, and therefore the colorimetric response, can be tuned by comonomer composition.

In this work, we investigated the interaction of merocyanine to different divalent metal ions by adding a second chelating group on the nitro ring of the chromophore, as well as by varying the comonomer with which spiropyran was polymerized. We fabricated a series of copolymers containing spiropyran moieties with controlled molecular weight and polydispersity using atom transfer radical polymerization (ATRP). We synthesized a spiropyran methacrylate with a methoxy substituent in the 8' position of the nitro ring (MEO) to study the effect of a second chelating group on metal ion binding. The composition of MEO contained in the polymer backbone was also varied from 10 to 100 mol% to investigate the influence of free volume and sterics on the photochromic response when a second chelating group is on the chromophore. We also investigated the impact of the comonomer, 2, 2, 2-trifluoroethyl methacrylate (TFEMA), on the metal ion binding by synthesizing spiropyran-containing copolymers with TFEMA and comparing these to methyl methacrylate (MMA) copolymers. By using a polymeric backbone, the microenvironment for the merocyanine-divalent metal ion (MC-M^{2+}) complex, and therefore the colorimetric response, can be tuned by polymer composition.

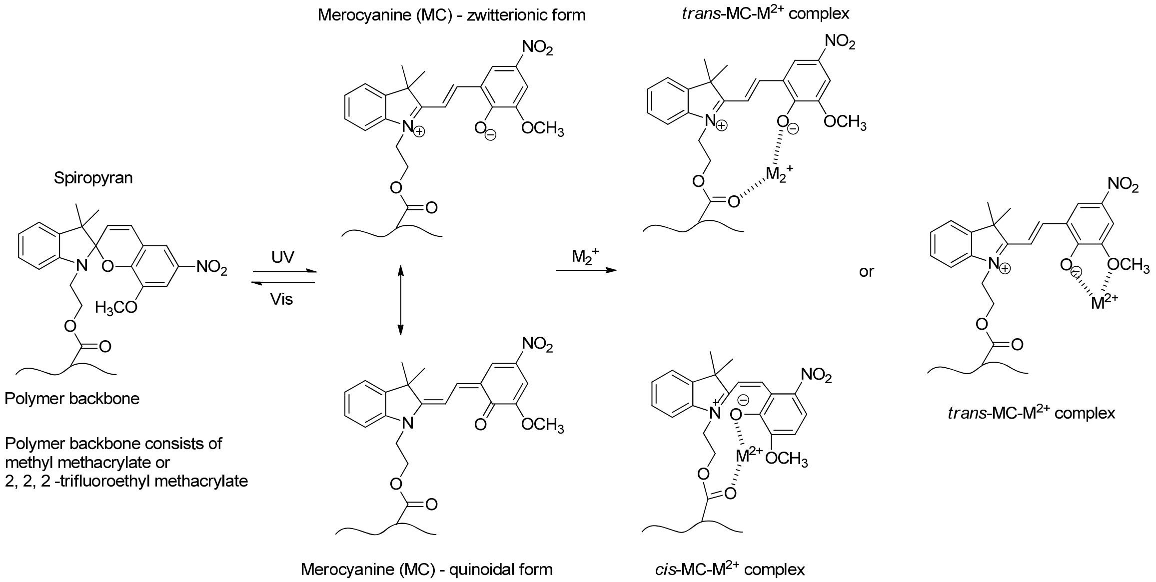

Figure 5.1. Isomeric structures of spiropyran and merocyanine and the MC-M^{2+} complex.

Experimental Section

Materials

Silicon wafers (orientation <100>, native oxide) were purchased from University Wafer. BK7 microscope slides (RI = 1.514) were purchased from VWR. THF, purchased from BDH, was distilled from sodium-ketyl. Methyl methacrylate (MMA), purchased from Alfa Aesar, and 2, 2, 2 – trifluoroethyl methacrylate (TFEMA), purchased from Sigma Aldrich, were flashed through a basic alumina column to remove inhibitor and degassed before polymerization. 2-Hydroxy-3-methoxybenzaldehyde, methacrylic acid, and diethyl azodicarboxylate were purchased from Alfa Aesar and used as received. Triphenylphosphine was purchased from TCI and used as received. Ethanol and glacial acetic acid were purchased from EMD, and methanol, chloroform, hexane, and ethyl acetate were purchased from BDH. All metal salts were purchased from either TCI or Alfa Aesar and used as received. N, N, N', N'', N''-pentamethyldiethylenetriamine (PMDETA) and ethyl-2-bromoisobutyrate (Et2BriB) were purchased from either TCI or Alfa Aesar and degassed prior to polymerization.

Synthesis of Spiropyran Methyl Methacrylate (SPMA)

1-(2-Hydroxyethyl)-3-dimethyl-6-nitrospiro(2H-1-benzopyran-2,2-indole) (SP alcohol)[14] was subsequently coupled to methacrylic acid following standard procedures.[32]

Synthesis of 2-Hydroxy-3-Methoxy-5-Nitrobenzaldehyde

6.00 g (39.4 mmol) of 2-hydroxy-3-methoxybenzaldehyde were added to 40 mL of glacial acetic acid. The solution was cooled to 15 $^{\circ}$C with an ice-water bath. A solution of 2.63 mL (63.16 mmol) of concentrated nitric acid and 6.10 mL (106 mmol) of glacial acetic acid was added dropwise over an hour. An orange precipitate formed. The solution was allowed to warm to room temperature and left to stir overnight. The precipitate was filtered, washed with ethanol, and dried on high vacuum. The yellow solid was used without further purification. Yield: 4.5g (75%) ^{1}H NMR (300 MHz, DMSO-d_6) δ (ppm): 10.36 (s, 1H); 8.13 (s, 1H); 7.95 (s, 1H); 4.02 (s, 3H).

Synthesis of Methoxy-Substituted Spiropyran Methacrylate (MEO)

2-(8-Methoxy-3',3'-dimethyl-6-nitrospiro[chromene-2,2'-indolin]-1'-yl)ethanol (MEO-OH) was subsequently coupled to methacrylic acid. 4.00 g (10.5 mmol) of MEO-OH and 4.95 g (18.8 mmol) of triphenylphosphine were added to 70 mL of dry THF. The solution was cooled to 0 °C. 1.60 mL (18.8 mmol) of methacrylic acid were added, and the solution was stirred for 20 min. While the reaction mixture was still at 0 °C, a solution of 3.03 mL (18.8 mmol) of diethyl azodicarboxylate and 10 mL of dry THF was added dropwise over one hour. The reaction mixture was stirred at room temperature for 24 h. The solution was concentrated to dryness using a rotary evaporator. A blue solid was isolated by column chromatography on a neutral alumina column using hexane:ethyl acetate (4:1 v/v) as the eluent. Yield: 3.5 g (87.5%) ^{1}H NMR (300 MHz, $CDCl_3$) δ (ppm): 7.68 (s, 1H); 7.61 (s, 1H); 7.18 (t, 1H); 7.06 (d, 1H); 6.87-6.70 (m, 3H); 6.05 (s, 1H); 5.82 (s, 1H); 5.54 (d, 1H); 4.29 (m, 2H); 3.75 (s, 3H); 3.57 (m, 1H); 3.48 (1H); 1.90 (3H); 1.27 (s, 3H); 1.15 (s, 3H).

Synthesis of Poly(MMA$_{90}$-co-MEO$_{10}$)

MEO (0.408 g, 0.906 mmol), MMA (0.816 g, 8.15 mmol), CuBr (0.005 g, 0.035 mmol), and Et2BriB (0.007 g, 0.035 mmol) were added to a dry, 25 mL schlenk flask. Anhydrous THF (5 mL) was then added, and the solution was degassed under Ar for 2 h. After degassing, PMDETA (0.060 g, 0.346 mmol), which was also degassed under Ar for 2 h, was added to the reaction mixture. The rubber septum on the schlenk flask was then replaced with a glass stopper while still under Ar to avoid any possible oxygen poisoning. The reaction was then placed in an oil bath for 16 h at 65 ºC. The flask was then opened and exposed to air. The solution was precipitated in approximately 50 mL of cold methanol, and the precipitate was filtered through a medium frit funnel. The polymer was re-dissolved in THF and the precipitation repeated. A blue powder was collected (M_w = 29,997 kDa, M_n = 29,103 kDa, M_w/M_n = 1.031, as obtained by gel permeation chromatography). ^{1}H NMR (500 MHz, $CDCl_3$) δ (ppm): 8.14 (s, 0.3H); 7.70 (s, 1.4H); 7.62 (s, 1.1H); 7.18 (s, 1.2H); 7.07 (s, 1.2H); 6.89 (s, 2.5H); 6.67 (d, 0.8H); 5.84 (s, 1H); 4.06 (s, 3.6H); 3.90 (s, 1.2H); 3.75 (s, 5.5H); 3.59 (s, 17.7H); 3.51 (s, 9H); 1.79 (m, 17.4H); 1.59 (s, 3.8H); 1.40 (s, 1.8H); 1.27 (s, 5.1H); 1.17 (s, 5.2H); 1.01 (s, 9.2H); 0.81 (s, 17.1H).

Synthesis of Poly(MMA$_{70}$-co-MEO$_{30}$)

MEO (0.817 g, 1.81 mmol), MMA (0.452 g, 4.52 mmol), CuBr (0.005 g, 0.035 mmol), and Et2BriB (0.007 g, 0.035 mmol) were added to a dry, 25 mL schlenk flask. Anhydrous THF (5 mL) was then added, and the solution was degassed under Ar for 2 h. After degassing, PMDETA (0.060 g, 0.346 mmol), which was also degassed under Ar for 2 h, was added to the reaction mixture. The rubber septum on the schlenk flask was then replaced with a glass stopper while still under Ar to avoid any possible oxygen poisoning. The reaction was then placed in an oil bath for 16 h at 65 ºC. The flask was then opened and exposed to air. The solution was precipitated in approximately 50 mL of cold methanol, and the precipitate was filtered through a medium frit funnel. The polymer was re-dissolved in THF and the precipitation repeated. A blue powder was collected (M_w = 35,498 kDa, M_n = 33,467 kDa, M_w/M_n = 1.061, as obtained by gel permeation chromatography). ^{1}H NMR (500 MHz, $CDCl_3$) δ (ppm): 8.12 (s, 0.3H); 7.61 – 7.17 (d, 2.4H); 7.08-7.17 (d, 2.8H); 6.87 (s, 2.8H); 6.66 (d, 1H); 6.47 (s, 0.2H); 5.85 (s, 1H); 4.05 (s, 2H); 3.88 (s, 0.9H); 3.72 (s, 3.2H); 3.59 (s, 6.3H); 3.51 (s, 8.3H); 1.78 (m, 7.4H); 1.57 (s, 1.3H); 1.40 (s, 1.2H); 1.27 (m, 4.3H); 1.17 (s, 5.8H); 0.98 (s, 4.8H); 0.81 (s, 8.7H).

Synthesis of Poly(TFEMA$_{90}$-co-MEO$_{10}$)

MEO (0.408 g, 0.906 mmol), TFEMA (1.37 g, 8.15 mmol), CuBr (0.005 g, 0.035 mmol), and Et2BriB (0.007 g, 0.035 mmol) were added to a dry, 25 mL schlenk flask. Anhydrous THF (5 mL) was then added, and the solution was degassed under Ar for 2 h. After degassing, PMDETA (0.060 g, 0.346 mmol), which was also degassed under Ar for 2 h, was added to the reaction mixture. The rubber septum on the schlenk flask was then replaced with a glass stopper while still under Ar to avoid any possible oxygen poisoning. The reaction was then placed in an oil bath for 16 h at 65 ºC. The flask was then opened and exposed to air. The solution was precipitated in approximately 50 mL of cold methanol, and the precipitate was filtered through a medium frit funnel. The polymer was re-dissolved in THF and the precipitation repeated. A blue powder was collected (M_w = 110,832 kDa, M_n = 95,983 kDa, M_w/M_n = 1.155, as obtained by gel permeation chromatography). ^{1}H NMR (500 MHz, $CDCl_3$) δ (ppm): 8.14 (s, 0.4H); 7.73 (d, 1.5H); 7.63 (m, 1.8H); 7.19 (m, 1.8H); 7.08 (m, 2H); 6.95 (s, 0.6H); 6.86 (m, 3.4H); 6.67 (m, 3.4H); 6.47 (s, 0.5H); 5.84 (d, 1H); 4.34 (s, 35H); 4.05 (d, 3.3H); 3.94 (d, 1.5H); 3.75 (m, 7.1H); 3.50 (d, 4.3H); 1.84 – 2.00 (m, 32.5H); 1.61 (s, 7.3H); 1.47 (s, 3.2H); 1.40 (s, 2.6H); 1.27 (m, 7.1H); 1.16 (m, 7H); 1.08 (s, 18H); 0.93 (m, 34H).

Synthesis of Poly(TFEMA$_{50}$-co-MEO$_{50}$)

MEO (0.785 g, 1.74 mmol), TFEMA (0.29 g, 1.73 mmol), CuBr (0.005 g, 0.035 mmol), and Et2BriB (0.007 g, 0.035 mmol) were added to a dry, 25 mL schlenk flask. Anhydrous THF (5 mL) was then added, and the solution was degassed under Ar for 2 h. After degassing, PMDETA (0.060 g, 0.346 mmol), which was also degassed under Ar for 2 h, was added to the reaction mixture. The rubber septum on the schlenk flask was then replaced with a glass stopper while still under Ar to avoid any possible oxygen poisoning. The reaction was then placed in an oil bath for 16 h at 65 ºC. The flask was then opened and exposed to air. The solution was precipitated in approximately 50 mL of cold methanol, and the precipitate was filtered through a medium frit funnel. The polymer was re-dissolved in THF and the precipitation repeated. A blue powder was collected (M_w = 37,842 kDa, M_n = 27,700 kDa, M_w/M_n = 1.366, as obtained by gel permeation chromatography). ^{1}H NMR (500 MHz, $CDCl_3$) δ (ppm): 8.14 (s, 0.6H); 7.61 – 7.67 (d, 3H); 7.08 – 7.13 (d, 3.7H); 6.85 (s, 3.8H); 6.64 (s, 1.1H); 6.50 (s, 0.3H); 5.80 (s, 1H); 4.32 (s, 5.4H); 4.05 (s, 2.8H); 3.84 (s, 1.2H); 3.70 (s, 5H); 3.38 – 3.52 (d, 3.5H); 1.85 (m, 7.9H); 1.38 (s, 2H); 1.26 (s, 5.1H); 1.14 (s, 8.6H); 0.85 (d, 8.2H).

Synthesis of Poly(TFEMA$_{90}$-co-SPMA$_{10}$)

SPMA (0.381 g, 0.906 mmol), TFEMA (1.37 g, 8.15 mmol), CuBr (0.005 g, 0.035 mmol), and Et2BriB (0.007 g, 0.035 mmol) were added to a dry, 25 mL schlenk flask. Anhydrous THF (5 mL) was then added, and the solution was degassed under Ar for 2 h. After degassing, PMDETA (0.060 g, 0.346 mmol), which was also degassed under Ar for 2 h, was added to the reaction mixture. The rubber septum on the schlenk flask was then replaced with a glass stopper while still under Ar to avoid any possible oxygen poisoning. The reaction was then placed in an oil bath for 16 h at 65 ºC. The flask was then opened and exposed to air. The solution was precipitated in approximately 50 mL of cold methanol, and the precipitate was filtered through a medium frit funnel. The polymer was re-dissolved in THF and the precipitation repeated. A pink powder was collected (M_w = 120,265 kDa, M_n = 71,040 kDa, M_w/M_n = 1.693, as obtained by gel permeation chromatography). ^1H NMR (500 MHz, $CDCl_3$) δ (ppm): 8.02 (s, 2H); 7.42 (s, 1H); 7.09 – 7.19 (d, 1H); 6.91 (s, 2H); 6.77 (m, 2H); 5.87 (s, 1H); 4.34 (s, 20H); 4.06 (s, 2H); 3.75 (s, 3.4H); 3.38 – 3.50 (d, 2H); 1.85 – 2.16 (m, 24H); 1.54 (s, 19H); 1.29 (d, 5H); 1.17 (s, 5H); 1.09 (s, 10H); 0.92 (d, 21H).

Synthesis of Poly(MEO)

MEO (0.845 g, 3.49 mmol), CuBr (0.005 g, 0.035 mmol), and Et2BriB (0.007 g, 0.035 mmol) were added to a dry, 25 mL schlenk flask. Anhydrous THF was then added, and the solution was degassed under Ar for 2 h. After degassing, PMDETA (0.060 g, 0.346 mmol), which was also degassed under Ar for 2 h, was added to the reaction mixture. The rubber septum on the schlenk flask was then replaced with a glass stopper while still under Ar to avoid any possible oxygen poisoning. The reaction was then placed in a 65 ºC oil bath for 16 h. The flask was then opened and exposed to air. The solution was precipitated in approximately 50 mL of cold methanol. Precipitate was filtered through a medium frit funnel. It was then re-dissolved in THF and the procedure was repeated. A blue powder was collected (unable to determine molecular weight using gel-permeation chromatography, and end group analysis was not possible with ^1H NMR). ^1H NMR (500 MHz, $CDCl_3$) δ (ppm): 8.11 (s, 0.2H); 7.54 (s, 2.5H); 6.44 – 7.00 (m, 7H); 5.76 (s, 1H); 4.00 (s, 2.5H); 3.50 (d, 7.7H); 1.62 – 1.85 (m, 2.3H); 1.23 (s, 3.8H); 1.09 (s, 4.6H); 0.75 (s, 3.3H).

Characterization

Fourier transform-infrared (FT-IR) measurements were taken with a Nicolet model 6700 instrument with a grazing angle attenuated total reflectance accessory (GATR, Harrick Scientific) at 264 scans with 4 cm^{-1} resolution. UV-vis spectroscopy was performed on a Cary 50 spectrophotometer (Varian). Number and weight average molecular weights of all polymers were estimated using gel permeation chromatography (Viscotek, Malvern Inc.) with two high molecular weight columns (I-MBHMW-3078) and one low molecular weight column (I-MBLMW-3078). Triple point detection, consisting of refractive index, light scattering, and viscometry, was used. Polystyrene standards were used to determine molecular weights from universal calibration. The film thickness was measured using null ellipsometry performed on a Multiskop (Optrel GbR) with a 632.8 nm He-Ne laser beam as the light source. Both δ and ψ value thickness data were measured and calculated by integrated specialized software. At least three measurements were taken for each wafer and the average thickness recorded.

Light Source

An OmniCure, series 1000 (EXFO, Inc.) with 365 nm wavelength light, was used as the UV light source. The substrates were held 2 cm from the source and irradiated at a power of 30 mW/cm^2. The visible light source was a Fiber-Lite Model with a 30 W quartz halogen fiber optic illuminator.

Spin-Coating Polymer Films on Silicon and Glass Substrates

Silicon wafers and glass substrates were cut into approximately 1 x 1 cm^2 squares. They were sonicated in isopropanol for 5 min and blown dry with a stream of nitrogen. A solution of 15 mg of polymer in 1 mL $CHCl_3$ (filtered with a 0.2 μm poly(tetrafluoroethylene) filter) was spin-coated on the clean substrates at 1600 rpm for 30 s (Chemat Technology Spin Coater KW-4A). The thickness of the films was held constant at 80 nm for each experiment, as measured by ellipsometry.

Merocyanine-Metal Ion Complexation Experiments

Initial UV-vis spectra and GATR-FT-IR spectra were recorded for the spin-coated film before UV irradiation. The substrate was then irradiated with 365 nm light for 1 minute, and a UV-vis spectrum and GATR-FT-IR spectrum were recorded for the merocyanine form. The substrate was then immersed in a 25 mM solution of metal(II) chloride in degassed ethanol for 3 min, blown dry under a stream of nitrogen, and UV-vis and GATR-FT-IR spectra recorded.

Chemometric Data Analysis

FT-IR and UV-visible absorption spectra were analyzed using chemometric methods to aid in spectral interpretation with respect to molecular conformation. MATLAB 7.5 environment (The Mathworks, Inc., Natick, MA) was utilized for spectral pretreatment and principal component analysis (PCA).

Spectral Preprocessing

Several spectroscopic pretreatments were investigated to optimize qualitative and quantitative predictive models. Spectral range, baseline correction, normalization, mean centering, and combinations of these steps were explored to optimize the PCA models.

Using a leave-one-out cross validation algorithm, minimization of the root-mean-square error of cross validation (RMSECV) was used as the criterion to identify the optimum preprocessing steps. Optimal preprocessing of the IR dataset consisted of analyzing the spectral range of 1000-1800 cm^{-1} by taking the 2nd derivative of each spectrum using a fifteen-point, 2nd-order polynomial Savitzky-Golay algorithm, followed by normalization to unit-vector length and mean centering.

Principal Component Analysis

PCA was used as an unsupervised method to explore variation in the sample spectra and to visualize clustering of similar spectra.[33] PCA models were built using the IR data for pre- and post-UV irradiated polymer films and FT-IR spectra for the polymer films complexed to each of the six metal ions, as well as the nonbinding polymer film. Principal component (PC) scores plots were constructed to search for clustering of samples according to their identity. Loadings plots for the FT-IR datasets identified the spectral bands responsible for spectral variation to aid interpretation of conformational changes due to metal ion complexation and determine differences in binding among the metal ions.

Results and Discussion

Design and Synthesis of the Chromophore

Figure 5.2 outlines the synthetic pathway to the **MEO** monomer. A methoxy substituent in the 8' position on the benzopyran ring has previously been used in several spiropyran derivatives aimed at metal ion coordination.[20, 22, 34, 35] This functional group can cooperate with the phenolate anion of the ring-opened merocyanine in the binding of metal ions. The nitrogen on the indol ring can also be functionalized, and as such, methacrylic acid was coupled to **MEO-OH** to yield a **MEO**-methacrylate derivative. This serves two purposes: 1) provides a means for polymerization by atom transfer radical polymerization, and 2) adds another potential chelating moiety with the carbonyl on the ester side chain.

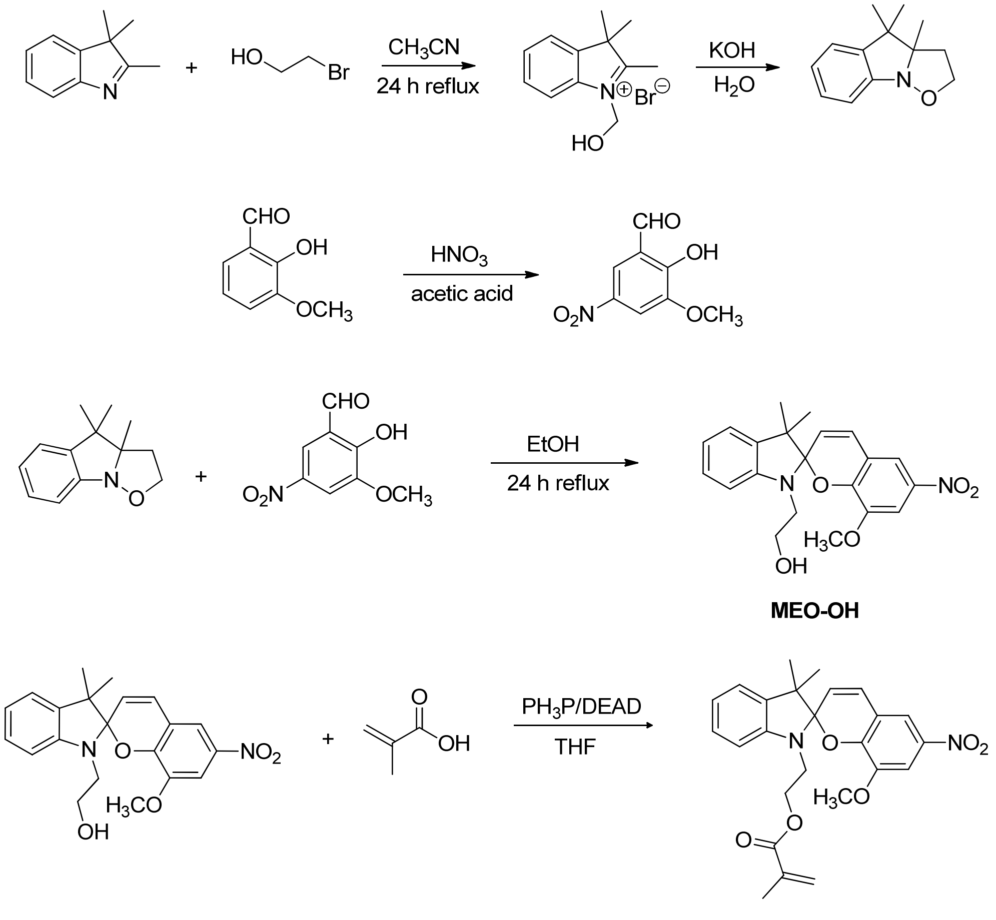

Figure 5.2. Synthetic route to **MEO** monomer.

Solution Polymerization

The SPMA or MEO monomer was copolymerized with either MMA or TFEMA at various concentrations using atom transfer radical polymerization (Figure 5.3). The content of either SPMA or MEO in the backbone of the copolymer and the molecular weight of each copolymer are summarized in Table 5.1. In each polymerization, the mol% of SPMA or MEO content found in the copolymer compares well to the monomer feed composition, as determined by integration of NMR resonances for each monomer on the polymer backbone (Figures C-1 - C-5 in Appendix C). The table shows that the experimental M_n determined by gel permeation chromatography agrees well with the theoretical M_n for the most of the copolymer ratios. This combined with the low polydispersity indicates a living polymerization.

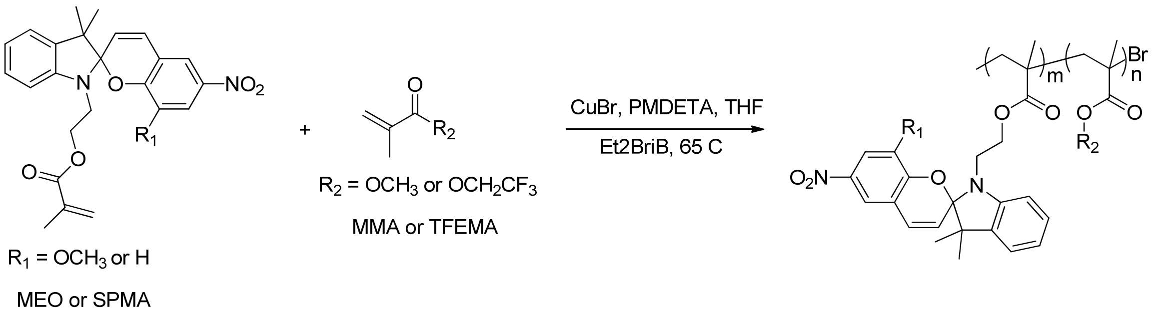

Figure 5.3. ATRP copolymerization conditions and structure of copolymers.

Table 5.1. Content of MEO or SPMA in copolymer.

Polymer	Content of SPMA or MEO in monomer feed	Content of SPMA or MEO in copolymer (mol %)[a]	M_w[b]	M_n[b]	M_w/M_n[b]	Theoretical M_n
poly(MMA_{90}-*co*-MEO_{10})	10	14	29 997	29 103	1.031	34 559
poly(MMA_{70}-*co*-MEO_{30})	30	33	35 498	33 467	1.061	36 332
poly($TFEMA_{90}$-*co*-MEO_{10})	10	10	110 832	95 983	1.155	50 953
poly($TFEMA_{50}$-*co*-MEO_{50})	50	38	37 842	27 700	1.366	30 794
poly($TFEMA_{90}$-*co*-$SPMA_{10}$)	10	9	120 265	71 040	1.693	50 173
poly(MEO)	100	100	*	*	*	27 367

[a] Calculated from ^{1}H NMR (Figures C-1 – C-6 in Appendix C). [b] Average molecular weight was obtained by gel-permeation chromatography (GPC). * Unable to determine molecular weight using GPC, and end group analysis was not possible by ^{1}H NMR.

In a previous study, we polymerized SPMA-MMA copolymers containing different concentrations of spiropyran to investigate the influence of free volume and sterics on the photochromic response of the MC-M^{2+} complex.[31] As the concentration of SPMA in the polymer backbone is increased, the chromophore is more sterically hindered and less accessible to accommodate binding to metal ions. In this work, we varied the concentration of MEO in the backbone when copolymerized with either MMA or TFEMA. We hypothesize that with MEO-containing copolymers, the metal ions will coordinate to the methoxy substituent on the nitro ring, along with the phenolate anion, and not involve the carbonyl on the ester side chain (Figure 5.1). If this is the case, merocyanine will not need to form a "binding pocket" around the metal ions, and increasing the concentration of MEO in the copolymer should have very little effect on the response of the MC-M^{2+} complex. TFEMA was used as a comonomer to study the effects of a more hydrophobic polymer on metal ion binding. It was found that poly($TFEMA_{90}$-*co*-MEO_{10}) provided a more unique colorimetric response for each MC-M^{2+} complex than did poly(MMA_{90}-*co*-MEO_{10}). For the purposes of studying the binding interaction of MC to the metal ions for the MEO-containing copolymers, TFEMA was used as the comonomer.

Photoinduced Conversion of SP to MC

The ring-opening of SP to MC in the copolymer thin films was monitored by GATR-FT-IR. Figure 5.4 shows the FT-IR spectra of the ring-closed SP and the ring-opened MC for the poly($TFEMA_{90}$-co-MEO_{10}) thin film which was spin-coated on a Si/SiO_2 wafer from $CHCl_3$. The thickness of the film was held constant at 80 nm for each experiment. Bands that are particularly important are the tertiary C-N stretching band at 1340 cm^{-1} and the C-C-N bend at 1070 cm^{-1} which disappeared upon UV irradiation, while new bands emerged at 1592, 1456, and 1311 cm^{-1} that are assigned to the $C=N^+$, $C-O^-$, and $C-N^+$, respectively. Also, the symmetrical stretching band of the aryl nitro group shifted to lower energy from 1525 to 1519 cm^{-1} upon irradiation due to the increased conjugation brought about in the planar merocyanine. Other bands that are important to note are the symmetric and asymmetric alkyl aryl ether ($-OCH_3$) at 1282 and 1118 cm^{-1}, respectively. Complete characterization and assignments are listed in Table 5.2.

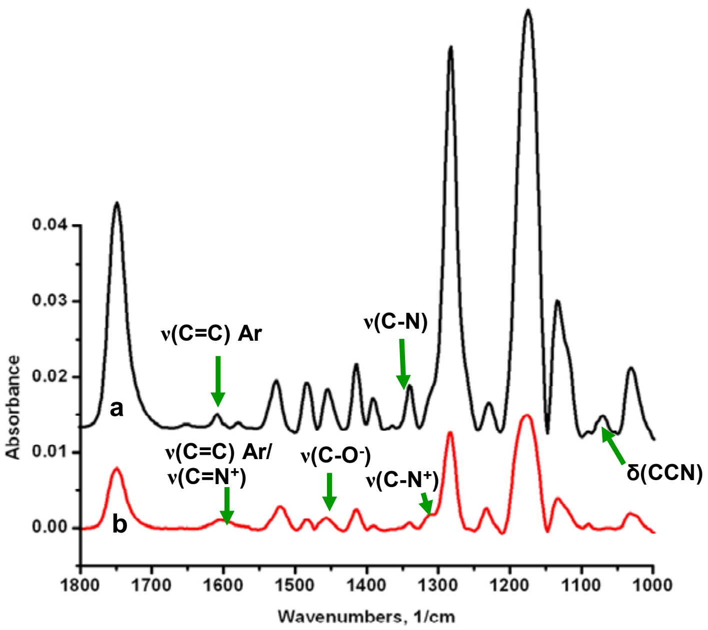

Figure 5.4. FT-IR spectra of poly(TFEMA$_{90}$-*co*-MEO$_{10}$) (a) before UV irradiation and (b) after UV irradiation. Peaks that indicate the photoconversion of spiropyran to merocyanine are labeled.

Table 5.2. Main FT-IR frequencies for poly(TFEMA$_{90}$-*co*-MEO$_{10}$) before (spiropyran) and after (merocyanine) UV irradiation.

	Spiropyran	**Merocyanine**
Assignments	**Wavenumbers (cm^{-1})**	**Wavenumbers (cm^{-1})**
C=O	1748	1748
Ar C=C	1655	-
Ar C=C	1608	1608
C=N$^+$	-	1592
NO$_2$ sym stretch	1525	1519
C-O$^-$	-	1456
NO$_2$ asym stretch	1340	1340
C-N (tertiary) stretch	1340	-
C-N$^+$	-	1311
OCH$_3$ sym stretch	1282	1283
C-F stretch	1282	1283
C-O-C ether sym stretch	1282	-
TFEMA	1230	1228
C-O-C ether asym stretch	1174	-
C-O ester stetch (TFEMA and SPMA)	1174	1173
C-O ester stretch (TFEMA)	1133	1133
OCH$_3$ asym stretch	1118	1118
C-O ester (SPMA)	1090	1090
C-C-N bend	1070	-

Principal component analysis was used to analyze the FT-IR spectra for multiple spin-coated films of poly(TFEMA$_{90}$-*co*-MEO$_{10}$) before and after UV irradiation. PCA involves finding combinations of latent variables, or factors, which describe the key trends in the data. It computes a new orthogonal coordinate system from the latent variables, such that new principal component (PC) axes, which are linear combinations of the original, *n*, axes, describe the maximum variance in the data set. PCA allows visualization of clusters of similar spectra to assess spectral reproducibility, identification of different sample types, and identification of variables responsible for spectral differences that can be interpreted with respect to chemical or physical phenomenon. For each data set, FT-IR spectra were obtained before and after UV irradiation for five poly(TFEMA$_{90}$-*co*-MEO$_{10}$) spin-coated films. The spectra were preprocessed using standard methods described above (experimental section) prior to performing PCA. A single principal component, PC1, describes 95.2 % of the spectral variance in the dataset. A plot of the scores on PC1 shows an obvious separation in the spectra acquired before and after UV irradiation (Figure 5.5). In addition, spectra collected for the same sample type cluster tightly, indicating the reproducibility in the preparation method of the thin films, as well as the consistency of the photoinduced conversion from SP to MC.

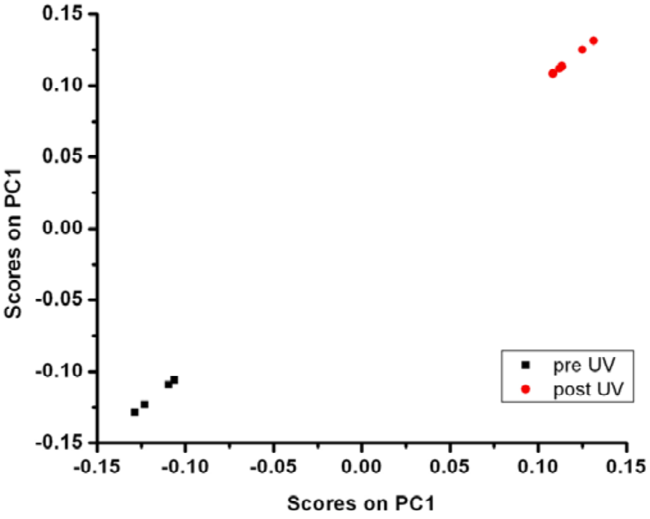

Figure 5.5. Scores plot for PC1 computed from the FT-IR spectra of poly(TFEMA$_{90}$-*co*-MEO$_{10}$) before UV irradiation (black) and after UV irradiation (red) for independently prepared films.

Evaluation of the loadings on PC1 provides information regarding the contribution of each wavenumber in the FT-IR spectra to the newly defined PC1 axis. Effectively, these are the wavenumbers responsible for the observed separation along PC1. The PC1 loadings plot (Figure 5.6) identifies the bands corresponding to the C-N$^+$, tertiary C-N, and symmetric NO_2 stretches (1311, 1340, and 1525 cm^{-1}, respectively) as the most significant variation between pre- and post-UV irradiation. The band assigned to the asymmetric C-O-C ether stretch at 1174 cm^{-1} can also be identified. The symmetric C-O-C ether stretch is masked by the strong C-F stretch of the TFEMA copolymer (1282 cm^{-1}), so no change in this band is observed upon UV irradiation. It is important to note that the phenolate anion stretch is also masked by a band from TFEMA, and as such, the appearance of the phenolic oxygen cannot be seen in the FT-IR spectra. These results are consistent with the ring-opening of SP to MC and the results provided in Table 5.2.

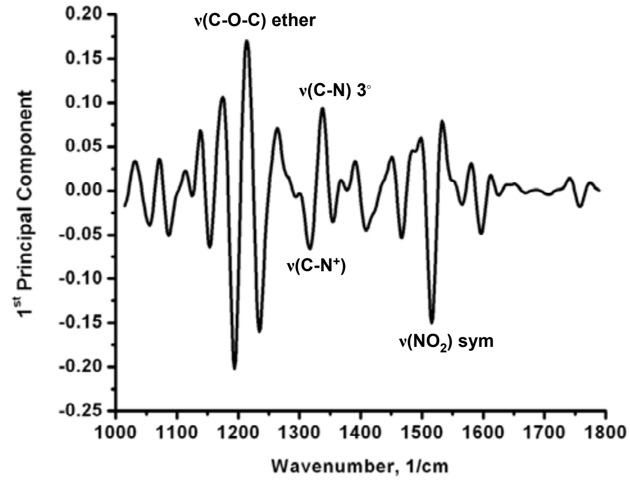

Figure 5.6. Loadings plot for PC1 computed from spectra of pre- and post-UV irradiated poly(TFEMA$_{90}$-*co*-MEO$_{10}$).

Ultimately, the purpose of this polymer design is to investigate the effect of a second chelating group on the nitro ring on the MC-M^{2+} complex and compare the complex in MEO-containing copolymers with SPMA-containing copolymers; as such, GATR-FT-IR was also used to characterize the photoinduced conversion of SP to MC for poly(TFEMA$_{90}$-*co*-SPMA$_{10}$) thin films (Figure 5.7). Again, the copolymers were spin-coated onto Si/SiO$_2$ wafers from CHCl$_3$, and the thickness was held constant at 80 nm. Complete characterization and assignments for poly(TFEMA$_{90}$-*co*-SPMA$_{10}$) are listed in Table 5.3. PCA was also used to analyze the FT-IR spectra and identify the bands that are important to the ring-opening process. One principal component, PC1, describes 96.8% of the spectral variance in the data set. Figure 5.8 shows a plot of the scores on PC1, where there is a distinct separation between the spectra of the ring-closed spiropyran and the spectra of the ring-opened merocyanine. The loadings on PC1 are plotted in Figure 5.9 and show that the bands identified as important to the ring-opening process are very similar to those identified for the poly(TFEMA$_{90}$-*co*-MEO$_{10}$) thin film (Figure 5.6). In both cases, the tertiary C-N stretching band and the C-N$^+$ stretching band are identified as the most significant to the variation between pre- and post-UV irradiation. Again, the disappearance of the asymmetrical C-O-C ether stretch (1174 cm^{-1}) and the shift to lower energy of the symmetric aryl nitro stretch upon UV irradiation are also identified as important to the ring-opening process.

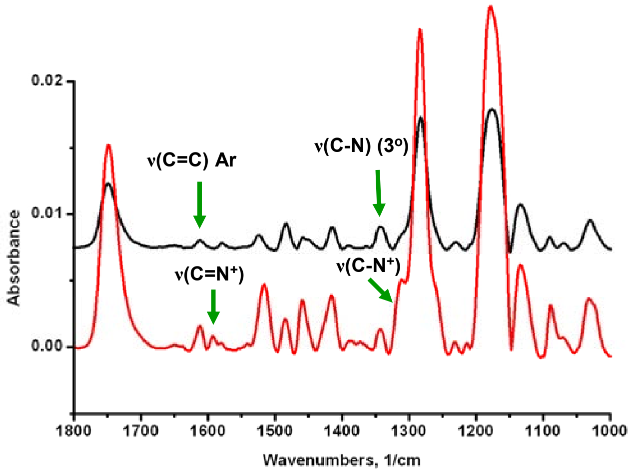

Figure 5.7. FT-IR spectra of poly(TFEMA$_{90}$-*co*-SPMA$_{10}$) (a) before UV irradiation and (b) after UV irradiation. Peaks that indicate the photoconversion of spiropyran to merocyanine are labeled.

Table 5.3. Main FT-IR frequencies for poly(TFEMA$_{90}$-*co*-SPMA$_{10}$) before (spiropyran) and after (merocyanine) UV irradiation.

	Spiropyran	**Merocyanine**
Assignments	**Wavenumbers (cm^{-1})**	**Wavenumbers (cm^{-1})**
C=O	1748	1748
C=N$^+$	-	1592
NO$_2$ sym stretch	1525	1519
C-O$^-$	-	1456
NO$_2$ asym stretch	1340	1340
C-N (tertiary) stretch	1342	-
C-N$^+$	-	1311
OCH$_3$ sym	1282	1283
C-F stretch	1282	1283
C-O-C ether sym stretch	1282	-
TFEMA	1230	1228
C-O-C ether asym stretch	1174	-
C-O ester stetch (TFEMA and SPMA)	1174	1173
C-O ester stretch (TFEMA)	1133	1133
OCH$_3$ aysm	1118	1118
C-O ester (SPMA)	1090	1090
C-C-N bend	1070	-

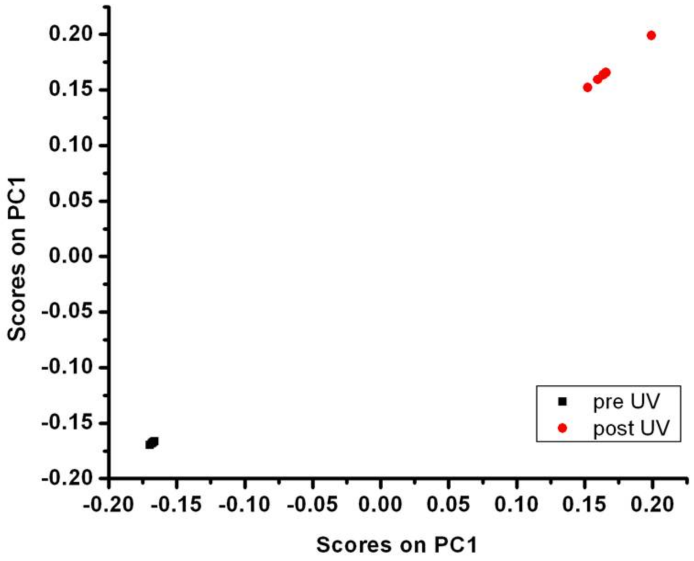

Figure 5.8. Scores plot for PC1 computed from the FT-IR spectra of poly(TFEMA$_{90}$-*co*-SPMA$_{10}$) before UV irradiation (black) and after UV irradiation (red) for independently prepared films.

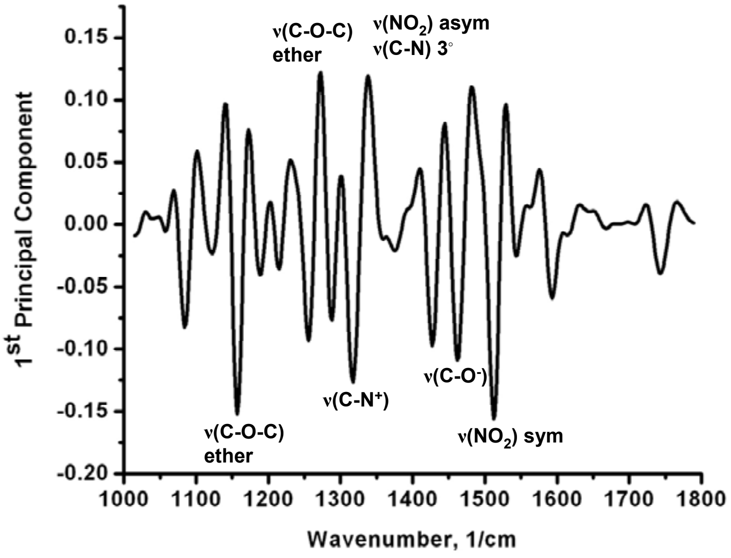

Figure 5.9. Loadings plot for PC1 computed from spectra of pre- and post-UV irradiated poly(TFEMA$_{90}$-*co*-SPMA$_{10}$).

UV-Vis Studies of the MC-M^{2+} Complex

In order to examine and compare the MC-M^{2+} complex for the different copolymers studied, UV-vis absorbance spectra were recorded for each of the spin-coated polymer films before and after UV irradiation. The substrates were then immersed in a 25 mM solution of metal(II) chloride in ethanol for 1 min and blown dry with nitrogen prior to recording UV-vis absorption spectra. Figure 5.10 shows the UV-vis spectra of poly(MMA_{90}-*co*-MEO_{10}) in response to different divalent metal ions. As can be seen from the figure, the colorless, ring-closed spiropyran (SP trace) was characterized by an absorption tail below 400 nm. After the photoinduced change to the ring-opened merocyanine, the copolymer thin film was characterized by an intense absorption band at λ_{max} = 600 nm, with a second band centered at 396 nm. Upon complexation with each divalent metal ion, there is a decrease in the long wavelength absorbance band, accompanied by a hypsochromic shift in absorbance maxima, which is dependent upon the metal ion contained in the solution. The MC-Fe^{2+}, MC-Cu^{2+}, and MC-Zn^{2+} complexes for the poly(MMA_{90}-*co*-MEO_{10}) have very similar absorbance bands of λ_{max} = 501 nm, λ_{max} = 506 nm, and λ_{max} = 512 nm, respectively, while the MC-Co^{2+} and MC-Ni^{2+} complexes provide the smallest hypsochromic shifts in absorbance maxima of 69 nm (λ_{max} = 531 nm) and 31 nm (λ_{max} = 569 nm), respectively. This shift to higher energy accompanying binding is attributed to the disruption of planarity of the *trans*-MC^{2+} that occurs upon complexation.[31, 36]

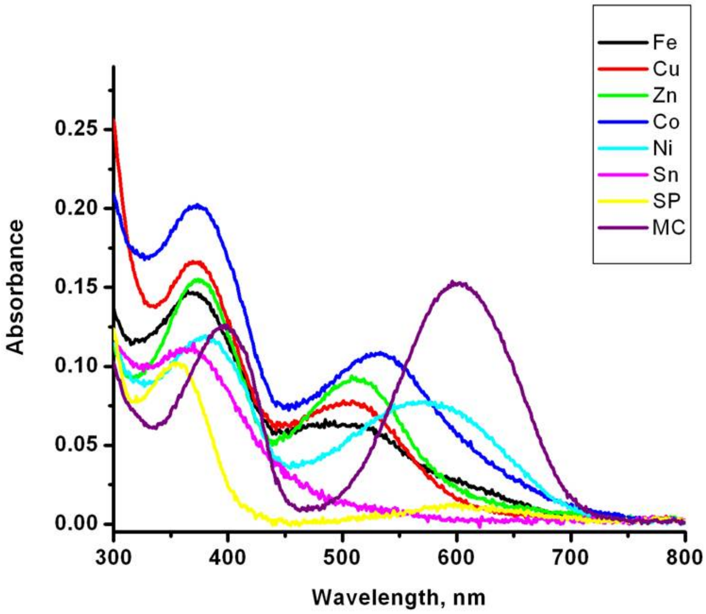

Figure 5.10. UV-vis absorbance spectra of poly(MMA_{90}-*co*-MEO_{10}) in the presence of different divalent metal ions: Fe, Cu, Zn, Co, Ni, Sn. SP and MC refer to the absorbance spectra of the polymer thin films in the ring-closed (SP) and ring-opened (MC) state.

In comparing the colorimetric response of these MC-M^{2+} complexes to that of poly(MMA_{90}-*co*-$SPMA_{10}$) (Figure 5.11), several differences exist. While there are changes in the absorbance peak shape, there is very little spectral variation between the MC-Cu^{2+}, MC-Fe^{2+}, and MC-Zn^{2+} complexes for the MEO-containing copolymer, with the change in λ_{max} from MC only 94, 99, and 90 nm, respectively. In comparison to SPMA, there are large differences in the blue shifts for the complexes for the SPMA-containing copolymer (174, 147, and 90 nm, respectively). Further, it does not appear that Cu^{2+} and Fe^{2+} bind in a *cis*-MC-M^{2+} complex with the MEO copolymer as with SPMA, as there is not a partially overlapping absorbance band for either of these two complexes. We observed evidence for a *cis*-MC-M^{2+} complex for Cu^{2+} and Fe^{2+} in poly(MMA_{90}-*co*-$SPMA_{10}$),[31] where the carbonyl in the ester side chain, as well as the phenolate anion, are involved in the binding. These UV-vis absorbance spectra suggest that with the MEO-containing copolymer, the – OCH_3 substituent on the nitro ring, along with the phenolate anion, are involved in the binding of these metal ions, while the carbonyl is not an important factor.

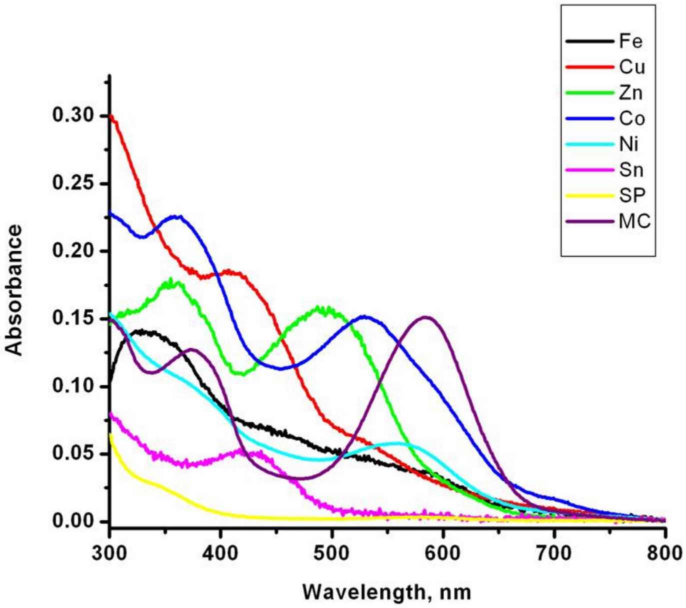

Figure 5.11. UV-vis absorbance spectra of poly(MMA_{90}-*co*-$SPMA_{10}$) in the presence of different divalent metal ions: Fe, Cu, Zn, Co, Ni, Sn. SP and MC refer to the absorbance spectra of the polymer thin films in the ring-closed (SP) and ring-opened (MC) state.

The MC-Sn^{2+} complex in the poly(MMA_{90}-*co*-MEO_{10}) thin film gives the largest blue shift of 234 nm (λ_{max} = 366 nm), which is indicative of a *cis*-MC-Sn^{2+} complex through complexation with the phenolate anion and the carbonyl of the ester side chain. Unfortunately, from the UV-vis spectrum alone, it cannot be determined if the methoxy is also contributing to the MC-Sn^{2+} complex. This compares with the MC-Sn^{2+} complex of the poly(MMA_{90}-*co*-$SPMA_{10}$) thin film, where a large shift in absorbance band to lower energy (λ_{max} = 423 nm) also indicates a *cis*-MC-Sn^{2+} complex.

We also examined the UV-vis absorbance spectra of the MC-M^{2+} complex for poly($TFEMA_{90}$-*co*-$SPMA_{10}$) and poly($TFEMA_{90}$-*co*-MEO_{10}) thin films to (1) compare the effect of comonomer on the metal ion binding and (2) to provide further evidence that the – OCH_3 substituent is involved in the binding for the MEO copolymers. Table 5.4 summarizes the change in λ_{max} from MC to MC-M^{2+} for the metal ions studied for all four copolymers investigated. Figure 5.12 shows the UV-vis absorbance spectra of poly($TFEMA_{90}$-*co*-$SPMA_{10}$) in response to divalent metal ions. The copolymer thin film after the photoinduced change to the ring-opened state was characterized by an intense absorption band at λ_{max} = 583 nm, with a second short wavelength absorbance at 375 nm. Upon binding to Zn^{2+}, Co^{2+}, and Ni^{2+}, there is a decrease in the long wavelength absorbance at 583 nm, along with a significant hypsochromic shift in absorbance maxima, where λ_{max} = 505 nm, 556 nm, and 574 nm, respectively. With Fe^{2+} (λ_{max} = 559 nm) and Cu^{2+} (λ_{max} = 526 nm), however, the absorption band broadens and a shoulder is observed at 456 nm and 440 nm, respectively, indicating that these ions form a *cis*-MC-M^{2+} complex as they do in the poly(MMA_{90}-*co*-$SPMA_{10}$) thin film.[31] Again, Sn^{2+} also appears to form a *cis*-MC-M^{2+} complex with a large shift in absorbance maxima to lower energy at λ_{max} = 413 nm. As can be seen in Table 5.4, the absorbance spectra of the MC-M^{2+} complex in poly($TFEMA_{90}$-*co*-$SPMA_{10}$) thin films compare well to the poly(MMA_{90}-*co*-$SPMA_{10}$) film when bound to the same ions in that the spectral variation between each MC-M^{2+} complex is significant. With the TFEMA copolymer, however, there is a small decrease in the change in λ_{max} from MC to MC-M^{2+} complex for each metal ion except Sn^{2+}.

Table 5.4. Summary of the $\Delta\lambda_{max}$ for each metal ion when bound to the various copolymer thin films.

	Sn^{2+}	**Fe^{2+}**	**Cu^{2+}**	**Zn^{2+}**	**Ni^{2+}**	**Co^{2+}**
Poly(MMA$_{90}$-*co*-SPMA$_{10}$)	161 nm	147, 64 nm	174, 64 nm	90 nm	27 nm	54 nm
Poly(TFEMA$_{90}$-*co*-SPMA$_{10}$)	170 nm	127, 24 nm	143, 57 nm	78 nm	8 nm	27 nm
Poly(MMA$_{90}$-*co*-MEO$_{10}$)	234 nm	99 nm	94 nm	90 nm	31 nm	69 nm
Poly(TFEMA$_{90}$-*co*-MEO$_{10}$)	124 nm	25 nm	83 nm	72 nm	11 nm	37 nm

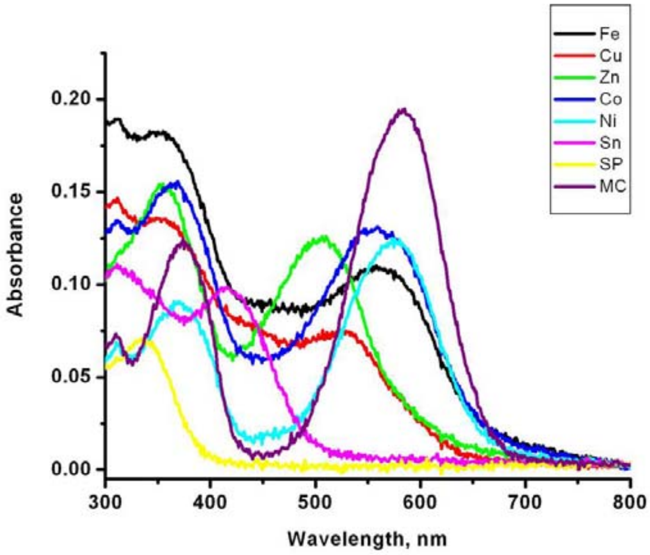

Figure 5.12. UV-vis absorbance spectra of poly(TFEMA$_{90}$-*co*-SPMA$_{10}$) in the presence of different divalent metal ions: Fe, Cu, Zn, Co, Ni, Sn. SP and MC refer to the absorbance spectra of the polymer thin films in the ring-closed (SP) and ring-opened (MC) state.

The UV-vis absorbance spectra for the poly(TFEMA$_{90}$-*co*-MEO$_{10}$) in response to the different metal ions were also examined (Figure 5.13). After the photoinduced change to the ring-opened merocyanine (MC trace), the copolymer thin film was characterized by an intense absorption band at λ_{max} = 602 nm, with a second band centered at 396 nm. As in the other copolymers, upon complexation with each divalent metal ion in the poly(TFEMA$_{90}$-*co*-MEO$_{10}$) thin film, there is a decrease in the long wavelength absorbance at 602 nm, accompanied by a hypsochromic shift in absorbance maxima, which is dependent upon the metal ion contained in the solution. The MC-Sn^{2+} complex gives the largest blue shift with an absorbance band at λ_{max} = 478 nm, indicating a *cis*-MC-M^{2+} complex. The MC-Cu^{2+} and MC-Zn^{2+} complexes show similar spectral responses with λ_{max} = 519 nm and λ_{max} = 530 nm, respectively. The MC-Fe^{2+}, MC-Co^{2+}, and MC-Ni^{2+} complexes also have a similar λ_{max} at 577 nm, 565 nm, and 591 nm, respectively. The spectral response for each of these complexes indicates a *trans*-MC-M^{2+} complex, and the change in λ_{max} for each metal ion is smaller than in the poly(MMA$_{90}$-*co*-MEO$_{10}$) thin films. With the MMA copolymer, however, the spectral variation between each complex is smaller than in the TFEMA copolymer. For this reason, poly(TFEMA$_{90}$-*co*-MEO$_{10}$) was used in the later FT-IR studies to examine the MC-M^{2+} complex in MEO-containing copolymers instead of poly(MMA$_{90}$-*co*-MEO$_{10}$).

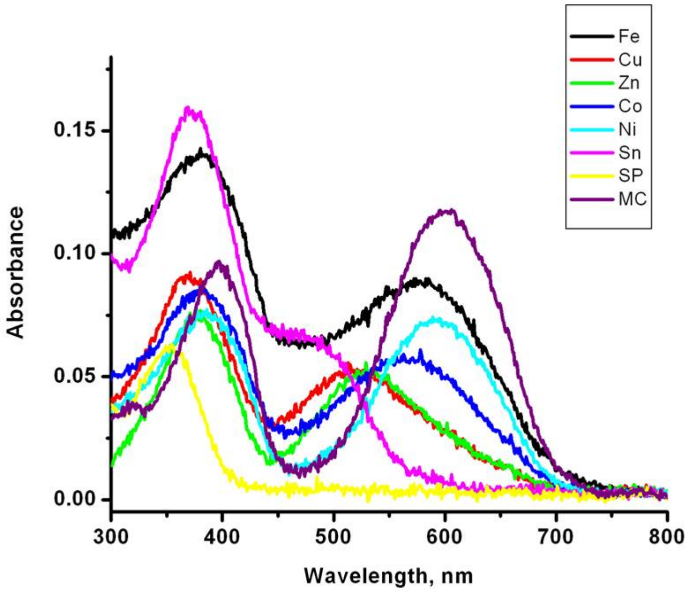

Figure 5.13. UV-vis absorbance spectra of poly(TFEMA$_{90}$-*co*-MEO$_{10}$) in the presence of different divalent metal ions: Fe, Cu, Zn, Co, Ni, Sn. SP and MC refer to the absorbance spectra of the polymer thin films in the ring-closed (SP) and ring-opened (MC) state.

Overall, the MC-M^{2+} complexes yield larger shifts in absorbance maxima in MMA copolymers than in TFEMA copolymers, and with SPMA-containing copolymers, the spectral variation between the complexes is larger than with MEO-containing copolymers. Poly(MMA$_{90}$-*co*-SPMA$_{10}$) yields the largest hypsochromic shifts in λ_{max} for each MC-M^{2+} complex, as well as provides the most variation in absorbance maxima between each complex. Interestingly, in poly(TFEMA$_{90}$-*co*-MEO$_{10}$), Fe^{2+} appears to have a much weaker interaction with MC. The MC-Fe^{2+} complex provides a much smaller shift in λ_{max} (25 nm) than in any of the other copolymers investigated. Upon close examination, Fe^{2+} also appears to have a weak interaction with MC in poly(TFEMA$_{90}$-*co*-SPMA$_{10}$). Even though a *cis*-MC-M^{2+} complex is observed, as supported by the shoulder in the absorbance peak, the long wavelength absorbance band only shifts 24 nm from the nonbinding merocyanine. The TFEMA in the copolymer appears to hinder the interaction of Fe^{2+} with MC. The absorbance shift for the MC-Ni^{2+} complex in both of the TFEMA copolymers is also very small (8 nm in SPMA-TFEMA and 11 nm in MEO-TFEMA). It appears that the TFEMA in the copolymer also hinders the interaction of MC with Ni^{2+}.

These UV-vis studies suggest that copolymers containing SPMA appear to bind differently to divalent metal ions than MEO-containing copolymers, as the metal ions do not bind in a *cis*-MC-M^{2+} complex with MEO. In previous studies we show through UV-vis and FT-IR spectroscopy that both the phenolate anion and the carbonyl of the ester side chain are involved in the binding of metal ions for the poly(MMA$_{90}$-*co*-SPMA$_{10}$) thin films, and that by increasing the concentration of SPMA in the copolymer, the chromophore becomes more sterically hindered and less accessible to accommodate metal ion binding.[31] We hypothesize that the methoxy substituent on the ring is involved in the binding for the copolymers containing MEO, and the carbonyl of the ester linkage is mostly likely not involved; therefore, steric congestion of the chromophore is not as important in these copolymer systems. If the concentration of MEO is increased in the backbone of the polymer, the colorimetric response of each MC-M^{2+} complex should be identical. In light of this, we synthesized a 30% MEO copolymer, poly(MMA$_{70}$-*co*-MEO$_{30}$), and the pure homopolymer, poly(MEO), to test the hypothesis that upon increasing the concentration of MEO in the copolymer, or by polymerizing the homopolymer, the differences between each complex in the UV-vis absorbance spectra will be minimal. Figures 5.14a and b show the UV-vis absorbance spectra for poly(MMA$_{70}$-*co*-MEO$_{30}$) and poly(MEO), respectively.

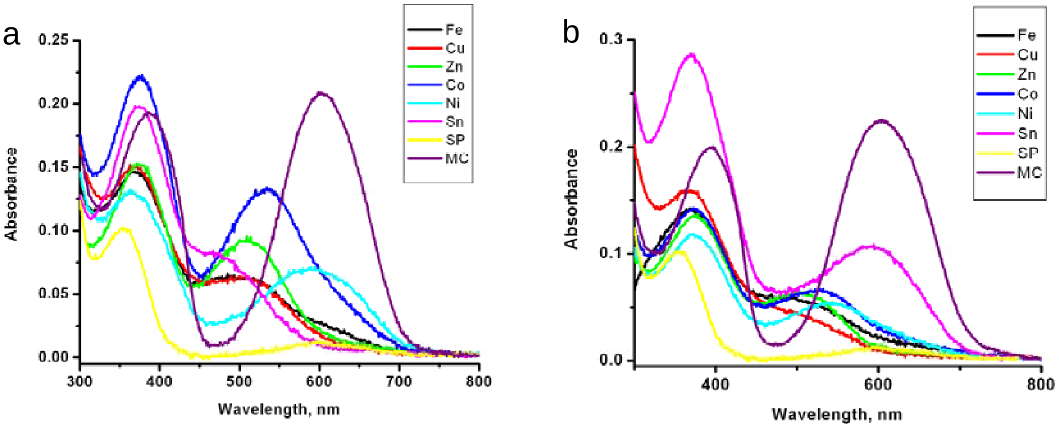

Figure 5.14. UV-vis absorbance spectra of (a) poly(MMA$_{70}$-*co*-MEO$_{30}$) and (b) poly(MEO) in the presence of different divalent metal ions.

As can be seen for poly(MMA$_{70}$-*co*-MEO$_{30}$) in Figure 5.14a, the blue shift in absorbance maxima for each MC-M^{2+} complex is very similar to that of poly(MMA$_{90}$-*co*-MEO$_{10}$). Table 5.5 summarizes the $\Delta\lambda_{max}$ for the MMA-MEO copolymers and poly(MEO). With poly(MMA$_{90}$-*co*-MEO$_{10}$), the MC-Fe^{2+}, MC-Cu^{2+}, MC-Zn^{2+}, and MC-Co^{2+} complexes have a hypsochromic shift of 99, 95, 90 and 68 nm, respectively, while with poly(MMA$_{70}$-*co*-MEO$_{30}$), the MC-Fe^{2+}, MC-Cu^{2+}, MC-Zn^{2+}, and MC-Co^{2+} complexes shift 95, 95, 92, and 68 nm respectively. The shift to lower energy for the MC-Ni^{2+} complex in the poly(MMA$_{90}$-*co*-MEO$_{10}$) (31 nm) does not compare as well to that of poly(MMA$_{70}$-*co*-MEO$_{30}$), which shifts only 12 nm. The difference, however, is still not very significant. Interestingly, increasing the concentration of MEO in the copolymer significantly affects the colorimetric response for Sn^{2+}. The absorbance maximum for the MC-Sn^{2+} complex in the poly(MMA_{70}-*co*-MEO_{30}) has a much smaller shift (129 nm) compared to a 234 nm shift for poly(MMA_{90}-*co*-MEO_{10}).

Table 5.5. Summary of the $\Delta\lambda_{max}$ for each metal ion when bound to the MMA-MEO copolymers at various concentrations of MEO and the MEO homopolymer.

Metal Ions	**MMA-MEO 90-10 $\Delta\lambda_{max}$ (nm)**	**MMA-MEO 70-30 $\Delta\lambda_{max}$ (nm)**	**MEO 100 $\Delta\lambda_{max}$ (nm)**
Sn^{2+}	234	129	14
Fe^{2+}	99	95	95
Cu^{2+}	53	95	95
Zn^{2+}	90	92	91
Co^{2+}	68	68	77
Ni^{2+}	31	12	64

Further increasing the concentration of MEO in the polymer backbone still does not affect the absorbance maxima significantly for most of the MC-M^{2+} complexes. Figure 5.14b shows that the MC-Fe^{2+}, MC-Cu^{2+}, MC-Zn^{2+}, and MC-Co^{2+} complexes in poly(MEO) produce a blue shift of 95, 95, 91, and 77 nm, respectively, which again, is very similar to that of the poly(MMA_{90}-*co*-MEO_{10}) thin film. The MC-Ni^{2+} complex yields a hypsochromic shift of 64 nm with poly(MEO), which is much larger than observed with any of the other MEO-containing copolymers. Further increasing the concentration of MEO leads to even less variation in the colorimetric response of the polymer to Sn^{2+}. The MC-Sn^{2+} complex in the poly(MEO) homopolymer thin film produces a blue shift of only 14 nm. This represents almost a 95% decrease in the blue shift of the absorbance maximum when the concentration of MEO is increased from 10-100 mol% in the polymer. These results suggest that Sn^{2+} still binds in a *cis*-MC-M^{2+} conformation in the poly(MMA_{90}-*co*-MEO_{10}) copolymers, and further, that Sn^{2+} requires this *cis*-MC-M^{2+} conformation to have any appreciable interaction with MEO-containing copolymers. With the exception of the MC-Sn^{2+} complex, there is very little difference in the absorbance maxima for each MC-M^{2+} complex lending support to the hypothesis that along with the phenolate anion, the methoxy substituent on the ring is involved in metal ion binding as well. With the methoxy involvement on the ring, and no involvement of the carbonyl on the ester side chain, MC does not need as much room to reorganize in order to accommodate the metal ions.

FT-IR Studies of the MC-M^{2+} Complex of Poly($TFEMA_{90}$-co-MEO_{10})

GATR-FT-IR spectroscopy was also used to characterize the MC-M^{2+} complex for the various copolymer films. Because there is a larger difference in colorimetric response of the metal ions in poly($TFEMA_{90}$-*co*-MEO_{10}) than in poly(MMA_{90}-*co*-MEO_{10}), TFEMA-containing copolymers were used primarily to study the MC-M^{2+} complex. Figure 5.15 shows the FT-IR spectra of a poly($TFEMA_{90}$-*co*-MEO_{10}) after binding to various metal ions. Complete characterization and assignments are listed in Table 5.6. Key differences in the FT-IR spectra of the MC-M^{2+} complex exist, revealing important insights into their binding interactions within the copolymer system. While the symmetrical – OCH_3 band (1118 cm^{-1}) is partially obscured by the C-O ester stretch of the TFEMA in the copolymer, changes in the shape of the peak when the merocyanine is bound to a metal ion still allow for inferences to be made. As can be seen in Figure 5.15, the shape of the – OCH_3 band at 1118 cm^{-1} for the MC-Ni^{2+} complex remains almost identical to the UV irradiated polymer (Figure 5.4). The shape of the peak is also very similar for the MC-Co^{2+} and MC-Cu^{2+} complexes as well. For the MC-Sn^{2+} and MC-Zn^{2+} complexes, the shape of the – OCH_3 stretch compares well together, but appears to be different than the MC-Co^{2+}, MC-Cu^{2+}, and MC-Ni^{2+} complex. The - OCH_3 band for the MC-Fe^{2+} complex appears to be the least similar to the others. Also of importance, the symmetrical stretching band of the aryl nitro group shifted from 1519 cm^{-1} for merocyanine to higher energy for each MC-M^{2+} complex, the magnitude of which is metal ion dependent. The nitro group stretching band for the Mc-Sn^{2+}, MC-Fe^{2+}, and MC-Cu^{2+} complexes have bands for the symmetrical stretching at 1527, 1527, and 1526 cm^{-1}, respectively, while the nitro group stretching bands for the MC-Zn^{2+}, MC-Co^{2+}, and MC-Ni^{2+} complexes are all observed at 1521 cm^{-1}, which is much closer to the nonbinding merocyanine band. As the metal ions interact with the phenolate and methoxy substituents, electron density is drawn away from the aromatic ring and the nitro group, shifting the symmetrical stretching bands of the aryl nitro group to higher energy. In general, the ions which have a weaker interaction with the phenolate anion and methoxy substituent, such as Ni^{2+}, Co^{2+}, and to some extent Zn^{2+}, do not afford the same shift to higher energy for the nitro stretching band. The only exception to this trend is Fe^{2+}, as the hypsochromic shift for the MC-Fe^{2+} complex in the UV-vis absorbance spectra is quite small (25 nm), but it still yields a larger shift in wavenumber for the symmetrical stretch of the aryl nitro group. The aromatic C=C stretching band is also important to note. The shape, as well as the shift in wavenumber, change depending upon the metal ion bound to MC. The shape remains almost identical to the UV irradiated merocyanine in the case of the MC-Ni^{2+} and MC-Co^{2+} complexes, whereas it is quite different for the MC-Sn^{2+}, MC-Cu^{2+}, MC-Fe^{2+}, and MC-Zn^{2+} complexes.

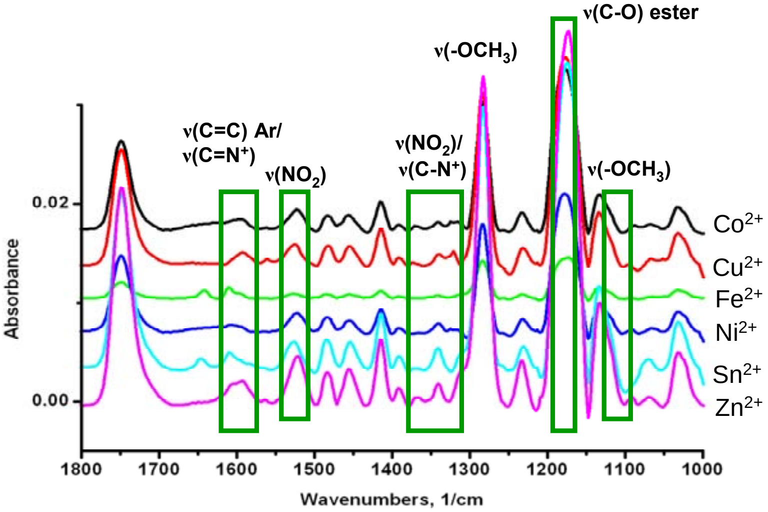

Figure 5.15. FT-IR spectra of poly(TFEMA$_{90}$-*co*-MEO$_{10}$) (a) after binding to Co^{2+}, (b) after binding to Cu^{2+}, (c) after binding Fe^{2+}, (d) after binding to Ni^{2+} (e) after binding to Sn^{2+}, and (f) after binding to Zn^{2+}. The green boxes highlight the major differences in the various merocyanine-metal ion complexes.

Table 5.6. Main FT-IR frequencies for poly(TFEMA$_{90}$-*co*-MEO$_{10}$) when bound to the different metal ions.

Assignments	Sn^{2+} (cm^{-1})	Fe^{2+} (cm^{-1})	Cu^{2+} (cm^{-1})	Zn^{2+} (cm^{-1})	Ni^{2+} (cm^{-1})	Co^{2+} (cm^{-1})
C=O	1748	1748	1748	1748	1748	1748
Ar C=C	1645	1641	n/a	1651	1651	1651
Ar C=C	1608	1609	n/a	1606	1606	1608
$C=N^+$	1592	1595	1592	1592	1595	1592
NO_2 sym stretch	1527	1527	1526	1521	1521	1521
NO_2 asym stretch	1341	1341	1341	1341	1341	1341
$C-N^+$	1308	1311	1320	1308	1318	1317
OCH_3 sym stretch	1283	1283	1283	1283	1283	1283
TFEMA	1232	1231	1231	1231	1231	1231
C-O ester stretch	1174	1174	1177	1174	1177	1177
OCH_3 asym stretch	1118	1118	1118	1118	1118	1118

In order to assess the reproducibility of the spectra and elucidate the binding interaction for each metal ion, PCA was performed on the spectra for each merocyanine-metal ion complex. PCA scores plots for PC1 and PC2 are shown in Figure 5.16. It can be seen from the plot of the scores on PC2 versus PC1 that spectra for each of the metal ion complexes cluster tightly, signifying the reproducibility of the spectral collection. Moreover, most of the clusters on PC1 are easily resolved from each other. The scores on PC1 reveal that while the FT-IR spectra for the MC-Co^{2+} and MC-Ni^{2+} complexes are very similar, the other complexes can be distinguished from each other, as well as the nonbinding merocyanine. Interestingly, with the exception of Fe^{2+}, the scores on PC1 correlate with the hypsochromic shifts seen in the UV-vis spectra (Figure 5.13) of the poly(TFEMA$_{90}$-*co*-MEO$_{10}$) bound to each metal ion. The MC-Sn^{2+} and MC-Cu^{2+} complexes give the largest blue shift in absorbance maxima, while the absorbance maxima for the MC-Co^{2+} and MC-Ni^{2+} complexes remain very close to the absorbance for the nonbinding merocyanine. Scores on PC2 do not show any more separation between the complexes than on PC1, and as such are not used to describe the data further.

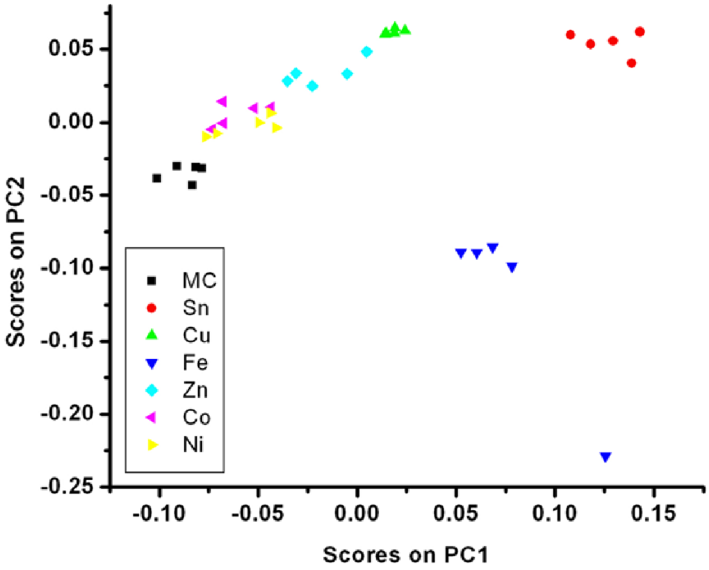

Figure 5.16. Scores plot for PC2 versus PC1 for the PCA model computed from the FT-IR spectra of poly(TFEMA$_{90}$-*co*-MEO$_{10}$) after UV irradiation, after binding to Sn^{2+}, after binding to Cu^{2+}, after binding to Fe^{2+}, after binding to Zn^{2+}, after binding to Co^{2+}, and after binding to Ni^{2+}.

The peaks that contribute to the differences between the clusters, as identified by the loadings on PC1 (Figure 5.17), are assigned to the symmetrical and asymmetrical stretching of the methoxy group (1118 and 1283 cm^{-1}), the C-O ester stretch (1174 cm^{-1}), the symmetrical stretch of the aryl nitro group (1520 cm^{-1}), the aromatic C=C stretch (1608 cm^{-1}), and the C=N^{+} stretching band (1592 cm^{-1}). In analyzing the loadings plot for PC1, it is clear that the peaks assigned to the aryl methoxy bands are not as important as some of the others. It is significant to note, however, that the C-F stretch (1283 cm^{-1}) and the ester C-O stretch (1174 cm^{-1}) from the TFEMA copolymer overshadow the symmetric and asymmetric methoxy stretches at 1283 cm^{-1} and 1174 cm^{-1}, respectively, which makes it more difficult to observe the changes in the band shape and frequency upon binding to the metal ions. It is also nearly impossible to observe changes in the band assigned to the phenolate anion as it is masked by a peak associated with the TFEMA in the copolymer. On the other hand, the aromatic C=C stretch appears to be very important in the variations seen among the different MC-M^{2+} complexes, suggesting that the methoxy is involved in the binding. As the metal ions interact with the methoxy substituent on the ring, electron density is drawn away from the ring affecting both the aromatic C=C stretching between 1600 and 1650 cm^{-1} and the symmetric stretch of the aryl nitro at 1520 cm^{-1}.

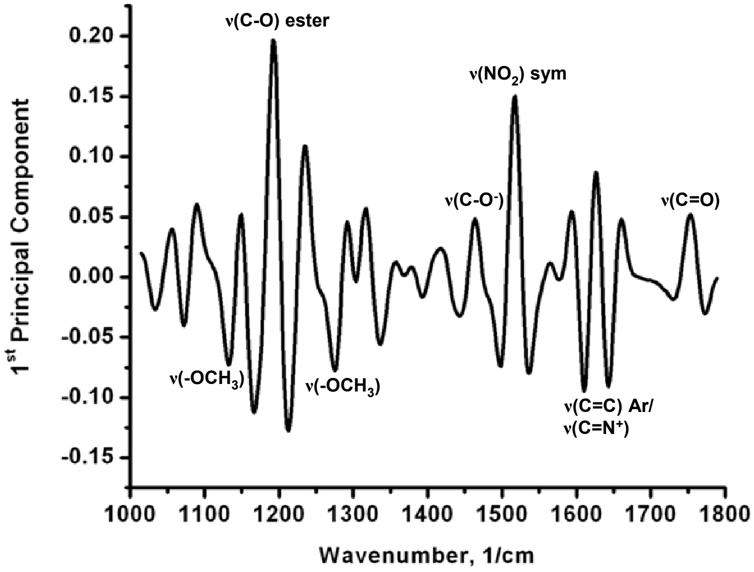

Figure 5.17. Loadings plot for PC1 computed from the PCA model built using FT-IR spectra of poly(TFEMA$_{90}$-*co*-MEO$_{10}$) after UV irradiation, after binding to Sn^{2+}, after binding to Fe^{2+}, after binding to Cu^{2+}, after binding to Zn^{2+}, after binding to Ni^{2+}, and after binding to Co^{2+}.

Comparison of FT-IR Spectra for the MC-M^{2+} Complex Between Poly(TFEMA$_{90}$-co-MEO$_{10}$) and Poly(MMA$_{90}$-co-SPMA$_{10}$)

With poly(MMA$_{90}$-*co*-SPMA$_{10}$) thin films, the merocyanine complexes to metal ions through the phenolate anion and the carbonyl on the ester side chain.[31] Depending upon the metal ion bound, this interaction can produce either a *trans*-MC-M^{2+} complex or a *cis*-MC-M^{2+} complex. By using PCA to analyze the FT-IR spectra of the poly(TFEMA$_{90}$-*co*-MEO$_{10}$) thin film when bound to various metal ions, we have shown that it is reasonable to assume that both the methoxy and the phenolic oxygen on the nitro ring of merocyanine are important in the binding of the metal ions. PCA shows that the bands assigned to the aromatic C=C stretching are responsible for a significant amount of variation in the FT-IR spectra of the different MC-M^{2+} complexes for poly($TFEMA_{90}$-*co*-MEO_{10}). In the case of the SPMA-containing copolymer, however, these bands are not responsible for the variation in the FT-IR spectra between the different MC-M^{2+} complexes, indicating that the aromatic C=C stretching is not as affected by the metal ion binding.[31] With the metal ions bound to the methoxy, as well as the phenolate, the electron density is drawn away from the ring affecting the C=C stretching.

FT-IR Studies of the MC-M^{2+} Complex of Poly($TFEMA_{90}$-co-$SPMA_{10}$)

To show that the TFEMA in the copolymer is not involved in the differences in binding between MEO and SPMA, the FT-IR spectra of the MC-M^{2+} complexes of poly($TFEMA_{90}$-*co*-$SPMA_{10}$) were investigated. Figure 5.18 shows the FT-IR spectra of the copolymer thin film when bound to various metal ions. A list of complete characterization and assignments are listed in Table 5.7. Bands assigned to the C=N^+ at 1593 cm^{-1}, the symmetrical stretching band of the aryl nitro group at 1523 cm^{-1}, the C-N^+ at 1310 cm^{-1}, and the C-O ester of the SPMA stretch at 1090 cm^{-1} show the most variation between the different MC-M^{2+} complexes. PCA was used to analyze the FT-IR spectra for the poly($TFEMA_{90}$-*co*-$SPMA_{10}$) thin film when bound to the metal ions to better understand the binding interaction between MC and each ion. Figure 5.19 shows the plot of the scores on PC1 versus PC1. In this case, the spectra do not cluster as tightly as with poly($TFEMA_{90}$-*co*-MEO_{10}) films when bound to metal ions, but distinctions between several of the complexes are still observed. The plot shows that the MC-Ni^{2+} and the MC-Co^{2+} complexes are very similar, as well as the MC-Cu^{2+} and the MC-Sn^{2+} complexes. It is still possible, however, to see a separation between each of these pairs as well as the rest of the MC-M^{2+} complexes and the nonbinding merocyanine. Again, interestingly, with the exception of the MC-Fe^{2+} complex, the scores on PC1 directly correlate with the UV-vis spectra (Figure 5.12) of the MC-M^{2+} complexes. The MC-Sn^{2+} and the MC-Cu^{2+} complexes yield the largest blue shift in absorbance maxima from the nonbinding merocyanine, while the MC-Co^{2+} and MC-Ni^{2+} complex are similar to merocyanine. The peaks that contribute to the differences between the clusters, as identified by the loadings on PC1 (Figure 5.20), are assigned to the ester C-O stretch in SPMA (1090 cm^{-1}), the ester C-O stretch for both TFEMA and SPMA (1176 cm^{-1}), the C-N^+ band (1311 cm^{-1}), the symmetrical and asymmetrical aryl nitro stretching band (1523 and 1342 cm^{-1}, respectively), the phenolate anion (1450 cm^{-1}), and the carbonyl of the ester side chain (1746 cm^{-1}). The aromatic C=C stretching of poly($TFEMA_{90}$-*co*-$SPMA_{10}$) is not affected by the metal ion binding, as it is for poly($TFEMA_{90}$-*co*-MEO_{10}) when bound to metal ions. These results provide further proof that with the introduction of a second chelating group on the nitro ring, the carbonyl of the ester side chain is no longer involved in the binding between MC and the metal ions, with the exception of Sn^{2+}.

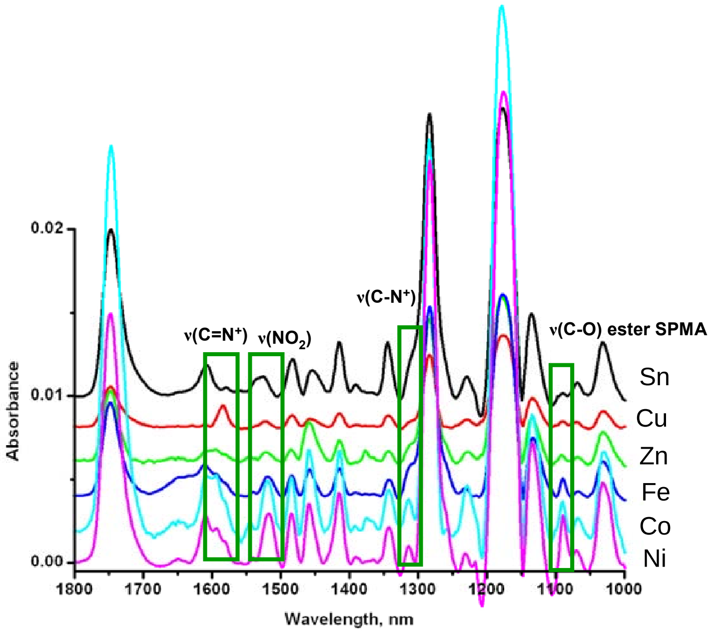

Figure 5.18. FT-IR spectra of poly(TFEMA$_{90}$-*co*-SPMA$_{10}$) (a) after binding to Sn^{2+}, (b) after binding to Cu^{2+}, (c) after binding Zn^{2+}, (d) after binding to Fe^{2+} (e) after binding to Co^{2+}, and (f) after binding to Ni^{2+}. The green boxes highlight the major differences in the various merocyanine-metal ion complexes.

Table 5.7. Main FT-IR frequencies for poly(TFEMA$_{90}$-*co*-SPMA$_{10}$) when bound to the different metal ions.

Assignments	**Sn^{2+} (cm^{-1})**	**Fe^{2+} (cm^{-1})**	**Cu^{2+} (cm^{-1})**	**Zn^{2+} (cm^{-1})**	**Ni^{2+} (cm^{-1})**	**Co^{2+} (cm^{-1})**
C=O	1746	1746	1746	1746	1746	1746
C=N$^+$	1577	1593	1584	1593	1593	1593
NO$_2$ sym stretch	1523	1518	1521	1521	1518	1518
C-O$^-$	1450s	1450s	1450s	1450s	1450s	1450s
NO$_2$ asym stretch	1343	1343	1343	1343	1343	1343
C-N$^+$	1311	1311	1311	1311	1313	1313
TFEMA	1232	1231	1231	1231	1231	1231
C-O ester stretch (SPMA)	1090	1090	1090	1090	1090	1090

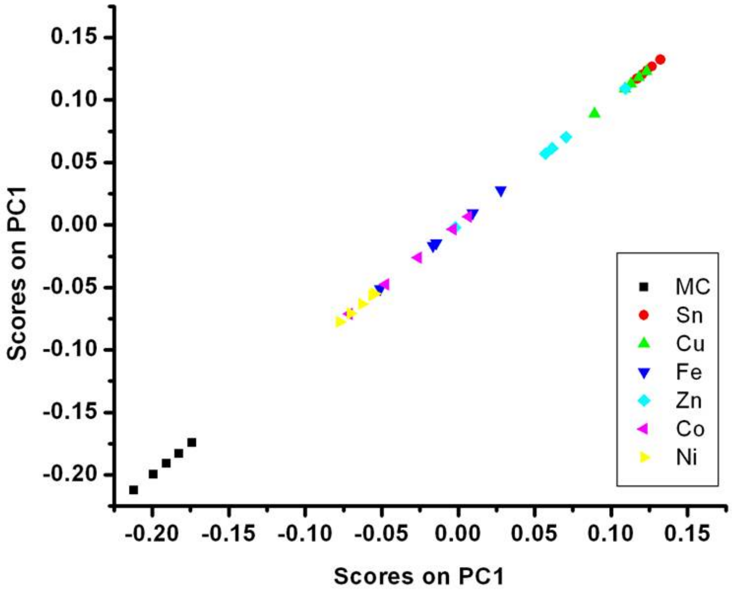

Figure 5.19. Scores plot for PC1 versus PC1 for the PCA model computed from the FT-IR spectra of poly(TFEMA$_{90}$-*co*-SPMA$_{10}$) after UV irradiation, after binding to Sn^{2+}, after binding to Cu^{2+}, after binding to Fe^{2+}, after binding to Zn^{2+}, after binding to Co^{2+}, and after binding to Ni^{2+}.

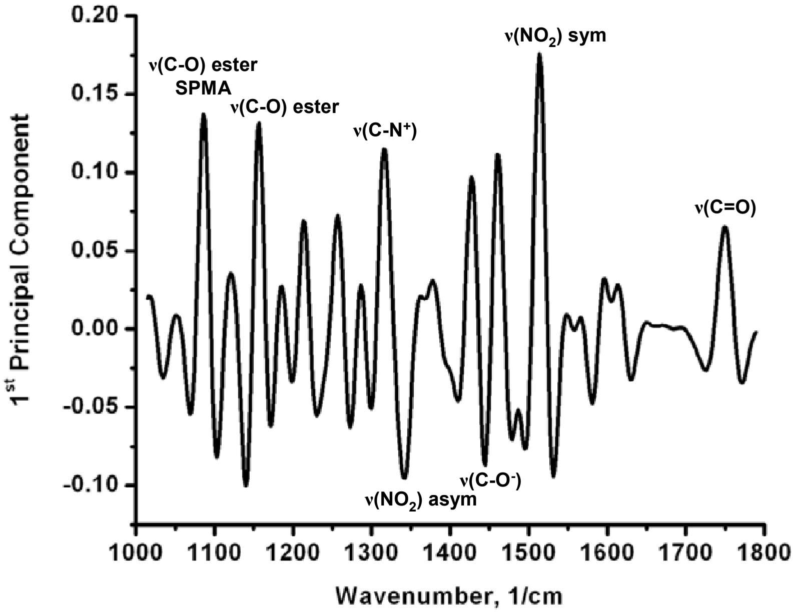

Figure 5.20. Loadings plot for PC1 computed from the PCA model built using FT-IR spectra of poly(TFEMA$_{90}$-*co*-SPMA$_{10}$) after UV irradiation, after binding to Sn^{2+}, after binding to Fe^{2+}, after binding to Cu^{2+}, after binding to Zn^{2+}, after binding to Ni^{2+}, and after binding to Co^{2+}.

Conclusions

In summary, we have investigated the interaction of merocyanine with different divalent metal ions by fabricating a series of copolymers containing spiropyran moieties. We have synthesized a spiropyran methacrylate functionalized with a methoxy substituent (MEO) in the 8' position on the benzopyran ring to study the effects of a second chelating group on the ring in the presence of metal ions, and compared the metal ion complexes to spiropyran methacrylate (SPMA). We also copolymerized the spiropyran derivatives with either MMA or TFEMA to investigate the influence of the comonomer on the binding of metal ions. Through UV-vis spectroscopy we showed that each metal ion gives a unique colorimetric response with all of the copolymers studied. Overall, the MEO-containing copolymers provide much smaller shifts in absorbance maxima than the SPMA-containing copolymers, and with MEO-containing copolymers, Fe^{2+} and Cu^{2+} do not bind in a *cis*-MC-M^{2+} complex as they do in SPMA-containing copolymers. We also showed that, with the exception of Sn^{2+}, there is no effect on the MC-M^{2+} complex as the concentration of MEO is increased in the copolymer, suggesting that the carbonyl is not involved in the binding of the other metal ions. Also through UV-vis absorption spectroscopy, we showed that with TFEMA copolymers, the hypsochromic shift in absorbance maxima is smaller than in MMA copolymers. Further, Fe^{2+} and Ni^{2+} appear to have much less interaction with merocyanine in the TFEMA copolymers than with MMA copolymers. FT-IR spectra of the various copolymers were analyzed using principal component analysis to elucidate the binding interaction of the MC-M^{2+} complex. Through these studies, we showed that the methoxy and the phenolate anion in the MEO-containing copolymers are involved in the binding of the metal ions. With more studies into the binding interaction between different spiropyran derivatives and metal ions, it will become possible to fabricate sensors from a single material that can be tuned to selectively and quantitatively distinguish specific metal ions.

References

1. Oehme, I. and O.S. Wolfbeis, *Microchim. Acta*, **1997**. *126*(3): p. 177.
2. Janata, J., M. Josowicz, P. Vanýsek and D.M. DeVaney, *Anal. Chem.*, **1998**. *70*(12): p. 179.
3. Nolan, E.M. and S.J. Lippard, *Chem. Rev.*, **2008**. *108*(9): p. 3443.
4. Prodi, L., F. Bolletta, M. Montalti and N. Zaccheroni, *Coord. Chem. Rev.*, **2000**. *205*(1): p. 59.
5. Buhlmann, P., E. Pretsch and E. Bakker, *Chem. Rev.*, **1998**. *98*(4): p. 1593.
6. Gabor, G., S. Chadha and D.R. Walt, *Anal. Chim. Acta*, **1995**. *313*(1-2): p. 131.
7. He, X. and G.A. Rechnitz, *Anal. Chem.*, **1995**. *67*(13): p. 2264.
8. Choi, M.M.F. and D. Xiao, *Anal. Chim. Acta*, **1999**. *387*(2): p. 197.
9. Rosatzin, T., P. Holy, K. Seiler, B. Rusterholz and W. Simon, *Anal. Chem.*, **1992**. *64*(18): p. 2029.
10. Oehme, I., S. Prattes, O.S. Wolfbeis and G.J. Mohr, *Talanta*, **1998**. *47*(3): p. 595.
11. Plaschke, M., R. Czolk and H.J. Ache, *Anal. Chim. Acta*, **1995**. *304*(1): p. 107.
12. Zhang, X.-B., C.-C. Guo, Z.-Z. Li, G.-L. Shen and R.-Q. Yu, *Anal. Chem.*, **2002**. *74*(4): p. 821.
13. Byrne, R. and D. Diamond, *Nat. Mater.*, **2006**. *5*(6): p. 421.
14. Hirshberg, Y., *J. Am. Chem. Soc.*, **1956**. *78*(10): p. 2304.
15. Saragi, T.P.I., T. Spehr, A. Siebert, T. Fuhrmann-Lieker and J. Salbeck, *Chem. Rev.*, **2007**. *107*(4): p. 1011.
16. Winkler, J.D., K. Deshayes and B. Shao, *J. Am. Chem. Soc.*, **1989**. *111*(2): p. 769.

17. Phillips, J.P., A. Mueller and F. Przystal, *J. Am. Chem. Soc.*, **1965**. *87*(17): p. 4020.

18. Byrne, R.J., S.E. Stitzel and D. Diamond, *J. Mater. Chem.*, **2006**. *16*(14): p. 1332.

19. Suzuki, T., Y. Kawata, S. Kahata and T. Kato, *Chem. Commun.*, **2003**(16): p. 2004.

20. Chibisov, A.K. and H. Görner, *Chem. Phys.*, **1998**. *237*(3): p. 425.

21. Samanta, S. and J. Locklin, *Langmuir*, **2008**. *24*(17): p. 9558.

22. Natali, M., C. Aakeroy, J. Desper and S. Giordani, *Dalton Trans.*, **2010**. *39*(35): p. 8269.

23. Winkler, J.D., C.M. Bowen and V. Michelet, *J. Am. Chem. Soc.*, **1998**. *120*(13): p. 3237.

24. Stauffer, M.T. and S.G. Weber, *Anal. Chem.*, **1999**. *71*(6): p. 1146.

25. Alhashimy, N., R. Byrne, S. Minkovska and D. Diamond, *Tetrahedron Lett.*, **2009**. *50*(21): p. 2573.

26. Shao, N., Y. Zhang, S. Cheung, R. Yang, W. Chan, T. Mo, K. Li and F. Liu, *Anal. Chem.*, **2005**. *77*(22): p. 7294.

27. Chernyshev, A.V., A.V. Metelitsa, E.B. Gaeva, N.A. Voloshin, G.S. Borodkin and V.I. Minkin, *J. Phys. Org. Chem.*, **2007**. *20*(11): p. 908.

28. Evans, L., G.E. Collins, R.E. Shaffer, V. Michelet and J.D. Winkler, *Anal. Chem.*, **1999**. *71*(23): p. 5322.

29. Khairutdinov, R.F. and J.K. Hurst, *Langmuir*, **2004**. *20*(5): p. 1781.

30. Fries, K., S. Samanta, S. Orski and J. Locklin, *Chem. Commun.*, **2008**(47): p. 6288.

31. Fries, K.H., J.D. Driskell, S. Samanta and J. Locklin, *Anal. Chem.*, **2010**. *82*(8): p. 3306.

32. Chung, D.-J., Y. Ito and Y. Imanishi, *J. Appl. Polym. Sci.*, **1994**. *51*(12): p. 2027.

33. Beebe, K.R., R.J. Pell and M.B. Seasholtz, *Chemometrics: A Practical Guide*. 1998, New York: John Wiley & Sons. 348.

34. Gorner, H. and A.K. Chibisov, *J. Chem. Soc., Faraday Trans.*, **1998**. *94*(17): p. 2557.

35. Natali, M., L. Soldi and S. Giordani, *Tetrahedron*, **2010**. *66*(38): p. 7612.

36. Wojtyk, J.T.C., P.M. Kazmaier and E. Buncel, *Chem. Mater.*, **2001**. *13*(8): p. 2547.

CHAPTER 6

CONCLUSIONS AND OUTLOOK

This dissertation has detailed the synthesis and investigation of spiropyran-containing copolymers used as colorimetric, thin film sensors for divalent metal ions. In Chapter 2, copolymer brushes containing spiropyran were synthesized using atom transfer radical polymerization (ATRP). The comonomer polymerized with spiropyran was varied between several different methacrylate monomers to investigate the influence of the comonomer on the photoinduced conversion of spiropyran (SP) to merocyanine (MC). The concentration of SP in the polymer backbone was also varied to study the influence of free volume and sterics on the photochromic response. Through UV-vis spectroscopy, we have shown that each metal ion gives rise to a unique colorimetric response. We have also shown through contact angle studies that with merocyanine complexed to various metal ions, contact angle changes of up to 70° are observed.

Chapter 3 describes the synthesis and characterization of a series of spiropyran-containing copolymers by ATRP and used as thin film sensors for the metal ions, Cu^{2+}, Fe^{2+}, Zn^{2+}, Co^{2+}, and Ni^{2+}. We showed that the unique colorimetric response of each merocyanine-metal ion ($MC\text{-}M^{2+}$) complex is dependent upon the amount of spiropyran comonomer that is contained in the polymer backbone. Principal component analysis (PCA) was used to analyze FT-IR spectra of each $MC\text{-}M^{2+}$ complex to elucidate the binding interaction between MC and M^{2+} and to selectively identify each metal ion bound to MC. We also showed that by using chemometric methods, UV-vis spectra can be analyzed to quantitatively identify metal ions in the micromolar to millimolar range. To our knowledge, this has not been observed with a single material before, and typically is only possible with an array of multiple compounds with varying affinity for a specific ion.

In Chapter 4, these same spiropyran-containing copolymers were used to identify multiple metal ions simultaneously. Using chemometric methods, UV-vis spectra of the MC-M^{2+} complexes can be analyzed to selectively identify both metal ions in a binary solution. Further, with several binary mixtures, chemometric methods can be used to quantitatively determine both metal ions in solution. The affinity of MC to each metal ion was also investigated, and we demonstrate that quantitative determination depends on the relative binding preference of MC to each metal ion.

Chapter 5 describes the synthesis and characterization of spiropyran-containing copolymers that were used to investigate the influence of two different spiropyran derivatives, spiropyran methacrylate (SPMA) and spiropyran methacrylate with a methoxy substituent in the 8' position of the benzopyran ring (MEO), on metal ion complexation. We also varied the comonomer with which SPMA was polymerized to investigate the influence of the comonomer on the binding interaction. Through UV-vis and FT-IR spectroscopy, it is observed that the MC-M^{2+} interaction is not only affected by the second chelating group on the benzopyran ring, but also by the type of comonomer with which SPMA is copolymerized.

FT-IR spectra of the various copolymers complexed to metal ions were analyzed using principal component analysis to elucidate the binding interaction of the MC-M^{2+} complex. In the MEO-containing copolymers, it is observed that the methoxy and the phenolate anion are involved in the complexation of the metal ions and not the carbonyl of the ester linkage. Due to this, steric congestion of the chromophore is not as important, and as the concentration of MEO is increased in the copolymer backbone, the colorimetric response of each MC-M^{2+} complex is almost identical.

In summary, this dissertation has expanded on a new approach to optical sensing whereby the sensor surface can be reversibly switched between passive and active states, extending the lifetime of the sensor and simplifying calibration as a new sensing surface is generated each time it is switched to its active state. We have demonstrated the idea that a spiropyran-containing copolymer can be used to complex metal ions in a way that yields a unique colorimetric response for each metal ion. In addition, through chemometric methods, we can selectively and quantitatively identify each metal ion in a micromolar to millimolar range. As stated before, quantitative identification is generally not feasible for a single chromophore and is typically done with multiple sensors with compounds of differing affinity.

We have also made strides towards understanding the binding interaction between MC and the metal ions. While this work has focused on the detection of specific divalent metal ions, it is evident that modification of the molecular architecture or the microenvironment of the binding site could allow other ions, as well as other chemical species, to be targeted. The phenolate anion is considered a “hard” base; and therefore, could be quite sensitive to the “hard” acids, such as Fe^{3+}, Al^{3+}, Mg^{2+}, or Ca^{2+}. Further, the spiropyran-containing copolymer can potentially be tuned to complex to heavy metal ions, such as Hg^{2+} or Pb^{2+}, simply by designing a spiropyran derivative with a chelating group that is sensitive to these specific ions. Amino acids could also be potential guests due to their ability to form complementary zwitterionic forms. By tuning the copolymer with which spiropyran is polymerized, it may also become possible to fabricate a sensor capable of binding to ions in aqueous solutions.

In conclusion, spiropyrans offer an intriguing approach to host-guest binding of charged analytes on surfaces. It can easily be switched from active to passive forms using light, and irradiation of the $MC\text{-}M^{2+}$ complex with visible light will expel the target analyte and regenerate the passive, spiropyran form. Moreover, the spiropyran-containing copolymer is self-indicating, yielding a unique color for each $MC\text{-}M^{2+}$ complex. Ultimately, spiropyrans have the potential to provide a route to developing simple, low cost chemical sensors capable of autonomous operation and long lifetime use.

APPENDIX A

^{1}H NMR SPECTRA OF SPMA-MMA COPOLYMERS

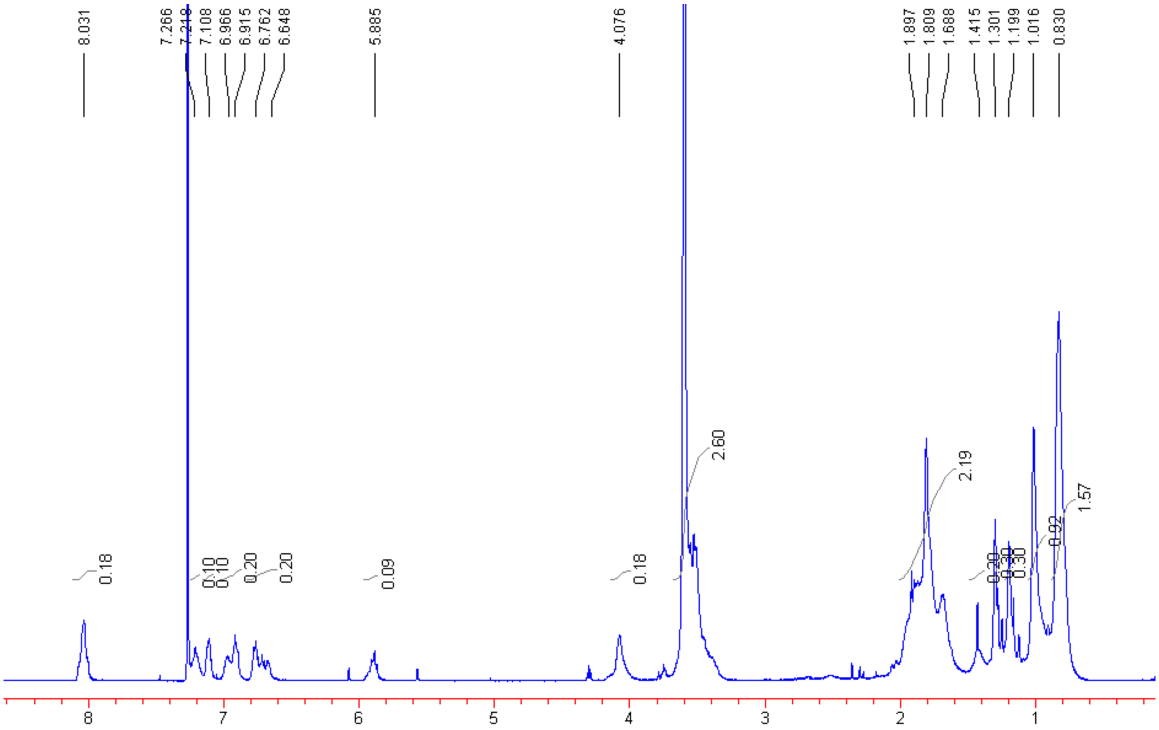

Figure A-1. ^{1}H NMR spectra of 10 mol% SPMA – 90 mol% MMA.

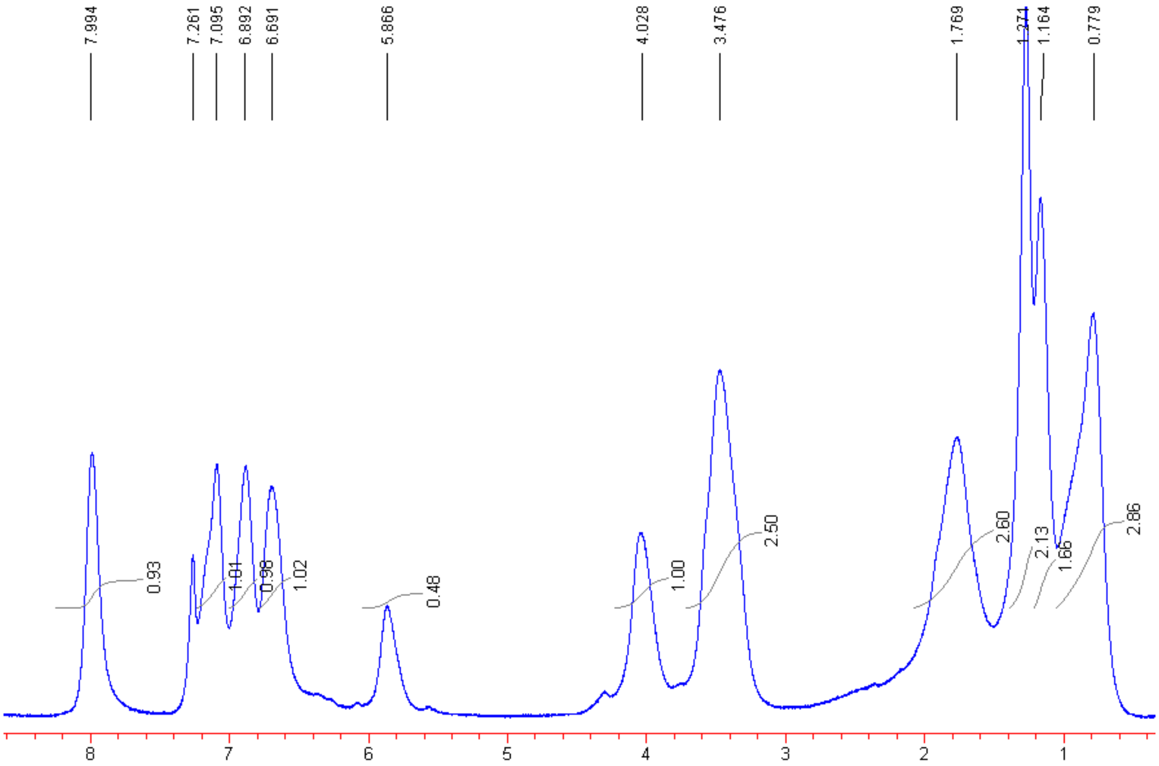

Figure A-2. ^{1}H NMR spectra of 50 mol% SPMA – 50 mol% MMA.

APPENDIX B

UV-VIS ABSORBANCE SPECTRA FOR DISPLACEMENT AND SELECTIVITY STUDIES

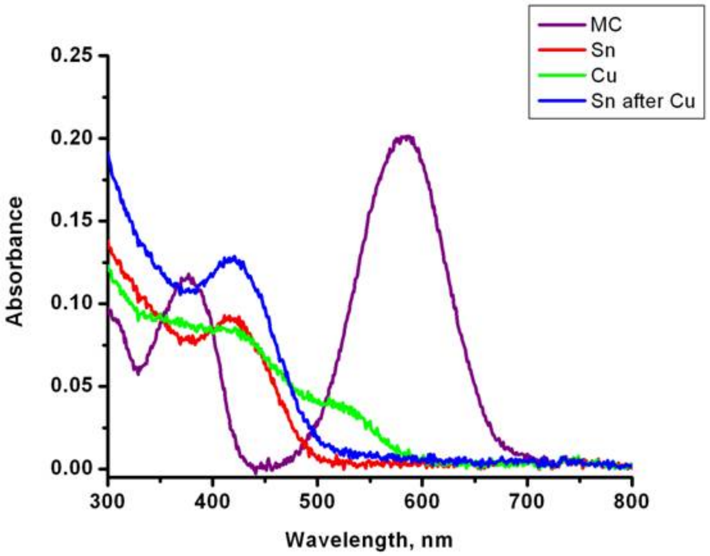

Figure B-1. UV-vis absorbance spectra of a poly(MMA$_{90}$-*co*-SPMA$_{10}$) thin film in response to immersion in 25 mM CuCl$_2$ followed by immersion in 25 mM SnCl$_2$.

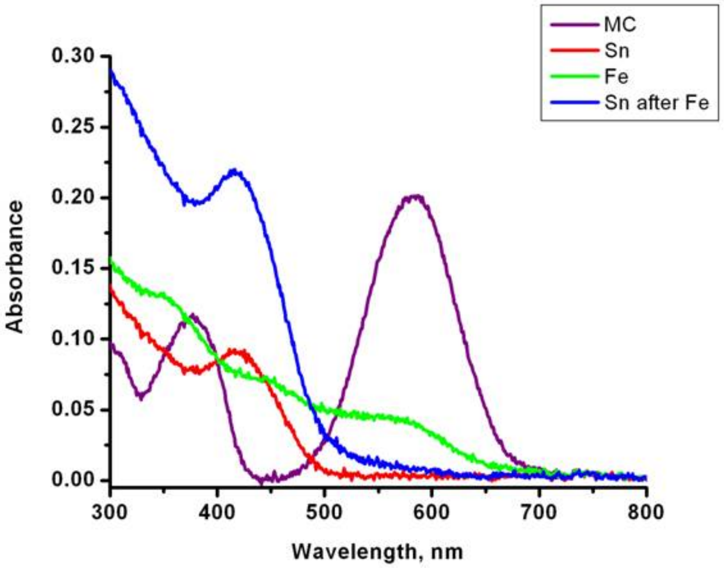

Figure B-2. UV-vis absorbance spectra of a poly(MMA_{90}-*co*-$SPMA_{10}$) thin film in response to immersion in 25 mM $FeCl_2$ followed by immersion in 25 mM $SnCl_2$.

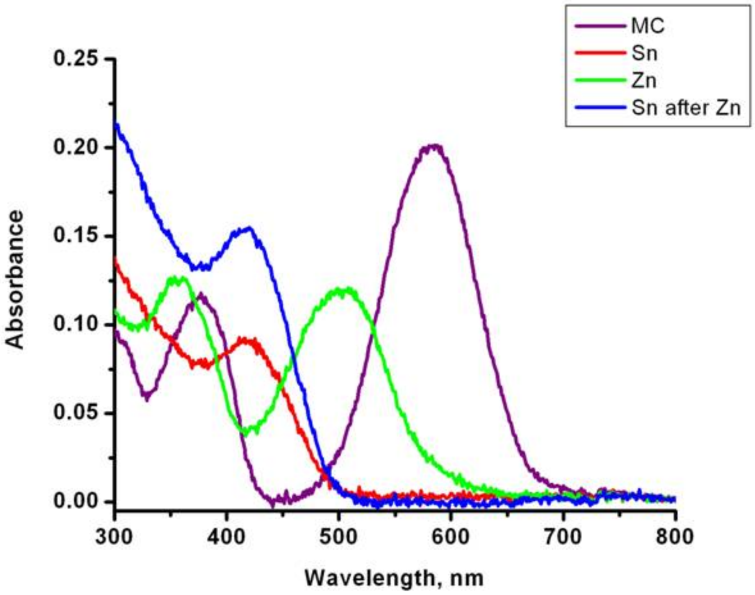

Figure B-3. UV-vis absorbance spectra of a poly(MMA_{90}-*co*-$SPMA_{10}$) thin film in response to immersion in 25 mM $ZnCl_2$ followed by immersion in 25 mM $SnCl_2$.

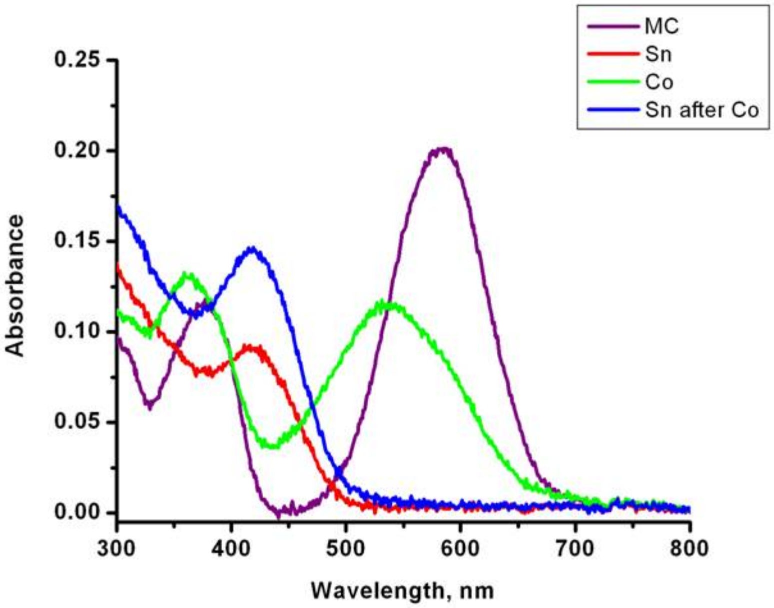

Figure B-4. UV-vis absorbance spectra of a poly(MMA_{90}-*co*-$SPMA_{10}$) thin film in response to immersion in 25 mM $CoCl_2$ followed by immersion in 25 mM $SnCl_2$.

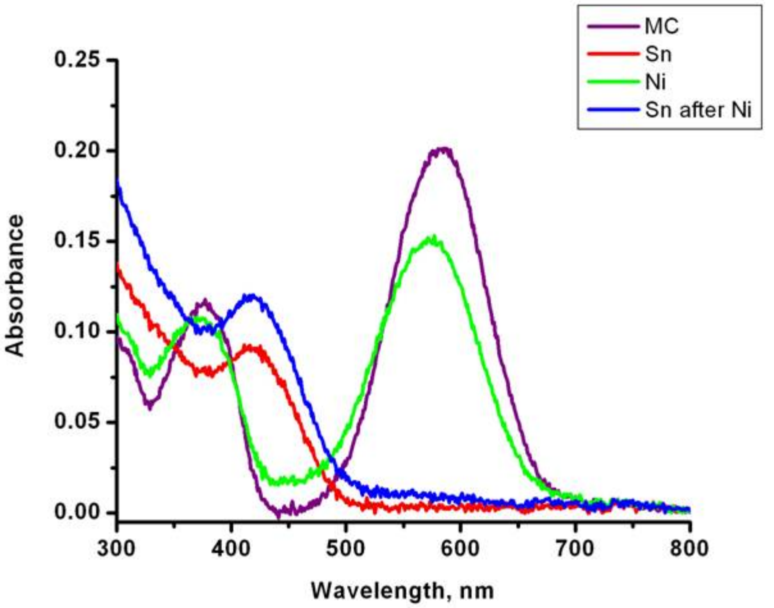

Figure B-5. UV-vis absorbance spectra of a poly(MMA_{90}-*co*-$SPMA_{10}$) thin film in response to immersion in 25 mM $NiCl_2$ followed by immersion in 25 mM $SnCl_2$.

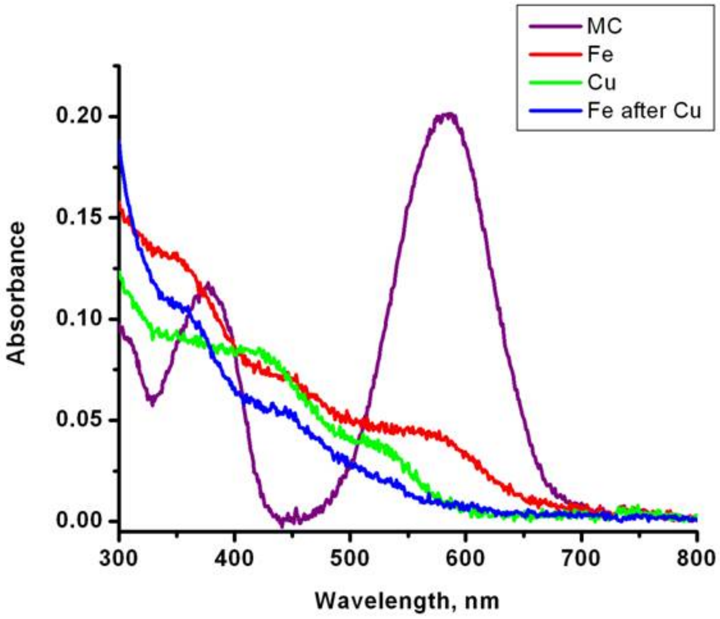

Figure B-6. UV-vis absorbance spectra of a poly(MMA_{90}-*co*-$SPMA_{10}$) thin film in response to immersion in 25 mM $CuCl_2$ followed by immersion in 25 mM $FeCl_2$.

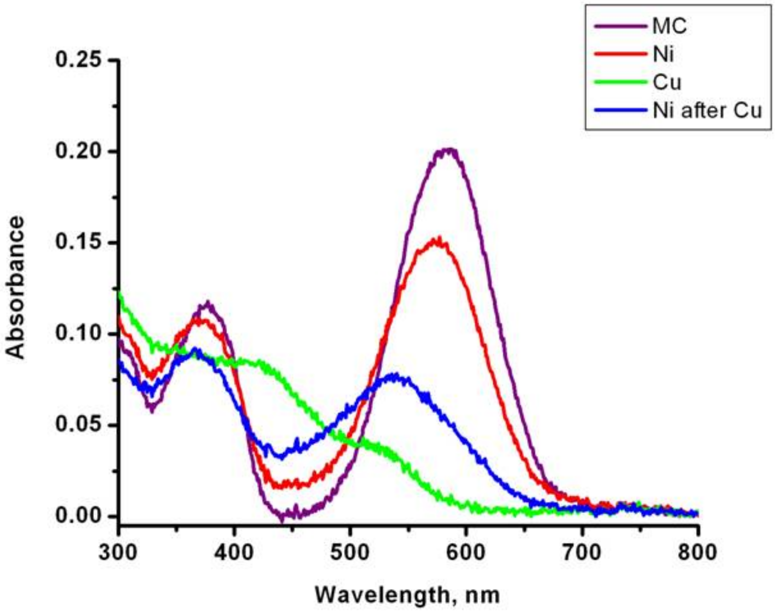

Figure B-7. UV-vis absorbance spectra of a poly(MMA_{90}-*co*-$SPMA_{10}$) thin film in response to immersion in 25 mM $CuCl_2$ followed by immersion in 25 mM $NiCl_2$.

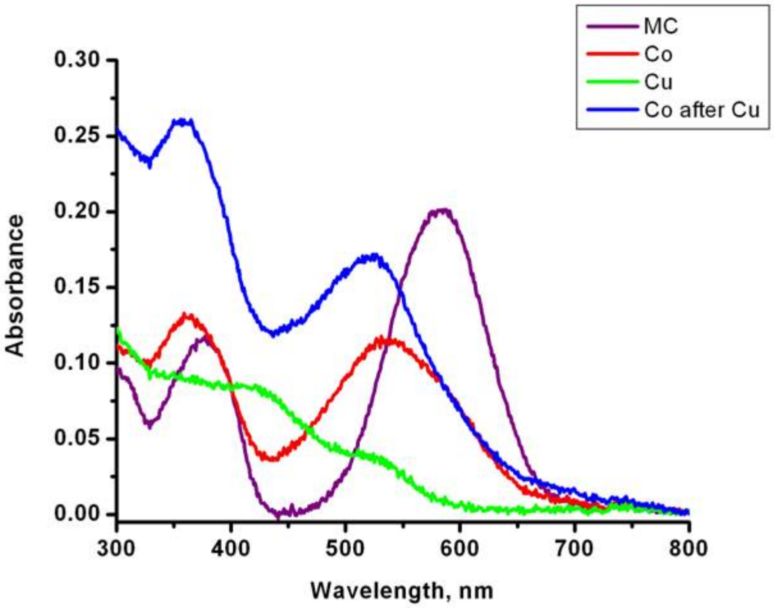

Figure B-8. UV-vis absorbance spectra of a poly(MMA$_{90}$-*co*-SPMA$_{10}$) thin film in response to immersion in 25 mM CuCl$_2$ followed by immersion in 25 mM CoCl$_2$.

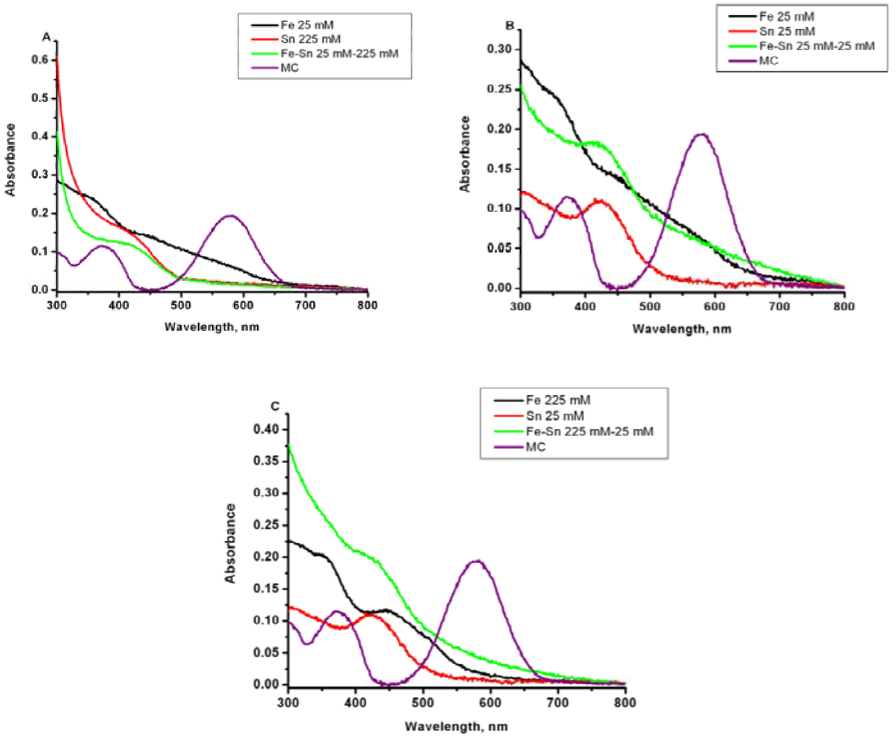

Figure B-9. UV-vis absorbance spectra of poly(MMA$_{90}$-*co*-SPMA$_{10}$) in response to a solution containing (a) 25 mM FeCl$_2$ and 225 mM SnCl$_2$ (b) 25 mM FeCl$_2$ and 25 mM SnCl$_2$ and (c) 225 mM FeCl$_2$ and 25 mM SnCl$_2$.

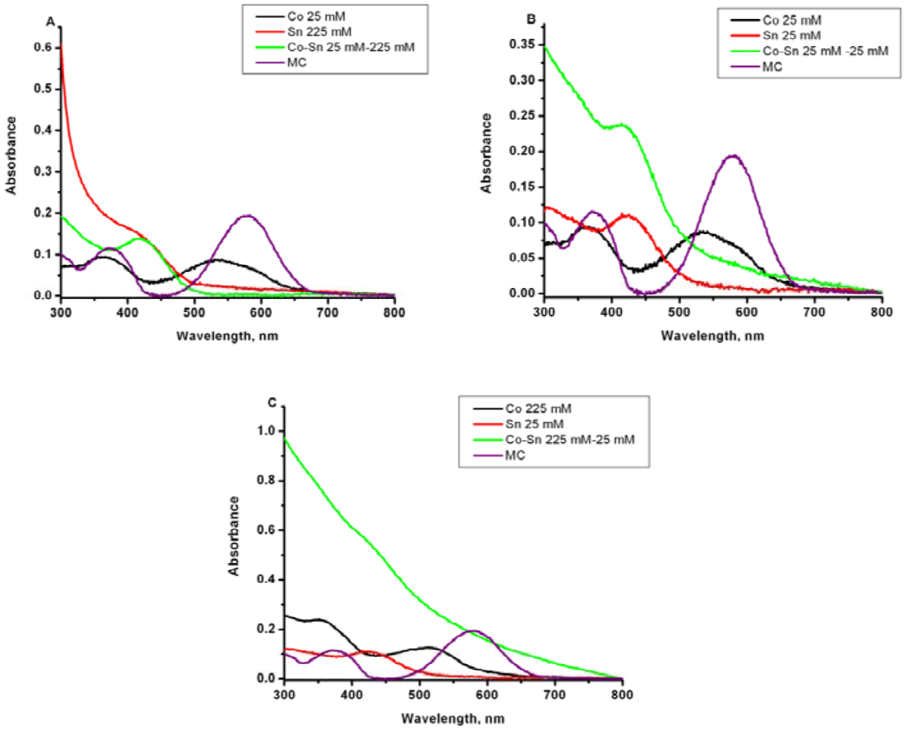

Figure B-10. UV-vis absorbance spectra of poly(MMA$_{90}$-*co*-SPMA$_{10}$) in response to a solution containing (a) 25 mM CoCl$_2$ and 225 mM SnCl$_2$ (b) 25 mM CoCl$_2$ and 25 mM SnCl$_2$ and (c) 225 mM CoCl$_2$ and 25 mM SnCl$_2$.

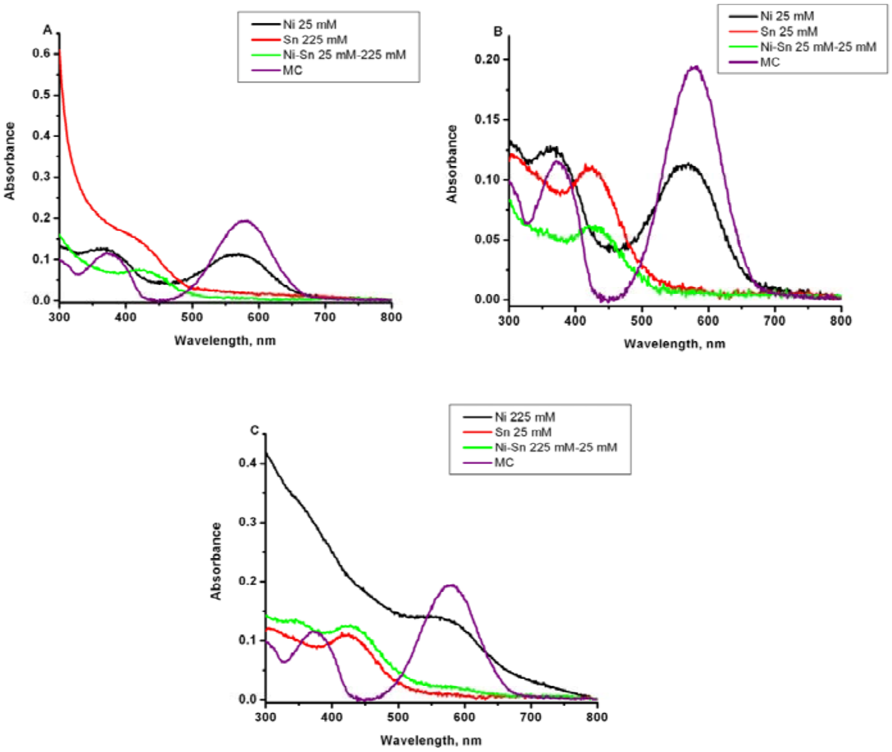

Figure B-11. UV-vis absorbance spectra of poly(MMA$_{90}$-*co*-SPMA$_{10}$) in response to a solution containing (a) 25 mM NiCl$_2$ and 225 mM SnCl$_2$ (b) 25 mM NiCl$_2$ and 25 mM SnCl$_2$ and (c) 225 mM NiCl$_2$ and 25 mM SnCl$_2$.

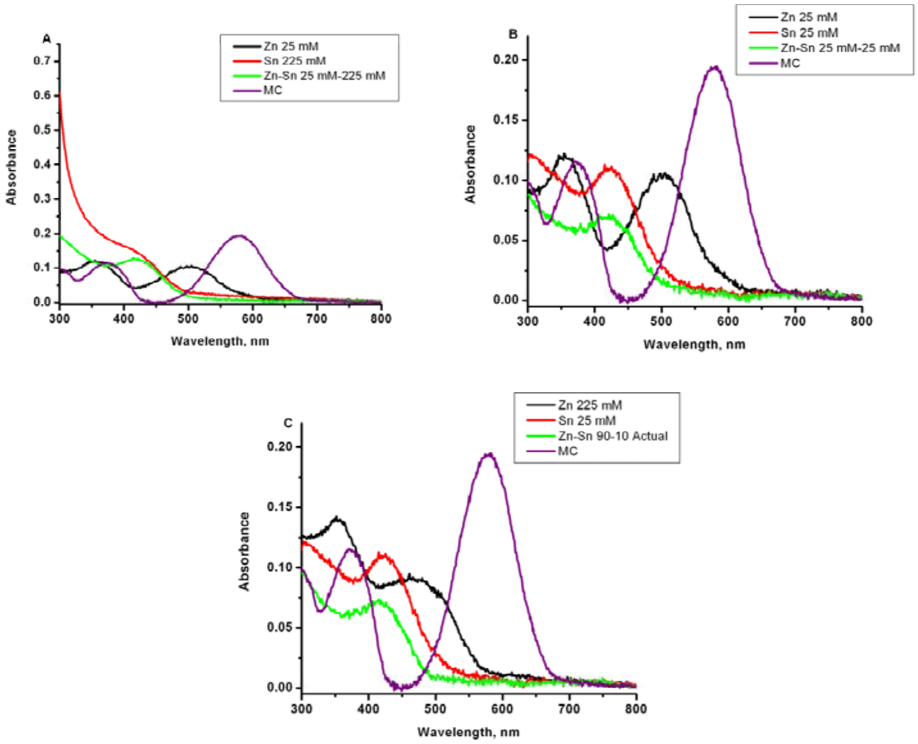

Figure B-12. UV-vis absorbance spectra of poly(MMA$_{90}$-*co*-SPMA$_{10}$) in response to a solution containing (a) 25 mM ZnCl$_2$ and 225 mM SnCl$_2$ (b) 25 mM ZnCl$_2$ and 25 mM SnCl$_2$ and (c) 225 mM ZnCl$_2$ and 25 mM SnCl$_2$.

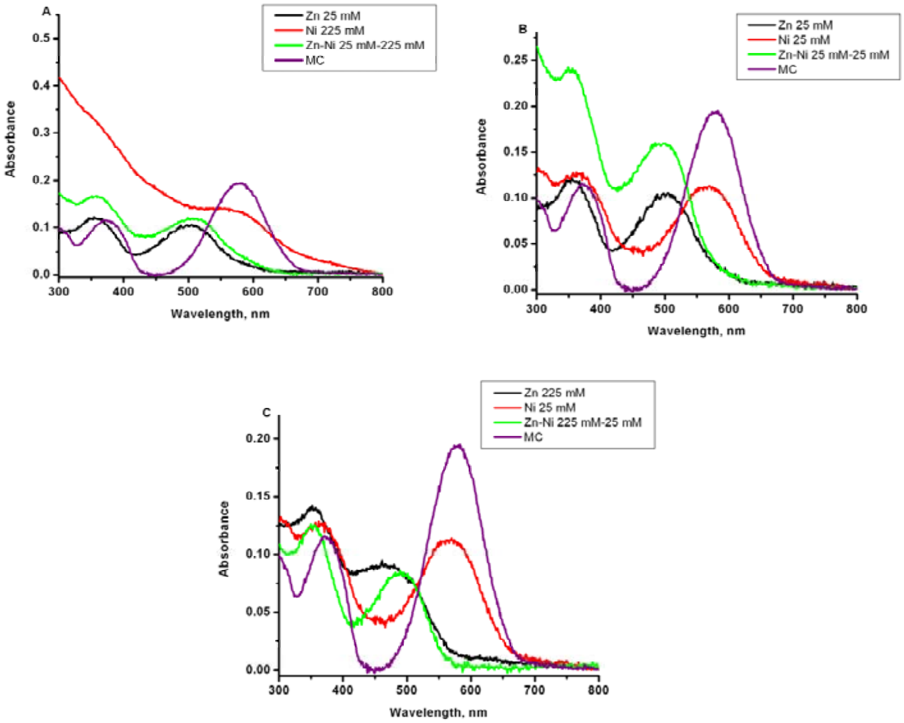

Figure B-13. UV-vis absorbance spectra of poly(MMA$_{90}$-*co*-SPMA$_{10}$) in response to a solution containing (a) 25 mM ZnCl$_2$ and 225 mM NiCl$_2$ (b) 25 mM ZnCl2 and 25 mM NiCl and (c) 225 mM ZnCl$_2$ and 25 mM NiCl$_2$.

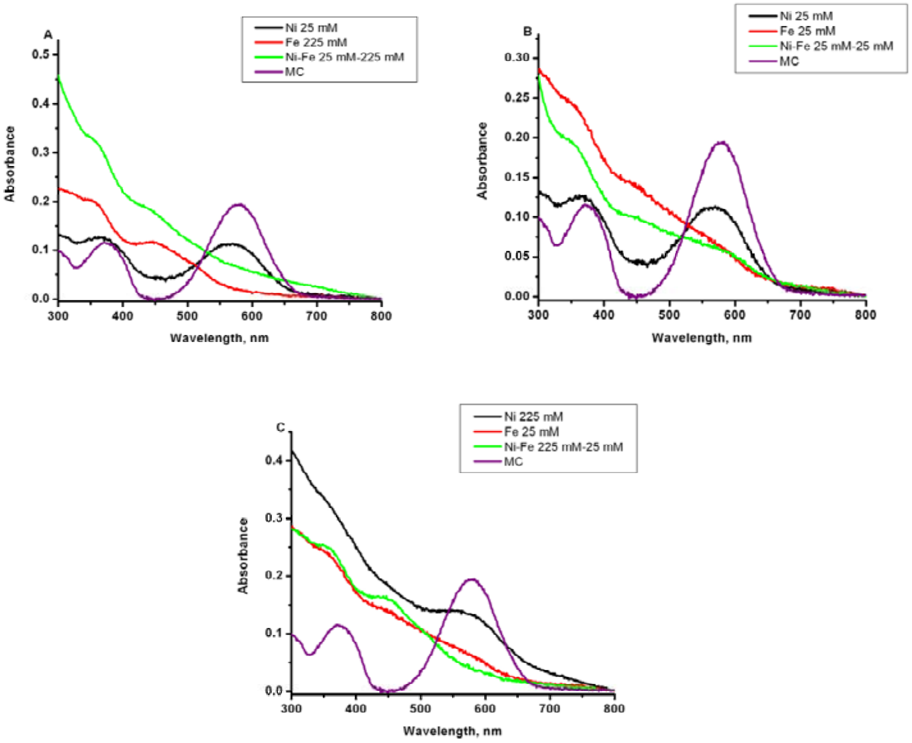

Figure B-14. UV-vis absorbance spectra of poly(MMA$_{90}$-*co*-SPMA$_{10}$) in response to a solution containing (a) 25 mM NiCl$_2$ and 225 mM FeCl$_2$ (b) 25 mM NiCl$_2$ and 25 mM FeCl$_2$ and (c) 225 mM NiCl$_2$ and 25 mM FeCl$_2$.

APPENDIX C

^{1}H NMR SPECTRA OF MMA-MEO, TFEMA-MEO, AND TFEMA-SPMA COPOLYMERS

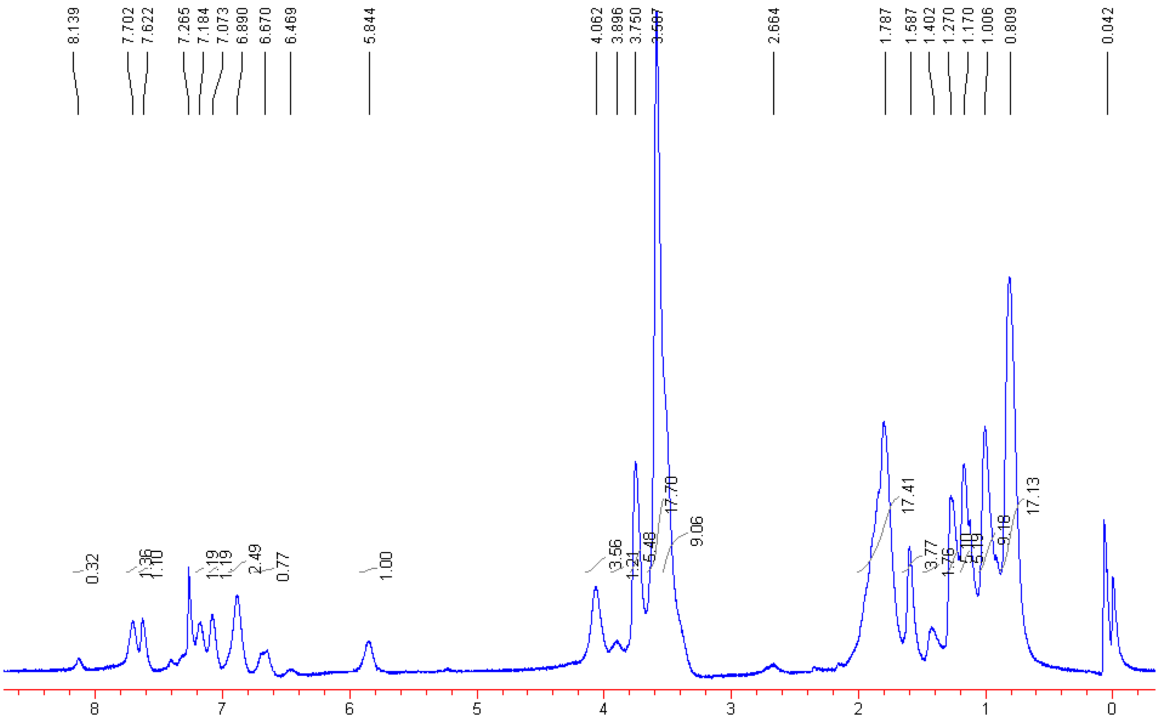

Figure C-1. ^{1}H NMR spectra of 10 mol% MEO – 90 mol% MMA.

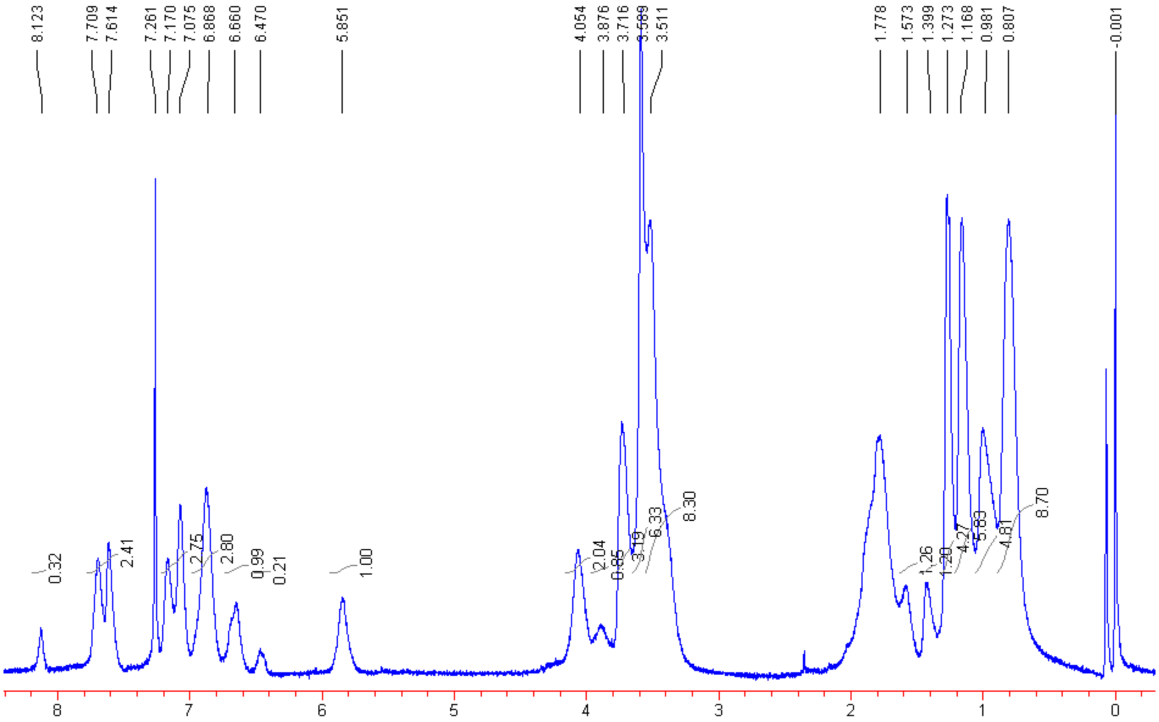

Figure C-2. ^{1}H NMR spectra of 30 mol% MEO – 70 mol% MMA.

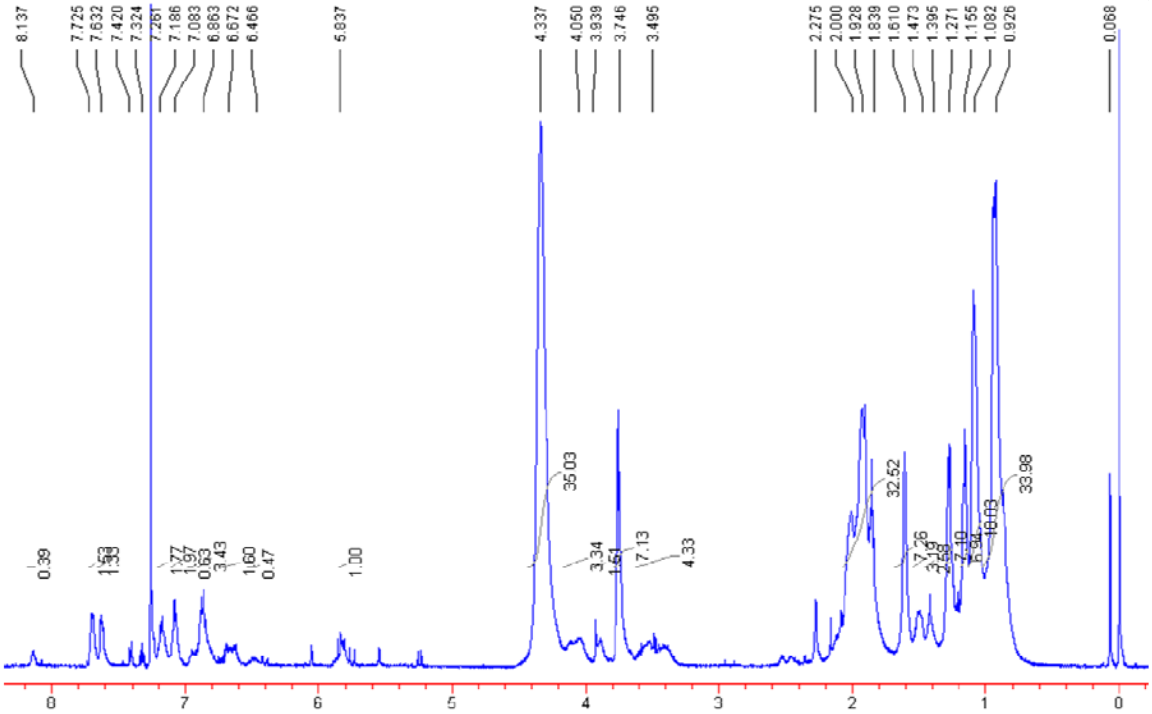

Figure C-3. ^{1}H NMR spectra of 10 mol% MEO – 90 mol% TFEMA.

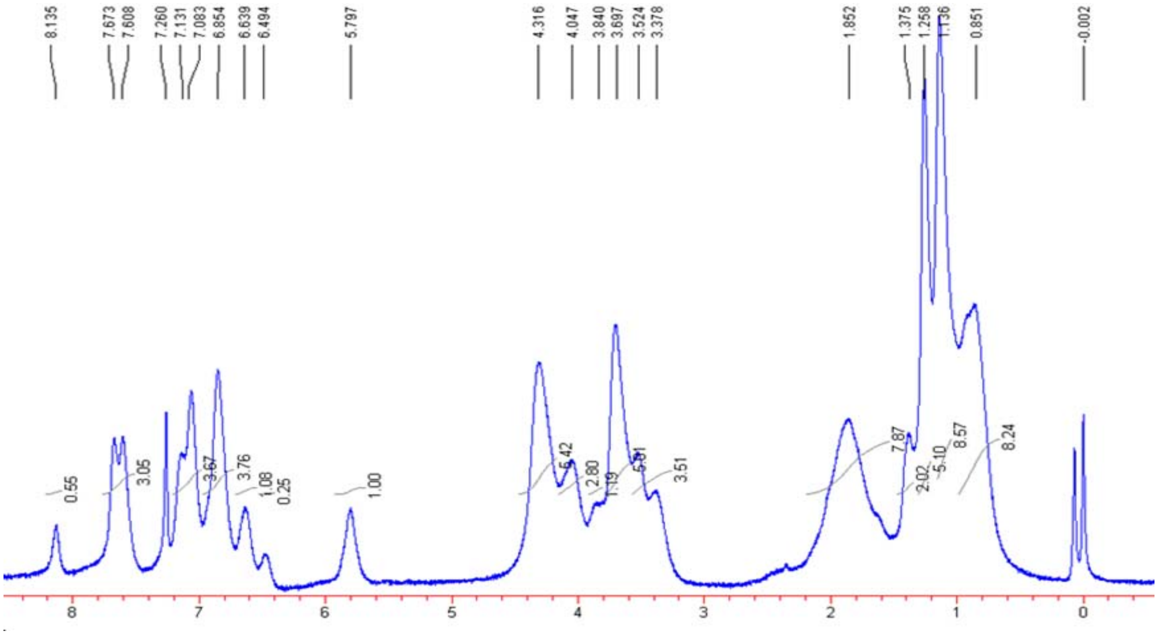

Figure C-4. ^{1}H NMR spectra of 50 mol% MEO – 50 mol% TFEMA.

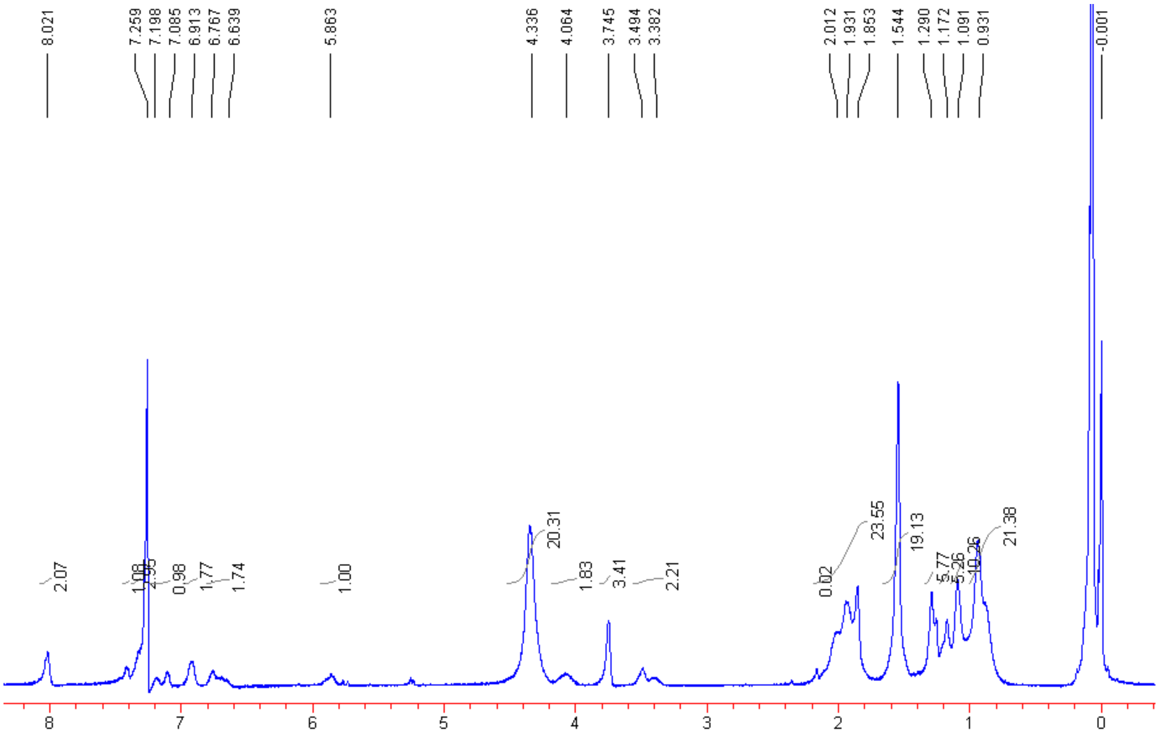

Figure C-5. ^{1}H NMR spectra of 10 mol% SPMA – 90 mol% TFEMA.